

System Design for a High Data Rate Wireless Infrared Multi language Distribution system

THESIS

Submitted in partial fulfillment of the
requirements for the degree of

MASTER OF SCIENCE
in
ELECTRICAL ENGINEERING
by
Fatemeh Badinrad



BOSCH
Invented for life

System Design for High Data Rate Wireless Infrared Multi Language Distribution System

Student Number: 1532472

Thesis Number:

COMMITTEE MEMBERS

Professor: Prof. Dr. ir. I.G.M.M. Niemegeers (WMC- TU Delft)

Supervisor: Dr. ir.G.J.M. Janssen (WMC-TU Delft)

Ir.H S.P. van der Schaar (Bosch Security System)

External Examiner: Dr.H.Nikookar (IRCTR - TU Delft)

Copyright ©2010 Bosch Security System

All rights reserved. No Section of the material protected by this copyright may be re-produced or utilized in any form or by any means, electronic or mechanical, including photocopying, recording or by any information storage and retrieval system, without the permission from the author, Delft University of Technology and Bosch Security System.

Abstract

This thesis investigates the feasibility of high speed wireless communication for an infrared multi language distribution system and concludes that data rates near 20Mbps are practical. We identify the impediments to high speed communication, namely, multipath dispersion and weak front-end design and propose different strategies to counter them. We characterize multipath optical propagation for diffuse-reflector environments by presenting a theoretical model. Bandwidth limiting factors are determined in transmitter and receiver front-ends and new components are introduced for supporting high data rate. We also determine the noise contribution at the receiver front-end which is a dominant source of noise. The performance of various modulation schemes is evaluated for the system and show how the data rate of the system can be improved.

Acknowledgement

I would like to gratefully acknowledge my supervisors Dr. Gerard Janssen and Hans van der Schaar for their guidance and help throughout the work. Dr.Janssen, thanks for steering me through the challenges with your wisdom, patience and your encouragements. Your valuable comments and remarks were always important and make me work harder. Hans, you are a champion for excellence. You have taught me to think positive and more importantly you inspired me to become a finer person in my life. I have enjoyed each moment of working with you over this period.

It has been a great pleasure to be a member of research group at Bosch and I would like to thank Patrick, Johan and Jacob and others for their discussions and suggestions on my work and providing me such friendly environment.

I am grateful to Dr.Nikookar for providing me this research opportunity at Bosch.

Here, I would like to thank all the teaching and non-teaching staff members of university for their nice cooperation for international students. Special thanks to John Stals, Paula Meesters and Gytha Rijnbeek

This thesis would have been impossible without support from my family members, and my friends. I would like to thank them all again.

Contents

Abstract	i
Acknowledgement.....	iii
1. Introduction	1
1.1 Bosch Infrared language distribution system	1
1.2 Technical characteristics of the system	2
1.3 Goal of the thesis	4
1.4 Outline of the thesis.....	4
2. Indoor wireless infrared communication.....	7
2.1 Infrared link configuration	8
2.2 Propagation in optical wireless channel	10
2.2.1 Power delay profile.....	11
2.2.2 Time delay spread.....	12
2.2.3 Coherence Bandwidth	12
2.2.4 Doppler Effect	13
2.3 Optical wireless channel model.....	13
2.3.1 LOS component.....	15
2.3.2 Diffuse component	16
2.4 Noise sources in optical wireless channel	18
3. Simulation model for the indoor infrared channel.....	21
3.1 Channel simulation model.....	21
3.2 Description of room and configuration	23
3.3 Simulation result of the single reflection model.....	24
3.4 Simulation result of the multiple reflections model	30
3.5 Simulation result of single reflection model with four radiators	32
3.6 Calculation of delay spread and RMS delay	35
4. Opto-Electronic Front-Ends	39
4.1 Optical source.....	39
4.2 Infrared receiver	42
4.2.1 Photo-detector.....	42

4.2.2	PIN diode with preamplifier	45
5.	Experimental investigation to increase the bandwidth.....	49
5.1	Light Emitting Diode	49
5.2	PIN-diode.....	51
5.3	Trans-impedance amplifier (TIA)	52
5.4	Summary of chosen components	53
5.5	Measurement set up	54
5.5.1	LED driver circuit	54
5.5.2	PIN diode driver circuit.....	55
5.6	Results of the measurement	56
6.	Digital Modulation Techniques	59
6.1	Modulation scheme classification	59
6.1.1	Constant envelop modulation (CE).....	60
6.1.2	Variable Envelop Modulation	60
6.2	Comparison of digital modulation schemes	62
6.2.1	Bandwidth and power efficiency	62
6.2.2	Bit error probability	64
6.2.3	Peak to average power ratio	65
7.	Multicarrier modulation-OFDM	67
7.1	Multicarrier	67
7.2	OFDM signal structure.....	71
7.3	Advantages of OFDM.....	73
7.4	OFDM challenges	73
7.4.1	Peak to average power ratio (PAPR)	73
7.4.2	Frequency and timing offset	75
7.5	Summary	76
8.	Modulation choice for the system.....	77
8.1	General system requirement.....	77
8.2	Single carrier approach with multilevel modulation	78
8.3	Non-overlapping multicarrier approach with multilevel digital modulation	79
8.3.1	Effective bandwidth per carrier.....	80

8.4	OFDM approach.....	81
8.4.1	OFDM system parameters.....	81
8.4.2	Challenges with chosen OFDM parameters	83
9.	Conclusion and further research.....	87
9.1	Conclusion.....	87
9.2	Further work	89
10.	References	91

List of Figures

Figure 1.1: Integrus system.....	1
Figure 1.2: Eight subcarriers in the assigned frequency band	2
Figure 1.3: Transmitter Architecture	3
Figure 1.4: Receiver Architecture.....	3
Figure 2.1: Configuration for wireless optical links	9
Figure 2.2: Example of power delay profile	11
Figure 2.3: Sketch of the impulse response	14
Figure 2.4: Normalized shape of the generalized Lambertian radiation pattern.....	15
Figure 2.5: Geometry of source (Tx) and detector (Rx) without reflectors	16
Figure 2.6: Multiple reflections propagation model	17
Figure 2.7: Optical power spectra of common ambient infrared sources	18
Figure 3.1: Algorithm implemented to simulate impulse response of an infrared channel	22
Figure 3.2: Communication scenario.....	23
Figure 3.3: Upper perspective of an empty room with several positions for receiver	24
Figure 3.4: Upper perspective of a room for single reflection propagation model.....	25
Figure 3.5: Received power vs. time delay for receiver at position (63m, 5m, 1m)	26
Figure 3.6: Received power vs. time delay for receiver at position (63m, 20m, 1m)	26
Figure 3.7: Received power vs. time delay for receiver at position (45m, 5m, 1m)	27
Figure 3.8: Received power vs. time delay for receiver at position (45m, 20m, 1m).....	28
Figure 3.9: Received power vs. time delay for receiver at position (10m, 5m, 1m)	29
Figure 3.10: Received power vs. time delay for receiver at position (10m, 20m, 1m).....	29
Figure 3.11: Upper perspective of a room with multiple reflection propagation.....	30
Figure 3.12: Received power vs. time delay for receiver at position (63m, 5m, 1m)	31
Figure 3.13: Received power vs. time delay for receiver at position (45m,5m,1m)	31
Figure 3.14: Received power vs. time delay for receiver at position (10m,5m,1m)	32
Figure 3.15: Two configurations of four radiators in the room	33
Figure 3.16: Received power vs. delay for the receiver shown in first conjuration.....	34
Figure 3.17: Received power vs. delay for the receiver shown in second configuration.....	34
Figure 3.18: 30dB delay spread with LOS and N-LOS in single reflection channel model	35
Figure 3.19: 40dB delay spread with LOS and N-LOS in single reflection channel model	36

Figure 3.20: RMS delay spread with LOS and N-LOS in single reflection channel model.....	36
Figure 3.21: 30dB delay spread with LOS and N-LOS in multi reflections channel model	37
Figure 3.22: 40dB delay spread with LOS and N-LOS in multi reflections channel model	37
Figure 3.23: RMS delay spread with LOS and N-LOS in multi reflections channel	38
Figure 4.1: A schematic of electrical-optical channel	39
Figure 4.2: A typical OW receiver	42
Figure 4.3: Circuit model and equivalent small circuit of a detector with low/ high impedance amplifier	45
Figure 4.4: Basic scheme of a detector with trans-impedance and its equivalent small circuit	46
Figure 4.5: Noise characteristic of a amplifier	47
Figure 5.1: Radiant intensity of the LEDs vs. angle of half intensity, $\lambda=870\text{nm}$	50
Figure 5.2: Radiant intensity of the LED vs. angle of half intensity, $\lambda=850\text{nm}$	51
Figure 5.3: Maximum achievable bandwidth for selected Op-amps	53
Figure 5.4: General measurement set up	54
Figure 5.5: LED driver circuit	55
Figure 5.6: PIN diode driver circuit	56
Figure 5.7: Measurement set up	57
Figure 5.8: Spectrum of the received signal	57
Figure 6.1: Modulation scheme classification.....	59
Figure 6.2: 16APSK constellation diagram.....	61
Figure 6.3: Bandwidth efficiency vs. power efficiency	63
Figure 6.4: Bit error rate vs. bit to noise ratio	64
Figure 7.1: Passing of baseband and MCM signal through a frequency selective channel.....	68
Figure 7.2: FDM spectrum with 8 subcarriers and guard bands	69
Figure 7.3: Spectrum of 8 equally modulated subcarriers in OFDM	70
Figure 7.4: Comparison of spectral efficiency of FDM and OFDM	70
Figure 7.5: Digital implementation of multi-cattier modulator. P/S denotes parallel-to-serial and DAC digital-to-analogue conversion.....	71
Figure 7.6: Generation of cyclic prefix guard interval	72
Figure 7.7: Simplified OFDM transmitter and receiver blocks.....	72
Figure 8.1: Raw data rate in different stages of transmitter	78
Figure 8.2: PAPR vs. number of subcarrier	85

Figure 8.3: Power penalty vs. number of subcarrier 85

List of Tables

Table 2.1: Comparison between radio and infrared properties for indoor wireless communication	8
Table 2.2: Comparison between wireless optical links	9
Table 4.1: Comparison between LED and LD	40
Table 4.2: Interpretation of LED safety classification for optical sources	40
Table 4.3: Comparison of PIN and APD for wireless optical link	43
Table 5.1: Light emitting diodes	49
Table 5.2: PIN diodes	52
Table 5.3: Summary of the OW components for target system	53
Table 6.1: Peak to average power ratio (PAPR) of several modulation schemes	65
Table 8.2: QPSK-OFDM parameters	83

Mathematical Symbol

A_{room}	Area of room
a_i	Amplitude of i -th copy of received signal
A_{Rx}	Detector area
B	Frequency bandwidth
B_G	Guard band
B_{avail}	Available bandwidth
B_{eff}	Effective bandwidth
B_N	Sub-channel bandwidth
B_T	Total transmission bandwidth
B_{coh}	Coherence bandwidth
C_t	Sum of the photodiode junction and input capacitances
c	Speed of light
C_{det}	Depletion capacitance of PIN diode
C_{stray}	Stray capacitance
C_{FET}	Preamplifier capacitance
C_f	Feedback capacitance
Cf	Compression factor
d	Depletion layer width
dP	Received power at reflector
dA	Area of reflectors
\bar{e}_n	Input voltage noise
E_b	Energy per bit
$E[J]$	Expectation
f_s	Sampling frequency
f_n	n -th subcarrier frequency
F	Band limiting frequency of a filter
f_c	PIN diode cutoff frequency
f_{3dB}	Modulation bandwidth of LED
FOV_{det}	Detector field of view
FOV_{ref}	Reflector field of view
f	Measurement bandwidth
GBP	Gain bandwidth product
$h^{(k)}$	Impulse response under k reflections
$h^{(0)}(t)$	LOS impulse response
$h(t)$	Multipath impulse response
$H(f)$	Frequency impulse response
I_{EQ}	Input equivalent noise
I_m	Total noise current generated in a photo-detector

I_p	Photocurrent
I_D	Dark current
I_{jn}	Johnson noise
\bar{i}_n	Input current noise
I_{ir}	Irradiance
$i(t)$	Received photo-current
k	Current shot noise
k_B	Boltzmann Constant
l	Number of bits per symbol
M_{path}	Number of multipath components
N_{data}	Number of data subcarrier
N_{pilot}	Number of pilot subcarriers
N_{null}	Number of null subcarriers
n_{wd}	Number of sample in sampling word
N_{CP}	Number of symbol in cyclic prefix
N_{sc}	Number of sub-channel in multicarrier system
N_0	Noise power spectral density
N_e	Number of reflecting element
\hat{n}_{Rx}	Receiver orientation vector
\hat{n}_{Tx}	Transmitter Orientation vector
\hat{n}_{ref}	Reflector orientation vector
n_L	Lambert radiation index
n_d	Lens index
P_n	Ambient light power
P_t	Transmitted optical power
P	Radiated power from reflector
$p_\tau(\tau)$	Density function of the power delay profile
$p_r(\tau)$	Power delay profile
P_r	Received power
q	Electron charge
R_{b-OFDM}	Data rate of an OFDM system
R_c	Coding rate
R_r	Raw bit rate per audio channel
R_T	Total data rate of 100 audio channel
r_N	Factor of Nyquist filter
R_f	Feedback resistor
R_b	Data rate
R_L	Load resistance
r	Distance

Rx	Receiver
r_s	Transmitter position vector
$rect$	Rectangular function
r_R	Receiver position vector
R_p	Responsivity of the detector
$R(\phi)$	radiation intensity
R_s	Symbol rate
s	Surface of all reflectors
T_g	Guard interval
T_u	Useful symbol time
T_{OFDM}	Duration of an OFDM symbol
T_N	Symbol time in multicarrier system
T_m	Temperature
t_{drift}	Drift transit time
t_{diff}	Diffusion time of carriers
t_{RC}	RC time constant
T_b	Bit duration
t	Time
Tx	Transmitter
V_R	Reverse voltage
$X(t)$	Instantaneous optical power
τ_{RMS}	Root mean square (RMS) delay
τ_{\max}	Maximum excess delay
τ_m	Mean excess delay
τ_0	First-arrival delay
τ	Excess time delay
τ_{rise}	Rise time
τ_{life}	Carrier lifetime
η	Bandwidth efficiency
$\phi_{1/2}$	Radiation half-angle
ψ	Angle between \hat{n}_{Rx} and $(r_s - r_R)$
ϕ	Direction angle of transmitter with respect to its normal vector
δ	Dirac delta function
φ_i	Phase of i -th copy of received signal
ΔA	Area of a reflecting element used in simulation
λ_p	Peak wavelength
ρ	Reflectivity
μ	Traveling rate

Acronyms

AEL	Allowable exposure limit
ACE	Active constellation extension
APD	Avalanche photodiodes
ASK	Amplitude shift keying
BER	Bit Error Rate
CE	Constant Envelope
CPM	Continuous phase modulation
CP	Cyclic prefix
DQPSK	Differential Quadrature Phase-Shift Keying
DC	Direct current
DFT	Discrete Fourier transform
DVB	Digital Video Broadcasting
FCC	Federal communication commission
FOV	Field-of-view
FFT	Fast Fourier transform
FDM	Frequency Division Multiplexing
FSK	Frequency shift keying
GMSK	Gaussian minimum shift key
IM/DD	Intensity modulation and direct detection
ISI	Inter-symbol inference
IR	Infrared radiation
IEC	Electro-technical Commission
ICI	Inter-carrier interference
LED	Light Emitting Diode
LD	Laser diodes
LOS	Line of sight
MCM	Multicarrier Modulation
MAPSK	Amplitude and phase shift keying
MSK	Minimum shift key
ML	Maximum likelihood estimator
NLOS	Non-Line-of- Sight
OFDM	Equivalent power
PIN	Positive-Intrinsic-Negative Diode
PSK	Phase shift keying
PAPR	Peak to average power ratio
PSD	Power spectral density
QAM	Quadrature amplitude modulation
RS	Reed Solomon
RF	Radio frequency
RMS	Root-mean-square
SFSK	Sinusoidal frequency shift key
SNR	Signal-to-noise ratio
SLM	Selective mapping
TR	Tone reservations
TIA	Trans-impedance amplifier
WPAN	Wireless personal area Network
ZP	Zero-padding

1. Introduction

Wireless communication systems have been evolving from one generation to the next and this is mostly due to the increasing demand for higher data rates and capacity of the channel.

Also for clients of Bosch conferencing systems, there was a clear need for a high system capacity which requires a high channel data rate. In that sense, the system can transmit more audio channels with high quality. This master's thesis is concerned with analysis of the feasible options to increase the capacity of the system. However, evaluating any method starts with studying of the requirements and the channel. In addition, it is necessary to look in more detail to challenges that arose when high speed transmission is required.

1.1 Bosch Infrared language distribution system

The infrared language distribution system is used in conferences to distribute the interpreted language of the speaker to participants. The two main reasons to use infrared are because the distributed infrared signals cannot pass beyond the conference hall and there is huge unregulated bandwidth at infrared frequency. This system consists of a transmitter, one or more radiators and a number of receivers as shown in Figure 1.1.



Figure 1.1: Integras system

The transmitter is the central element of the system. It receives inputs from either analog or digital sources and modulates these signals onto multiple carriers. Then, this base band signal is transmitted to infrared radiators mounted on the ceiling or walls in a conferencing hall. The output of the radiator is intensity modulated infrared radiation. The radiators provide a reliable infrared coverage from small meeting rooms up to very large conference halls.

Each delegate is equipped with a pocket receiver that has a lens to collect the infrared signal. The signal is decoded into the interpretation language selected by the delegate and finally passed to the headphone.

1.2 Technical characteristics of the system

The main infrared carrier of the radiators has an optical wavelength at 875nm. The baseband transmission bandwidth between 2 and 8MHz is used; however, according to the standard for infrared conferencing systems, only the bandwidth up to 6MHz is standardized.

The current system has up to 8 subcarriers with a bandwidth of 586.53 kHz each and uses a guard band of 444 kHz, as shown in Figure 1.2. For each subcarrier, a single carrier transmission with DQPSK modulation and a raised cosine pulse shaping with roll-off factor of 0.4 are used. This results in a data rate of 837kb/s per carrier and a total data rate of 6.7 Mb/s for 32 audio channels. Forward error correction with a (28, 24, 2) Reed-Solomon (RS) code and audio compression with a factor of 2.6 are applied on each subcarrier.

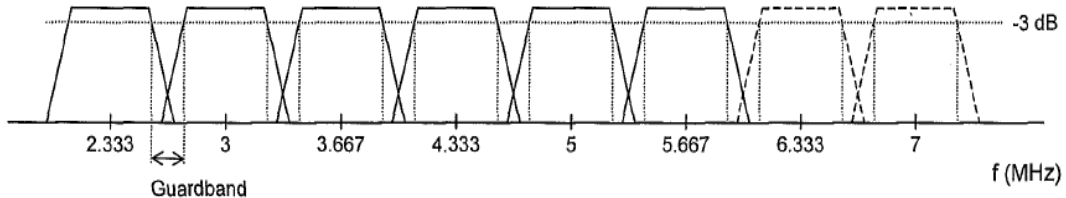


Figure 1.2: Eight subcarriers in the assigned frequency band

Figure 1.3 and Figure 1.4 show the functional block diagrams of the transmitter and receiver. The transmitter manages the following functions:

- Audio Digitalization: each analogue audio channel is converted to a digital signal;
- Audio compression: the digital signals are compressed in order to reduce the amount of information for transmission. The compression factor is related to the required audio quality.
- Protocol generation and framing
- Forward error correction: it is applied to protect the audio and data information from transmission error using RS code of (28, 24, 2)
- Synchronization insertion: to detect the start of the data.
- DQPSK modulation: the symbol information is encoded as the phase change from one symbol period to the next rather than as an absolute phase.
- Digital to analog convertor

- The front end of the transmitter uses intensity modulation by modulating the output power of infrared LEDs.

And the receiver manages the inverse of all the mentioned functions except audio de-compression.

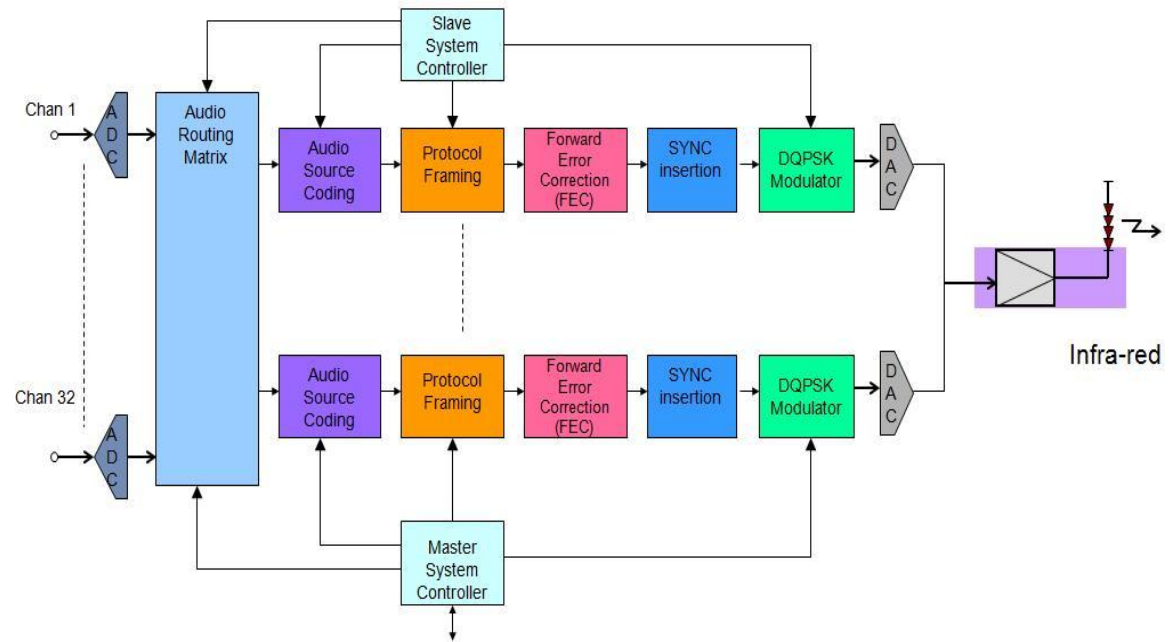


Figure 1.3: Transmitter Architecture

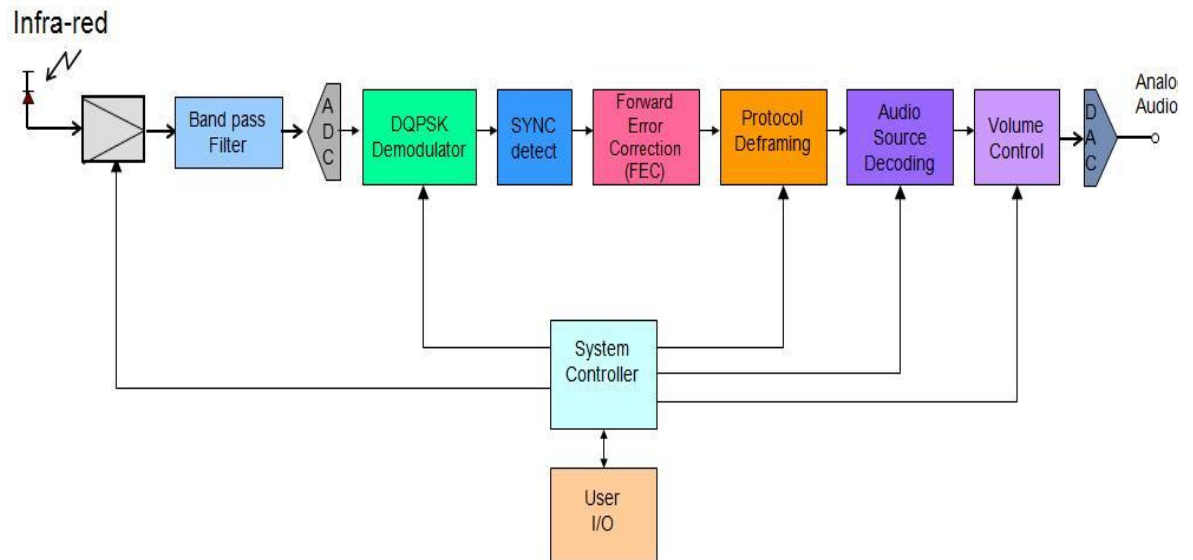


Figure 1.4: Receiver Architecture

1.3 Goal of the thesis

The overall goal of this thesis is to investigate the feasibility of increasing the data rate of the Bosch infrared language distribution system. The number of audio channels to be supported by new system shall be at least 100. In that case, the system shall have a transmission rate of at least 20Mb/s. Therefore, this thesis provides an insight on the performance of various modulation techniques for the system with which the requirement is met. In that context, two main questions are handled

What are the limits for transmission rate in an intensity modulation and direct detection (IM/DD) channel?

How and to what extent can these limitations affect the design choices in practice?

The transmission data rate of wireless communication system is strongly affected by multipath propagation. The delay of the channel causes stretching of the input signal which creates signal distortion referred to as inter-symbol inference (ISI). Therefore, it is necessary to investigate the behaviour of the channel.

Another limiting factor is created in the design of the system; the opto-electrical components used in the transmitter and receiver have speed limitations. For example the photo-detector is the main component in limiting the bandwidth of the system.

To answer these questions, this thesis investigates the following subjects

- Modelling of the optical wireless channel to determine the effect of the multipath on the bandwidth limitation (channel delay spread).
- Bandwidth limitation factors in the transmitter and receiver front-end designs are determined.
- Analyze several modulation techniques such as single and multicarrier modulations and select the appropriate scheme that fits with channel characteristics and meets the requirement.
- Identifying the issues related to the link budget analysis of the chosen modulation.

1.4 Outline of the thesis

This thesis consists of eight technical chapters with the main contributions in the chapters 3, 5 and 8. In the following the content of all chapters is outlined

Chapter 2 begins with a comparison between radio frequency (RF) and infrared (IR) radiation. It continues with a short review of basic optical links and fundamentals of propagation in the optical wireless channel. Furthermore, a mathematical channel model for line of sight (LOS) and diffuse links is discussed. In the last section the noise sources of an optical channel is discussed.

Chapter 3 consists of a set of simulation model for optical wireless channel to determine delay spread and root-mean-square (RMS) delay.

Chapter 4 defines the opto-electrical components in the front-end of the system. The aim of this chapter is to determine the factors which limit the bandwidth of the system.

Chapter 5 discusses the characteristics of the new opto-electrical components available in the market. The aim of this chapter is to determine the possibility of increasing the bandwidth by means of applying these new components. It is included a simple measurement set up to verify the feasibility of supporting large bandwidth.

Chapter 6 briefly describes different digital modulation techniques and compares them in terms of power, bandwidth efficiency and bit error probability.

Chapter 7 describes the concept of multipath channel and introduces multicarrier modulation as a promising technique to handle multipath dispersion. A mathematical model of the Orthogonal Frequency Division Multiplexing (OFDM) is presented and it is followed by discussing the challenges in designing an OFDM system.

Chapter 8 focuses on theoretical calculation of the total transmission rate of the system considering single and multicarrier modulation schemes as discussed in previous chapters. Also, the link budget analysis of these approaches is compared.

Chapter 9 summarizes the main results and offers an outlook for future work.

2.

Indoor wireless infrared communication

This chapter discusses advantages and disadvantages of IR over RF. A short review of basic optical links and fundamentals of propagation in optical channels will be given. A mathematical model for evaluating the impulse response of the infrared channel with as many reflections as required will be discussed. In the last section, the noise source of an optical channel will be discussed as well.

Wireless infrared communication refers to the propagation of light waves in the near infrared band (0.75-1.4 μm wavelength). It has several advantages over RF as a medium for short range wireless communication. The capacity of RF is limited because of the restricted bandwidth. Indeed, RF links are subject to regulations and the spectrum licensing fee has to be paid. The most important advantage of wireless infrared links is the license free spectrum at optical frequencies. More importantly, infrared signals are confined to the same room in which it is generated and it makes the infrared a secure medium against eavesdropping. Another advantage is that infrared components are small and relatively inexpensive. Therefore, infrared wireless can provide a low cost, secure and high speed transmission link in various indoor environments [1] [2].

Although infrared provides a number of advantages, it also has disadvantages. One of the disadvantages is that communication from one room to another room requires the installation of infrared base stations for which an extensive wiring is needed to connect these base stations [3]. Line-of-sight (LOS) links may easily be blocked by persons and objects between the transmitter and the receiver. The range is limited because of significant path loss leading to the requirement of higher transmission power. The last one is the speed limitation of the opto-electronic components in the transmitter and receiver front ends which limits the bandwidth of the system [4]. General characteristics of radio and infrared indoor wireless links are compared in Table 2.1.

As a consequence, the RF and IR are complementary media that can be used in different applications. Radio is the most convenient medium for applications over long ranges and when high mobility, penetration through a wall and minimization in transmitter power consumption are necessary. Infrared links are more favored in short range and high data rate applications [2] [3].

Properties	Radio Frequency	Infrared Radiation
regulation	Yes	No
Security	Possible	High
RF interference	Yes	No
Technology cost	Variable	Low
Main noise source	Other Users	Ambient light
Coverage	Medium	Low
Mobility	Yes	Some Configuration links
Multipath dispersion	Yes	Some Configuration links
Multipath fading	Yes	No
Path loss	High	High
Bandwidth limitation	Regulatory	Detector/Preamplifier/diffuse channel

Table 2.1: Comparison between radio and infrared properties for indoor wireless communication

2.1 Infrared link configuration

Wireless optical links can be classified as Line-of-Sight (LOS) or Non-Line-of- Sight (NLOS) links and they can further be classified as directed and non-directed links, as shown in Figure 2.1. A directed link consists of a narrow beam transmitter and a narrow field-of-view receiver (FOV). Similarly, a non-directed link consists of a wide beam transmitter and a wide FOV receiver. In addition, a hybrid link consists of either a narrow beam transmitter and wide FOV receiver or a wide beam transmitter and a narrow FOV receiver.

In general, LOS links rely on the existence of an unobstructed path between transmitter and receiver. Directed LOS links make the most efficient use of power consumption because the signal energy is concentrated into a very narrow beam and it also experience minimum reception of ambient light noise. Furthermore, they don't suffer from multipath dispersion.

On the other hand, directed LOS links require careful alignment of transmitter and receiver leading to very small coverage area. The main drawbacks of this configuration are its inability to cope with broadcast communication modes, mobility of the receiver and interruption in transmission caused by shadowing. The first drawback is solved by using directed NLOS configurations. In a direct NLOS configuration, energy from the transmitter is re-radiated from a large reflector in every direction; therefore, some of this radiation may be received by narrow FOV receiver [1].

By replacing the narrow FOV receiver with wide FOV one in directed LOS, hybrid LOS is generated which the narrow beam width still creates a pointing problem and susceptibility to LOS blocking. In hybrid LOS, if energy from the narrow beam transmitter is re-radiated from a large reflector and some of this radiation is received by wide FOV receiver, it is referred to as NLOS-hybrid.

In order to increase the coverage area and support receiver mobility, non-directed LOS and NLOS (diffuse link) configurations were proposed [5]. In this thesis, none directed LOS is considered as

optical link configuration. In such link, LOS and diffuse signal components are simultaneously presented at the receiver. Non-direct LOS makes better use of signal power than the diffuse like, but it requires that the LOS path be uninterrupted. Diffuse links rely on the reflected paths from objects in a room and operate without LOS. Because a diffuse transmitter does not need to be aimed at the receiver, it provides a wide degree of mobility which is the most convenient configuration from the user point of view. Therefore, a diffuse link is very robust against shadowing and no tight alignment is required for users. On the other hand, a diffuse system suffers from very high signal attenuation, so a large optical transmitted power is required. In addition, multipath reflection in diffuse links can cause inter-symbol-interference (ISI) [2]. Besides, the received optical power in NLOS links depends on properties of the room such as size and reflection coefficients of reflectors as well as orientation angles of transmitter and receiver.

Table 2.2 summarizes the characteristics of directed LOS and diffuse configurations.

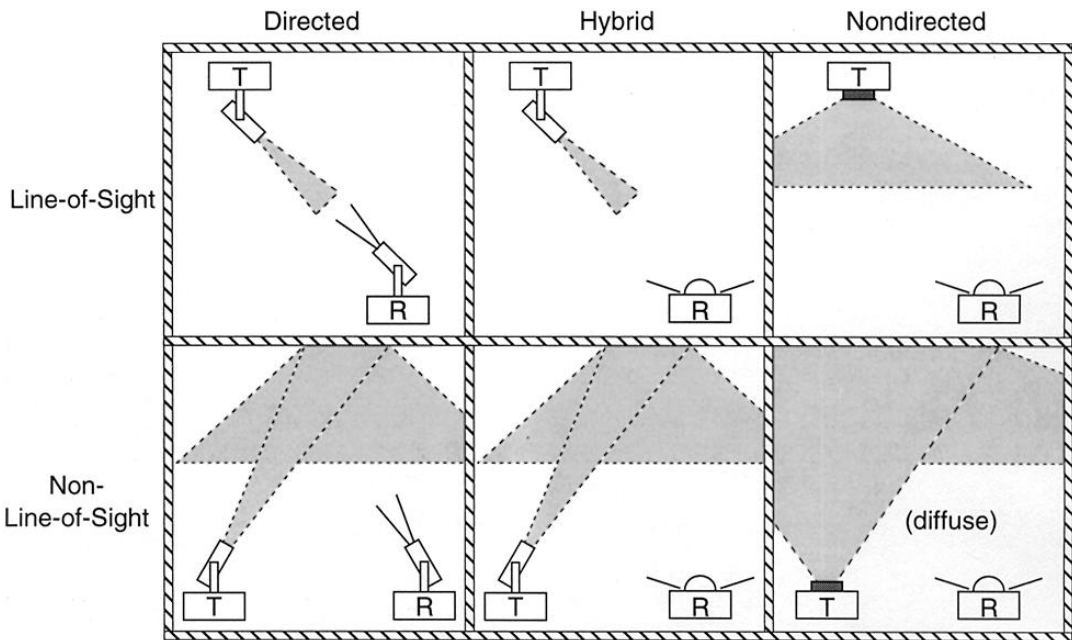


Figure 2.1: Configuration for wireless optical links [1]

Characteristic	Directed LOS Link	Diffuse Link
Data rate	High	Low-Moderate
Pointing required	Yes	No
Immunity to Blocking	Low	High
Mobility	Low	High
Complexity of Optics	Low	Low-Moderate
Ambient light Rejection	High	Low
Multipath Distortion	No	High
Path Loss	Low	High

Table 2.2: Comparison between wireless optical links [3]

In order to combine the mobility of the diffuse link and high speed capability of the LOS link, the multi-spot diffusing approach was proposed in [2]. In this approach, a diffuse transmitter is replaced by a quasi-diffuse transmitter which utilizes multiple narrow beams pointed in different directions which reduces the path loss. The reason is the narrow beams experience little path loss traveling from transmitter to receiver. Also, a single element receiver is replaced with an imaging light concentrator and a segmented photo-detector which can reduce received ambient light noise and multipath distortion [2].

2.2 Propagation in optical wireless channel

In optical communication, the most viable modulation is intensity modulation with direct detection (*IM/DD*) in which the information is modulated onto the intensity of the optical signal. Because of the intensity modulation, the channel input signal $X(t)$ is instantaneous optical power and it must be positive. The average power of the transmitted optical signal is given by [3]

$$P_t = \lim_{T \rightarrow \infty} \frac{1}{2T} \int_{-T}^T X(t) dt \quad (2.1)$$

The optical signals between transmitter and receiver in a wireless non-directed NLOS channel travel different paths and experience path loss and propagation delay. If a signal is transmitted over a multipath channel then the received signal is the superposition of attenuated and delayed copies of the transmitted signal which causes constructive and destructive interference of original signal [7].

The resulting effect of the multipath propagation of an optical signal is similar as observed for a RF signal. Consequently, multipath reflections create time dispersion of the received signal (multipath dispersion) and variation in amplitude of the received signal which is referred to as multipath fading.

One of the major differences between RF and IR systems is the size of the receiving antenna relative to the wavelength of the received signal. Typical photo-detector dimensions are thousand of the wavelength. Therefore, the total received power by a direct detection receiver may remain the same as the receiver changes its position by thousands of wavelength. In radio, as the receiver changes its position by a fraction of the wavelength, the channel properties change drastically [8]. The large detector area leads to efficient diversity which reduces the effect of multipath fading and simplifies the link design [3].

Multipath dispersion is, however, very much present in optical wireless channel. In the following section, the parameters that characterize propagation delay mechanism are presented.

2.2.1 Power delay profile

As it was said, a signal transmitted from a transmitter encounters multiple objects which generate reflected replicas of the transmitted signal and it is referred to as a multipath channel. This multipath channel is modelled by its impulse response $h(t)$ given by

$$h(t) = \sum_{i=1}^{M_{path}} a_i \delta(t - \tau_i) e^{j\varphi_i} \quad (2.2)$$

where t is the observation time at the receiver, $(t - \tau_i)$ is the application time of the impulse of the channel relative to t , M_{path} is the number of multipath components, a_i , τ_i and φ_i are amplitude, arrival time, and phase sequence of the i -th multipath component respectively and δ is the Dirac delta function.

The degree of multipath dispersion of a signal is measured by power delay profile. It represents distribution of transmitted power over different paths in time domain as seen in Figure 2.2. It is function of excess delay and calculated by

$$p_r(\tau) = \sum_{i=1}^{M_{path}} \bar{a}_i^2 \delta(t - \tau_i) \quad (2.3)$$

The density function of the power delay profile $p(\tau)$ is given by

$$p_\tau(\tau) = \frac{p(\tau_j)}{\sum_{i=1}^{M_{path}} p(\tau_j)} \quad (2.4)$$

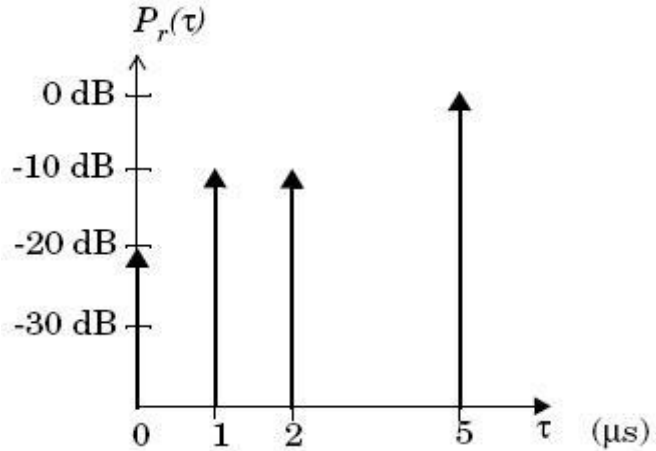


Figure 2.2: Example of power delay profile

2.2.2 Time delay spread

When a transmitted signal arrives at receiver through multipath propagation, it causes signal dispersion in time. There are some parameters which can quantify the multipath channel in time domain. The mean excess delay, RMS delay spread, and excess delay spread are multipath channel parameters that can be determined from a power delay profile and they are explained below

First-arrival delay (τ_0) is time delay corresponding to the arrival of the first transmitted signal at the receiver. It acts as a reference and any delay longer than this is called an excess delay.

Mean excess delay (τ_m) is the first moment of power delay profile with respect to the first delay.

Maximum excess delay (τ_{\max}) is an excess delay that is measured with respect to specific power level called the threshold of the signal. When the received signal is less than this threshold, it is not considered.

Root mean square (RMS) delay (τ_{RMS}) is square root of the second moment of the power delay profile. It is standard deviation about the mean excess delay.

RMS delay spread is a good measure of channel time's dispersion and shows an indication of nature of ISI in the received signal. It is expressed by the impulse response $h(t)$ and the multipath mean delay (τ_m) as

$$\tau_{RMS} = \left[\frac{\int (t - \tau_m)^2 h^2(t) dt}{\int h^2(t) dt} \right]^{1/2}, \quad \tau_m = \frac{\int t h^2(t) dt}{\int h^2(t) dt} \quad [s] \quad (2.5)$$

To avoid ISI, transmitted signal requires having a symbol period (T_s) that is large relative to RMS delay ($(T_s > \tau_{RMS})$). Conversely, if the symbol period is less than τ_{RMS} , the signal experience significant ISI. Thus, the maximum data rate of the system is limited by τ_{RMS} as $R_s = 1/10\tau_{RMS}$ where R_s is the symbol rate [9].

2.2.3 Coherence Bandwidth

Multipath dispersion can also be characterized in the frequency domain by coherence bandwidth (B_{coh}). Coherence bandwidth is the frequency range over which the frequency components of a signal experience correlated amplitude fading [9]. The relationship between B_{coh} and τ_{RMS} is given by

$$B_{coh} \approx \frac{1}{2\pi\tau_{RMS}} \quad [Hz] \quad (2.6)$$

Equivalently, to avoid ISI, the bandwidth of the signal must be much smaller than the coherence bandwidth ($B \ll B_{coh}$). Then the fading across the entire signal bandwidth is roughly equal

which is referred to as flat fading. On the other hand, if $B \gg B_{coh}$ then the amplitude values of different frequency components of a signal vary differently across the signal bandwidth which is referred to as frequency selectivity resulting to ISI [9].

2.2.4 Doppler Effect

For a fixed transmitter, receiver and reflectors, the optical channel impulse response is stationary. When these objects are moving relative to each other, then the frequency of the received signal is not the same as that at the source due to Doppler effect. It means when objects are approaching each other, the frequency of the received signal is higher and when they are moving away, it is lower than source.

Here, we ignore Doppler effect for the optical channel because the channel varies very slowly and it can be considered as time invariant [1], [3]. Therefore, if $X(t)$ is the instantaneous output power of the source, the received electrical current after detection in a noiseless multipath optical channel is given by

$$i(t) = R_p X(t) \otimes h(t) \quad (2.7)$$

where, \otimes indicates convolution and R_p [A/W] denotes the responsivity of the detector which is conversion factor at the receiver.

2.3 Optical wireless channel model

Many researchers have modelled the indoor infrared wireless channel to determine the delay spread and distribution of power throughout a room.

Gfeller *et al.* [5] introduced the idea of using infrared for indoor wireless communications. He studied various physical channel properties, namely, the reflection properties of several materials, bandwidth limitation due to multipath dispersion, ambient noise and distribution of diffuse optical radiation. In the paper, they suggested the Lambertian pattern as model for the reflections from the surface which will be explained in 2.3.1.

Barry *et al.* [1] proposed a general simulation method for evaluating characterization of the impulse response of an indoor optical channel. The model can compute the impulse response for as many reflections as required. Based on his model, the room is divided into numerous small reflecting elements. It is a recursive model so that to find the impulse response of the k^{th} reflections, the impulse response of $(k-1)^{\text{th}}$ reflections and LOS are required. One drawback of this method is its long simulation time.

Lopez-Hernandez *et al.* [10] proposed a novel algorithm called the “DUSTIN algorithm” for calculating the impulse response of the IR wireless indoor channels. The method is fast in computing the impulse response and it is split into three stages: initialization, wall processing and calculating of the photo diode response.

Lopez-Hernandez *et al.* [11] also developed a method to find the impulse response by using Monte Carlo analysis. It does not only evaluate the Lambertian but also specular reflections.

Carruthers *et al.* [12] described an iterative method for the estimation of the impulse response of the wireless infrared channels. This method can consider any order of reflections. Complex reflection environments with all types of obstructions, shadowing effects and related effects can be modeled. It can perform more accurately and efficiently than the recursive method used by Barry *et al* [1].

Cipriano *et al.* [13] developed a computationally efficient algorithm for simulation of the wireless infrared channel. Two new procedures, namely, Time Delay Agglutination and Time and Space Indexed Tables are defined to increase the efficiency of the simulation of the impulse response for the indoor wireless optical channel. The results presented in this paper show good agreement with those already published and verified experimentally [1] [8].

Large experimental measurements of indoor IR channel were performed at the University of Ottawa [8] over a 40 MHz band for many different configurations. They investigated impact of receiver rotation and shadowing on the properties of indoor infrared channels. The results demonstrate the effect of elevation angle of the receiver on path loss, correlation between the channel delay spread and path loss for LOS and diffuse configurations.

In this thesis, optical wireless channel model proposed by John Barry [1] is discussed and used for simulation because of good prediction of the channel properties. Other available methods are a more or less modified version of this model.

In general the impulse response of the non directed LOS channel consists of two components, discrete Dirac-pulse due to the LOS and a continuous signal due to contributions of diffuse reflections. Figure 2.3 illustrates a sketch of the channel impulse response model.

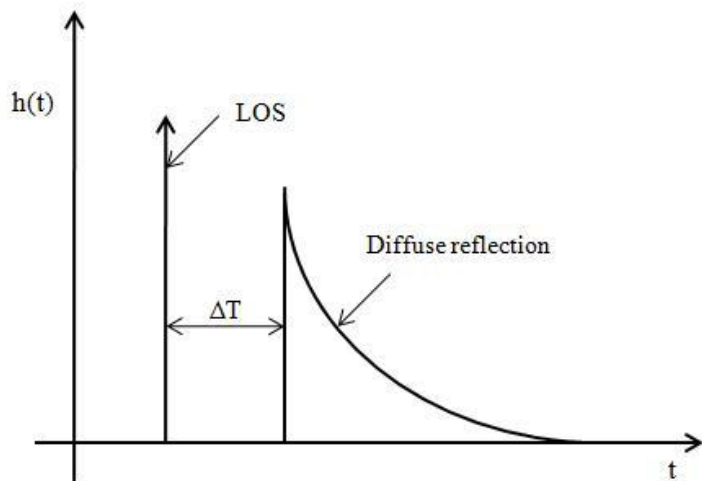


Figure2.3: Sketch of the impulse response

2.3.1 LOS component

The LOS impulse response is characterized by the geometric properties between transmitter and receiver such as transmitter radiation characteristic, distance and their orientation angles. The radiation pattern of the source is modelled approximately as a Lambertian radiation pattern

$$R(\phi) = \frac{n_L + 1}{2\pi} P_t \cos^{n_L}(\phi) \quad \text{for } \phi \in [-\frac{\pi}{2}, \frac{\pi}{2}] \quad (2.8)$$

where, $R(\phi)$ illustrates the radiation intensity in the direction ϕ , n_L is the Lambert radiation index and P_t is output optical power of the source.

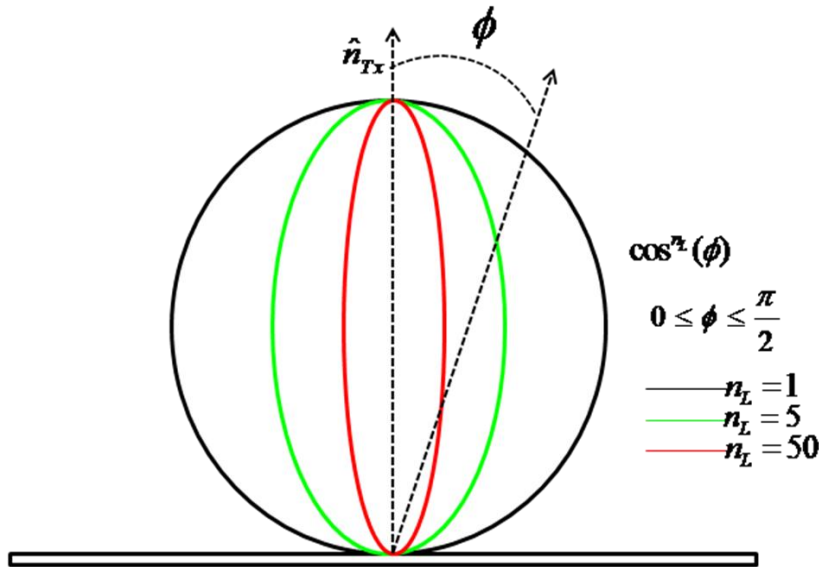


Figure 2.4: Normalized shape of the generalized Lambertian radiation pattern

The source or emitter is denoted by the following set of parameters $Tx = \{r_s, \hat{n}_{Tx}, n_L\}$ where r_s is its position and \hat{n}_{Tx} is its orientation. Similarly, a detector is denoted by four parameters $Rx = \{r_R, \hat{n}_{Rx}, A_{Rx}, FOV_{det}\}$ with an active area A_{Rx} , field of view angle (FOV_{det}) which is defined such that light whose angle of incidence is larger than the FOV_{det} cannot be detected, r_R is its position and \hat{n}_{Rx} is its orientation. Consider a receiver Rx placed at distance r from the source as shown in Figure 2.5. Then the LOS impulse response is represented by

$$h^{(0)}(t, Tx, Rx) = \frac{n_L + 1}{2\pi} \cos^n(\phi) \frac{A_{Rx} \cos(\psi)}{r^2} \cdot \text{rect} \cdot \delta(t - \frac{r}{c}) \quad (2.9)$$

ϕ is the angle between \hat{n}_{Tx} and $(r_R - r_s)$, ψ is the angle between \hat{n}_{Rx} and $(r_s - r_R)$, c is speed of light and the rect is rectangular function defined as

$$rect = \begin{cases} 1 & \text{for } \psi \leq FOV_{\text{det}} \\ 0 & \text{for } \psi \geq FOV_{\text{det}} \end{cases} \quad (2.10)$$

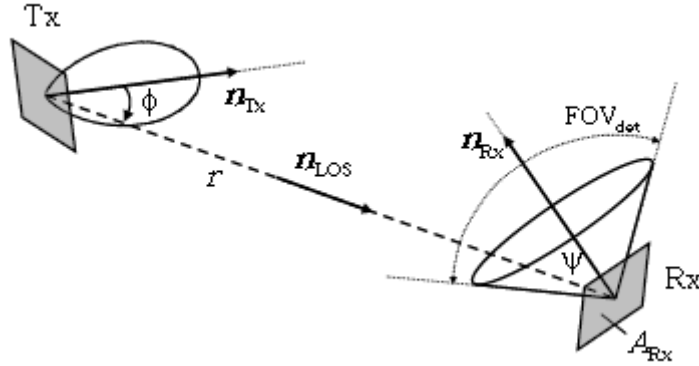


Figure 2.5: Geometry of source (Tx) and detector (Rx) without reflectors [7]

The Lambert radiation index n_L is related to the radiation half-angle by

$$\phi_{1/2} = \arccos \sqrt[n_L]{0.5} \quad (2.11)$$

For example, $\phi_{1/2} = 60^\circ$ corresponds to $n_L = 1$ and $\phi_{1/2} = 15^\circ$ corresponds to $n_L = 20$. Therefore, a higher Lambert index corresponds to narrower radiation beam width of the source. Also, a higher n_L implies an increase in DC gain of channel [3].

2.3.2 Diffuse component

Let us consider the effect of the multiple reflections from the reflecting surfaces within a room as shown in Figure 2.6. In a multipath channel, the emitted signal is reflected and absorbed by the room surfaces before collection by the detector. The surface reflectivity of a typical plaster walls and acoustical ceiling is in the range of 0.6 to 0.9 [3]. The radiation characteristics of building materials can be approximated as Lambertian reflectors.

So let's us considering a source Tx and receiver Rx in a room with reflecting surfaces in which light reaches the receiver after a number of reflections. To model the reflection of a surface with area dA and reflectivity ρ , first, the reflecting surface is considered as a receiver with area of dA , and then the received power (dP) by this reflector is calculated. Second, the reflecting surface is considered as a source that re-emits this power $P = \rho dP$ with Lambertian radiation pattern $n_L = 1$.

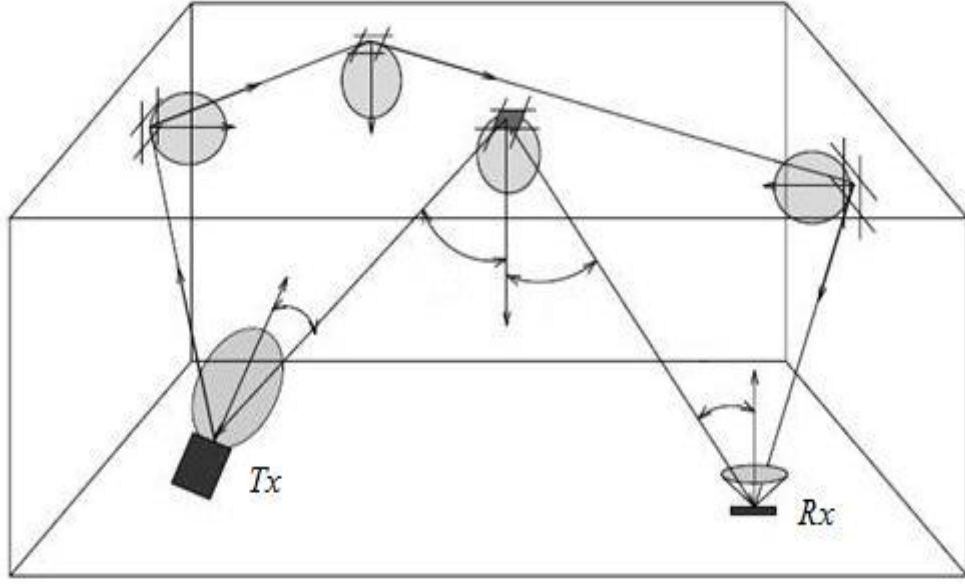


Figure2.6: Multiple reflections propagation model

Therefore, the impulse response of the light undergoing k reflections can be written as

$$h(t, Tx, Rx) = \sum_{k=0}^{\infty} h^k(t, Tx, Rx) \quad (2.12)$$

The LOS impulse response is represented by $h^{(0)}(t)$ while the higher order reflections are calculated by a recursive algorithm:

$$h^{(k)}(t, Tx, Rx) = \int_s h^{(0)}(t; Tx, \{r_p, \hat{n}_{ref}, FOV_{ref}, dA\}) \otimes h^{k-1}(t; \{r_p, \hat{n}_{ref}, n_L = 1\}, Rx) \quad (2.13)$$

where, \hat{n}_{ref} is orientation vector of the reflecting surface at position r_p and integration is performed over the surface (s) of all reflectors. Substituting Eq.2.9 in Eq.2.13 and performing convolution result in:

$$h^{(k)}(t, Tx, Rx) = \frac{n_L + 1}{2\pi} \int_s \frac{\rho \cos(\psi) \cos^{n_L}(\phi)}{r^2} \cdot rect \cdot h^{k-1}(t - r/c; \{r_p, \hat{n}_{ref}, n_L = 1\}, Rx) dA \quad (2.14)$$

2.4 Noise sources in optical wireless channel

In infrared systems, the noise is generated by internal and external components at the receiver front end. The internal noise is generated in the receiver is from front-end electronic components such as resistor, diode and transistor which referred to as thermal noise. The important source of noise in the optical channel is the background light referred to as external source of noise. Generally, the background light is presented as a mixture of light coming from the sun, incandescent and fluorescent lighting. The spectral power density of different sources including Light Emitting diode (LED), photo-detector (PD) and laser diode (LD) are shown in Figure 2.7.

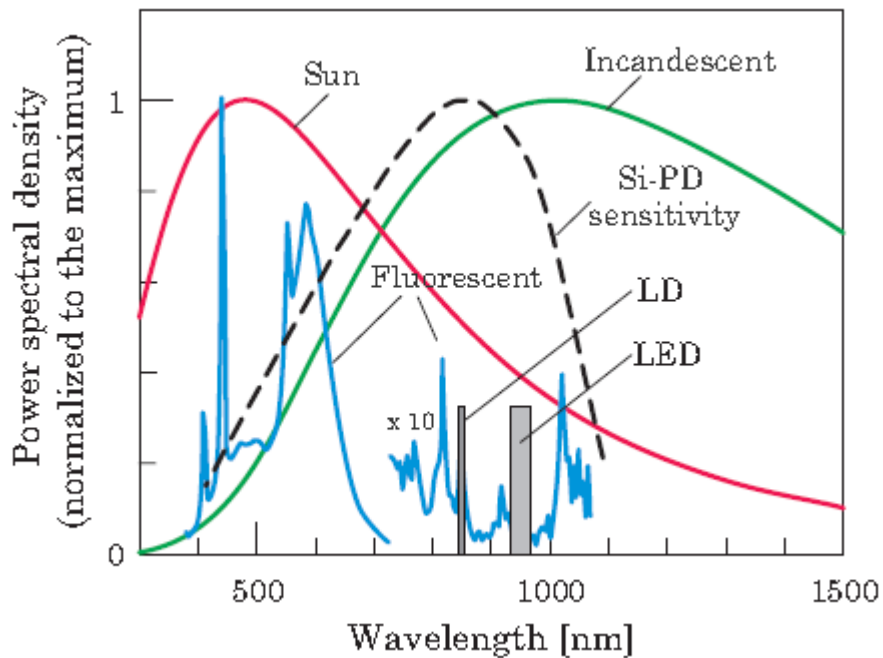


Figure2.7: Optical power spectra of common ambient infrared sources[7]

The natural light coming from sun is practically stationary whereas the light produced by artificial sources exhibits fast fluctuations in time. Hence, both natural and artificial sources produce a certain amount of background optical power impinging to the photo-detector. Because of this background optical power, a high level of shot noise current is generated in the photo-detector and increases the noise floor and decreases the sensitivity of an optical receiver. In addition, fluorescent artificial sources generate interference at frequencies of hundreds of kilohertz [7]. The shot noise is essentially white Gaussian noise, given by

$$I_{sn} = 2qR_p P_n, \quad (A) \quad (2.15)$$

where, $q = 1.6 \cdot 10^{-19} [\text{As}]$ denotes the electron charge, P_n is the ambient light power (W) and R_p is (A/w) responsivity of photo-detector.

In order to suppress the background noise, it is desired to use a narrow beam detector and day light filter before detection. The use of an optical filter reduces the amount of undesirable optical power producing shot noise at the receiver. It also provides an efficient reduction in the interference generated by artificial lighting. Therefore, the actual average photocurrent coming from background radiation depends on the receiver design [14] [15]. As mentioned, apart from shot noise, there is thermal noise which also contributes to the link performance degradation. The level of thermal noise depends on the receiver preamplifier circuit design. A more detailed analysis of thermal noise is given in Chapter 4 where the receiver front-end is discussed.

3.

Simulation model for the indoor infrared channel

In this chapter a simulation model is described to determine the delay spread and RMS delay spread of the optical channel in a room of arbitrary dimension. The investigation shows that the optical wireless channel varies for different scenarios and first order reflections have the most effect on the characteristics of the channel.

As it is mentioned in chapter 2, a simulation model of the indoor infrared channel has been introduced by Gfeller *et al* [5]. Barry *et al* [1] presented a general computer simulation method for infrared channel characterization. In this thesis, based on the mathematical model introduced in chapter 2, we present a recursive method in order to calculate the channel delay spread of an arbitrary room with Lambertian reflectors as well as channel path loss. This method can account for multiple reflections of the first and second order which evaluates the effect of multipath dispersion. It can be enhanced for any order of reflections but as we will see, considering first and second order reflections is sufficient.

This simulation model can benefit significantly the system design since the delay spread and RMS delay spread can be calculated from the impulse response by Eq. (2.5). In future investigations, it is necessary to verify the accuracy of this simulation model with experimental measurement of the optical multipath channel.

In the following sections we describe the recursive algorithm and three different scenarios that have been simulated. The first scenario is to consider a single reflection channel with only one source, and then multiple reflections channel with one source. The last scenario is to model the single reflection channel with four sources installed in the room.

3.1 Channel simulation model

Given a source and receiver with vectors Tx and Rx as defined in chapter 2 in a room with reflectors, light can reach a detector after any number of reflections. The reflectors are assumed to be ideal Lambertian because the experimental measurements have shown that many materials are well approximated as Lambertian reflectors [1]. To be reminded, the radiation intensity pattern of a reflector is given by Eq. (2.8). Eq. (2.12) is the major theoretical approach on which the simulation model is based to find the k -bounce impulse response.

To implement the integral in Eq. (2.12), the reflecting surfaces are subdivided into small reflecting elements (E_i) with area of ΔA . Therefore, the impulse response can be written as a summation with

$$h^{(k)}(t, Tx, Rx) = \frac{n_L + 1}{2\pi} \sum_{i=1}^{N_e} \frac{\rho_i \cos(\psi) \cos^{n_L}(\phi)}{r^2} rect \cdot h^{k-1}(t - r/c; \{r_p, \hat{n}_{ref}, n_L = 1\}, Rx) \Delta A \quad (3.1)$$

where i represents the i -th reflecting element and N_e is total number of reflecting elements.

The flowchart which implements this procedure is shown in Figure 3.1. In general, the required input parameters are in terms of transmitter and receiver vectors as explained in 2.3.1, transmitted optical power (P_t), N_e reflecting elements, room size (A_{room}) and reflectivity (ρ) of walls. Walls of the room are subdivided into a large set of reflectors with very small areas ΔA . LOS received power and its arrival time is calculated. To implement Eq. (3.1) to determine diffuse received power, two computations are performed where one computation is defined as the calculation of differential power and delay from a source to a reflecting element and the second computation is defined as calculation of the received power and delay from the reflecting element to the detector. The received power and delay of different paths are collected and by searching through the arrival times of the signal, the maximum and minimum arrival times are determined. The first arrival delay corresponds to the LOS received signal and in order to calculate received power via the reflections, continuous function of time observed up to the maximum arrival time is subdivided into the bins with width of Δt and the power received within each time bin is sum up.

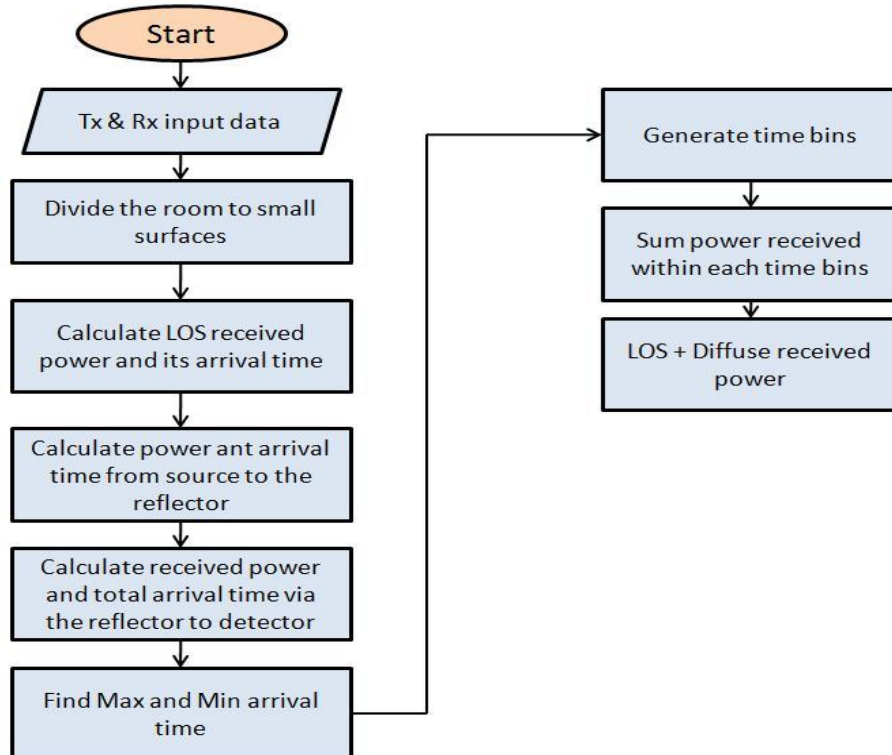


Figure 3.1: Algorithm implemented to simulate impulse response of an infrared channel

3.2 Description of room and configuration

The simulation is performed for an empty room with sizes of $65 \times 40 \times 4 \text{ m}^3$ as pictured in Figure 3.2. The selection of the room size is based on existing system deployments for which the system is capable of covering an area of 2600m^2 . However; the model can be adjusted for other rooms in an uncomplicated manner.

In this room, the walls are assumed to have a reflectivity of $\rho=0.7$ and they are subdivided into a large number of small surfaces with area of $\Delta A=1\text{m}^2$. As seen, the area of a reflecting surface is considered quite large in order to reduce the run time of the simulation. It is possible to make the area smaller and increase the number of reflecting elements but it only improves the resolution of the channel model and does not significantly impact the delay spread of the channel. The elevation angle is defined with respect to the horizontal plane so that the source pointing down has an elevation angle of -45° and the receiver pointing straight up has an elevation of 90° . The azimuth angle at position r_p is defined as the angle between the x axis and the projection of r_p onto the x - y plane so that y has an azimuth of 90° . The source and detector have azimuth angles of 0° .

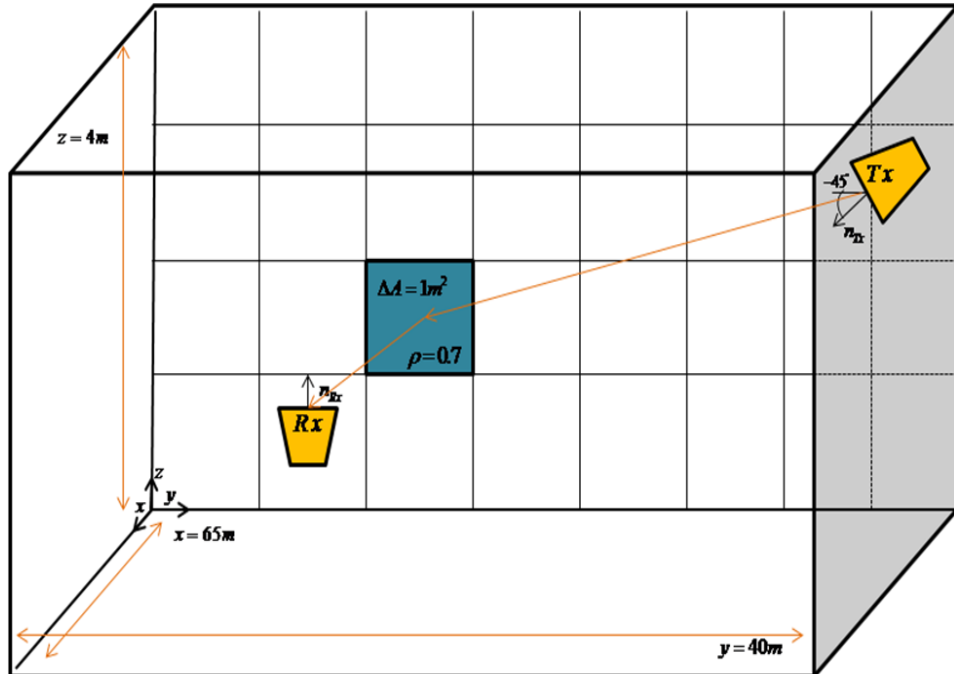


Figure 3.2: Communication scenario

The total transmitted optical power is 25W and the area of the receiver is considered $A_{Rx}=31.5\text{mm}^2$ which is the area of the current receiver. As seen from Figure 3.3, the transmitter is located at position (0m, 20m, 4m) and the receiver is located in 24 different positions as marked with blue circles. For all these points the height of the receiver remains unchanged and is placed 1m above the floor.

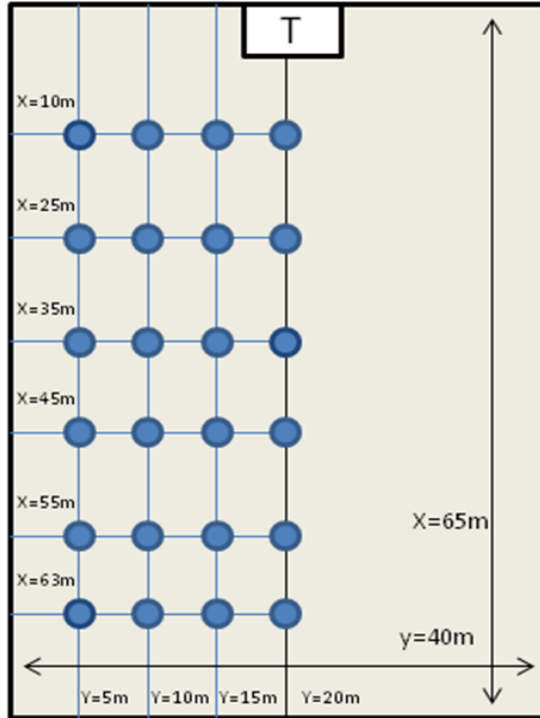


Figure 3.3: Upper perspective of an empty room with several positions for receiver

3.3 Simulation result of the single reflection model

The propagation of IR signals in this room is based on LOS and diffuse configurations. A diffuse configuration is based on a single reflection of the emitted signal. The model allows evaluating the effect of the reflection on the channel propagation loss and the signal propagation delay.

Figure 3.4 illustrates the geometry to obtain the single reflection propagation model considering only 3 walls as reflecting surfaces. In this model, the ceiling, floor and the wall behind transmitter are not considered as reflecting surfaces. Because of the orientation angle of transmitter (elevation angle = -45°), the ceiling and the wall behind transmitter don't have good reflection characteristics. In addition, it is assumed that the floor is covered with material which has very low reflectivity.

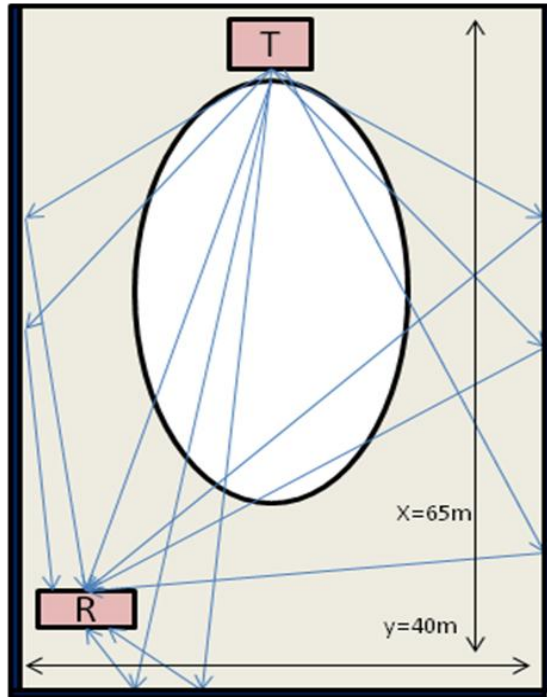


Figure 3.4: Upper perspective of a room for single reflection propagation model

In Figures 3.5 and 3.6 an illustrations of the impulse response are given when the receiver is located at positions (63m, 5m, 1m) and (63m, 20m, 1m). In this case, the distance between transmitter and receiver becomes very large and little optical power is collected.

The first point on the plots indicates LOS received power which is about -60dBm at a delay of 216ns in the first plot. It is interesting to be noted that the power received via reflections is more than LOS power at arrival time of 236ns. As seen, for arrivals afterwards, there is an exponentially decay in the power.

The same behavior is seen when the receiver is moved to the middle of the room at position (63m, 20m, 1m). The LOS received power slightly increases and, due to the location of the receiver, the excess delay is shorter compared to the first plot.

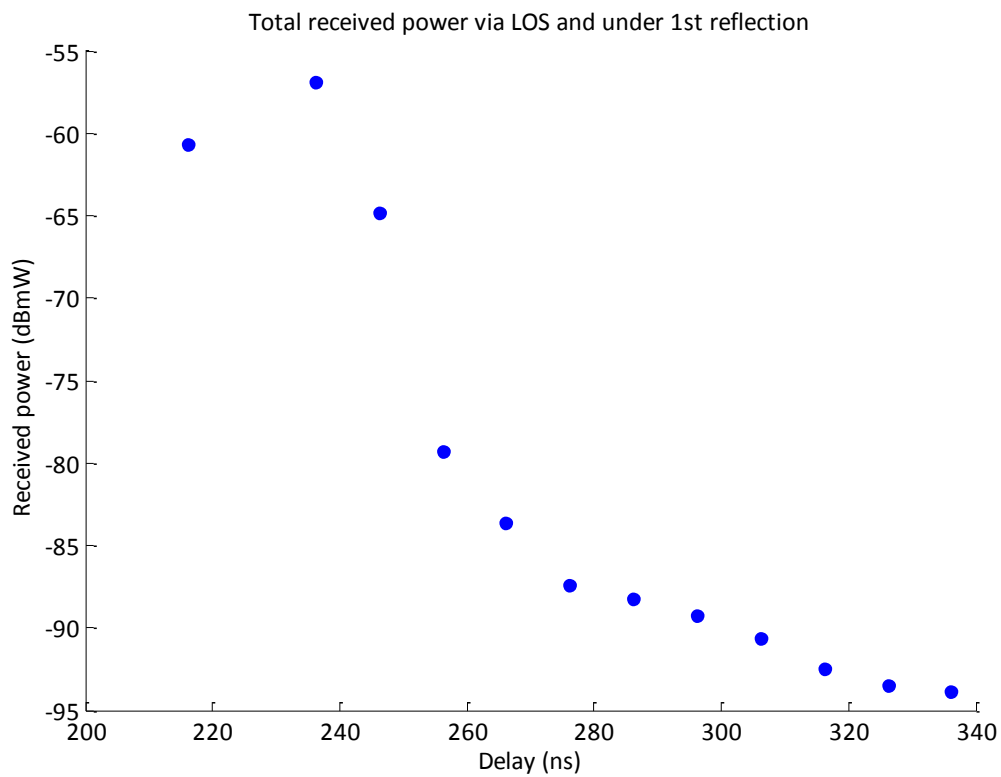


Figure 3.5: Received power vs. time delay for receiver at position (63m, 5m, 1m)

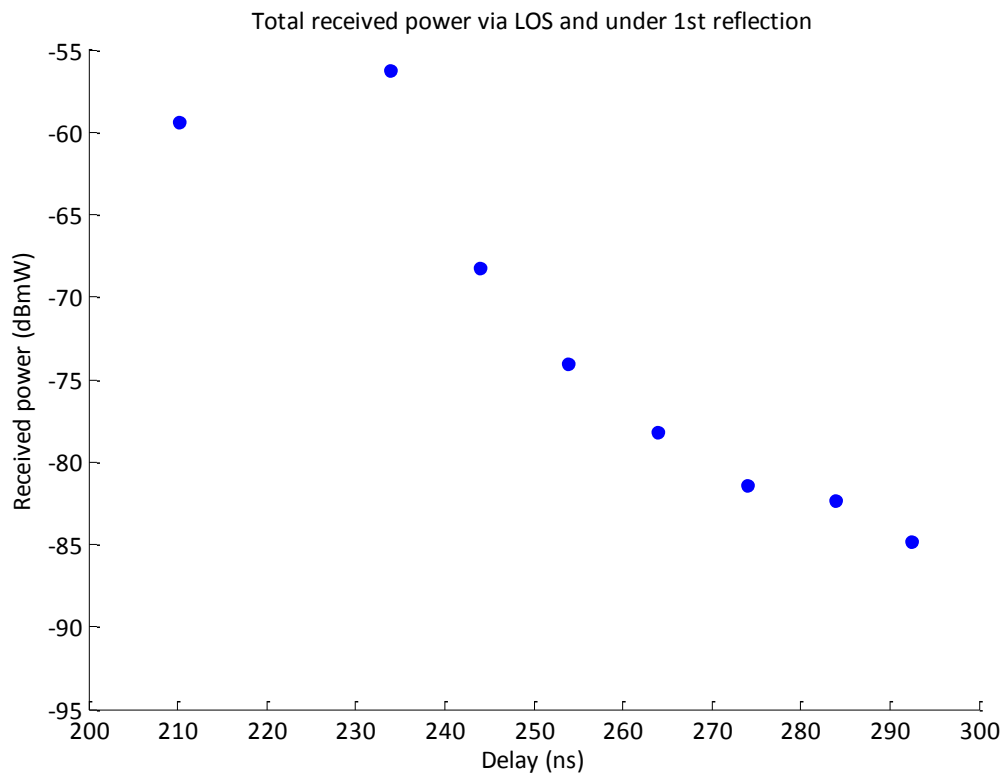


Figure 3.6: Received power vs. time delay for receiver at position (63m, 20m, 1m)

Figure 3.7 and 3.8 show the impulse responses of the channel when the receiver is located at positions (45m, 5m, 1m) and (45m, 20m, 1m). Clearly from the first plot, the LOS received power increases to -58dBm at a shorter delay of 158ns compared to the previous result. The LOS arrival time is shorter because the receiver is now close to the transmitter. The received power coming from the nearby reflectors decreases exponentially up to a time delay of 282ns. Afterwards, there are strong reflections with large excess delay at 292ns due to reflection from far away reflectors and result in a cluster of reflections.

This cluster contains multiple reflections from the same transmitted signal arriving at the receiver with different time delay and with different amplitudes, but from the same general direction. Here since the receiver is almost in the middle of the room, the reflecting element located at position $x = 65\text{m}$ on the back wall cause strong reflections with large excess delay because of their good orientation angles with respect to the transmitter. In addition, the larger the room being modeled the more clusters appear in the model resulting in a large RMS delay spread.

In Figure 3.8, the receiver moves to the middle of the room and the effect of LOS dominates any reflection paths. LOS received power is about -54dBm at a delay of 150ns. The same clustering effect also occurs here; however excess time delay is limited to 320ns which is less compared to the situation that the receiver is at left side of the room.

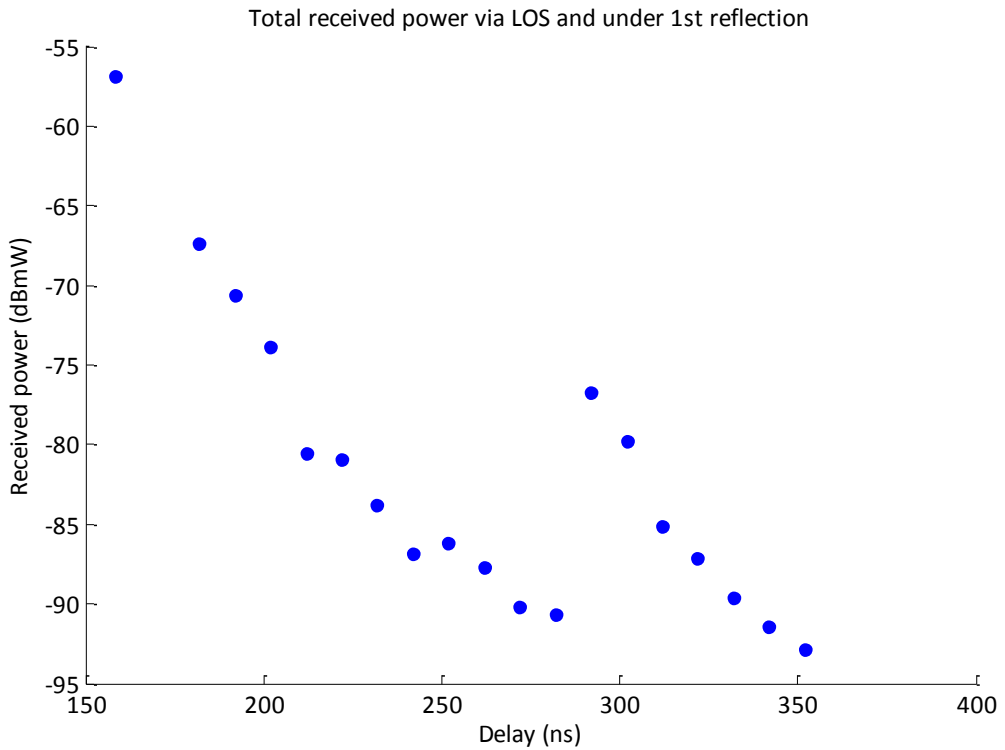


Figure 3.7: Received power vs. time delay for receiver at position (45m, 5m, 1m)

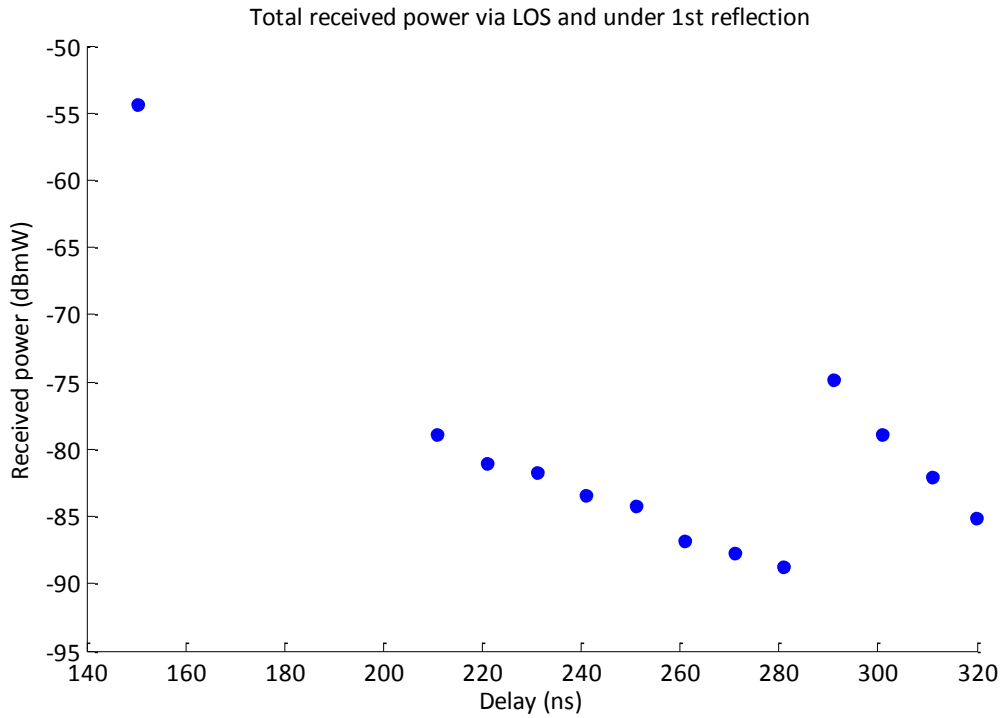


Figure 3.8: Received power vs. time delay for receiver at position (45m, 20m, 1m)

The last two plots in Figures 3.9 and 3.10 show the impulse response with the receiver at positions (10m, 5m, 1m) and (10m, 20m, 1m). Comparing the received power in Figures 3.5 and 3.9, we see that LOS received power are more less the same; however the received power coming from reflection is less than that shown in Figure 3.5. In addition, excess delay increases to 450ns because the receiver is now very close to the transmitter.

From Figure 3.10, it is seen that because transmitter and receiver are exactly directed to each other at a very short distance, LOS received power is significantly stronger than diffuse components.

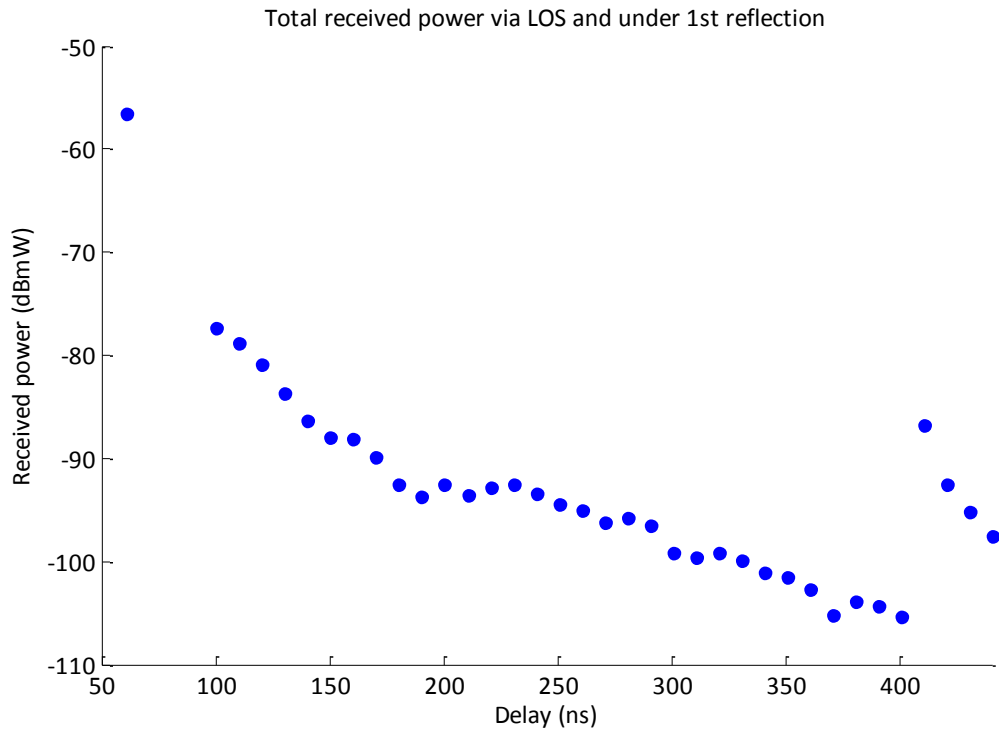


Figure 3.9: Received power vs. time delay for receiver at position (10m, 5m, 1m)

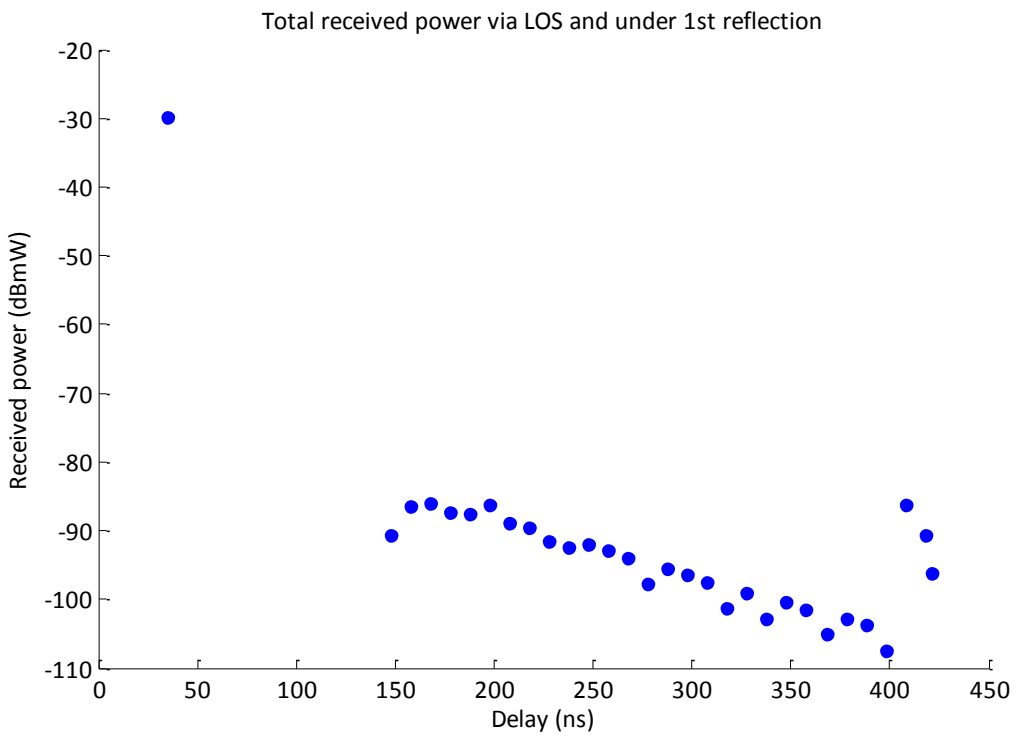


Figure 3.10: Received power vs. time delay for receiver at position (10m, 20m, 1m)

3.4 Simulation result of the multiple reflections model

In this model, room, transmitter and receiver configurations remain the same and the only new consideration is that also second order reflections are included in the detected signal. In this model, all the walls including the ceiling and the wall behind transmitter are taken as reflectors but the floor is not considered.

The impulse response of only three receiver positions is represented here to evaluate the effect of second order reflections. It has to be mentioned that we limited the number of second reflections such that the computation can be performed in a reasonable amount of time. In that sense, the following scenario as shown in Figure 3.11 is defined. The same algorithm shown in Figure 3.1 is applied to calculate the received power after a single reflection. Besides that, two walls remarked with the green rectangular are considered for second order reflection so that the emitted power from the green reflectors is reflected again from ceiling and other reflectors and then received by the detector.

Figure 3.12, 3.13 and 3.14 shows the power distribution vs. time delay considering second order reflections when the receiver is located at positions (63m, 5m, 1m), (45m, 5m, 1m) and (10m, 5m, 1m). It is observed that the excess delay becomes very large due to the large signal dispersion. In addition, because 2nd order reflected signals travel a long distance to reach the receiver, the received power is very low. Therefore, they don't influence strongly received power from single reflections. The tail of the impulse response appears due the second order reflections from far reflector which carry only little power.

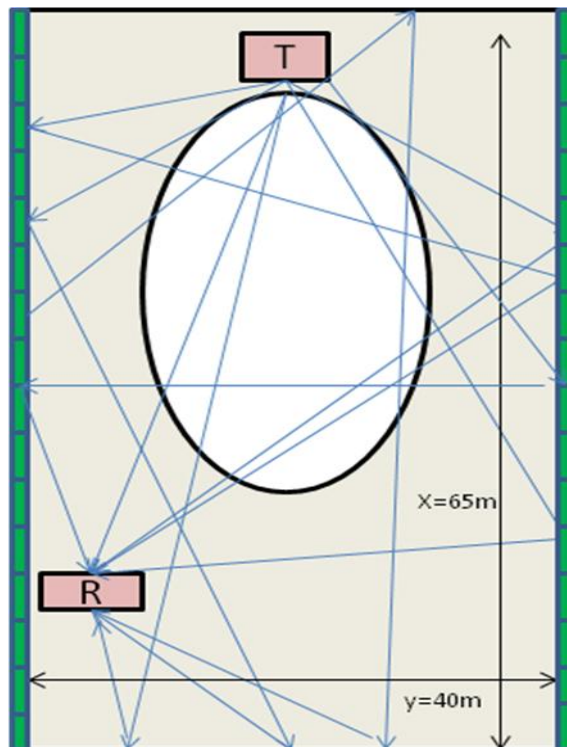


Figure 3.11: Upper perspective of a room with multiple reflection propagation

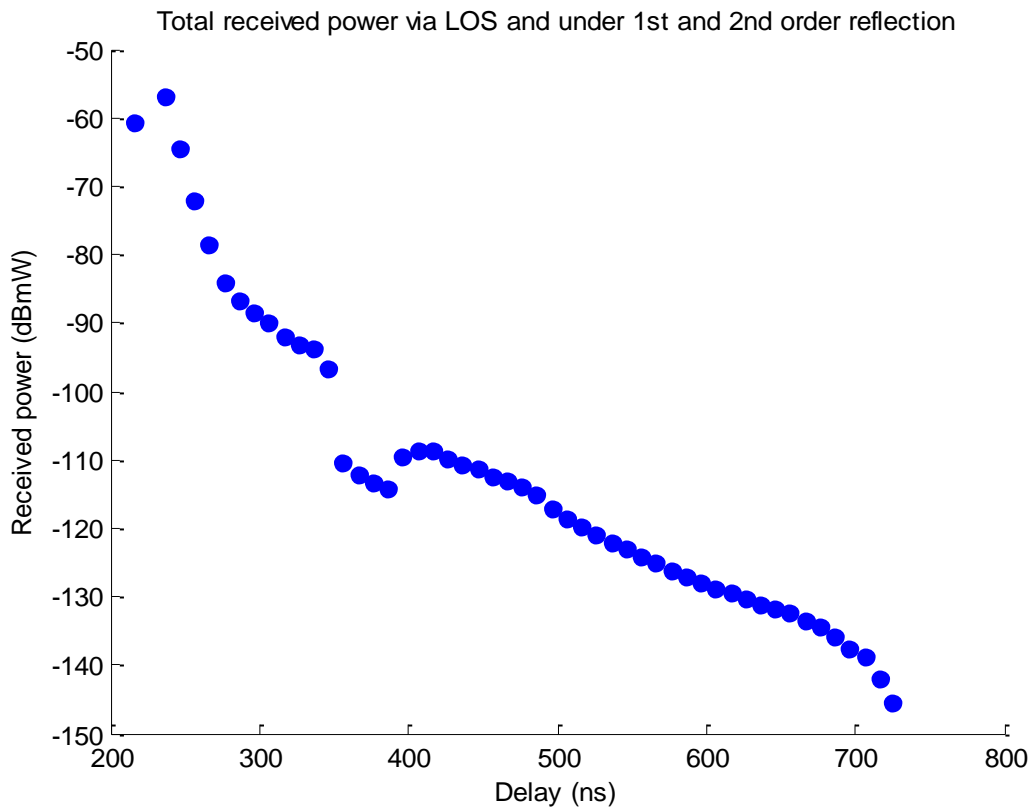


Figure 3.12: Received power vs. time delay for receiver at position (63m, 5m, 1m)

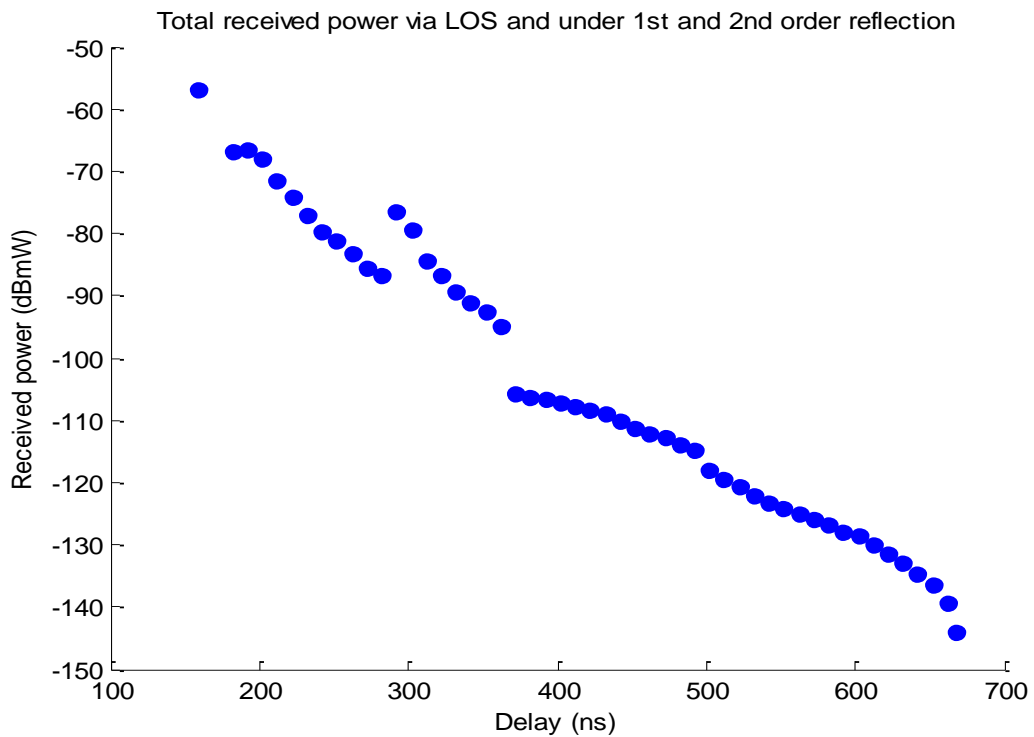


Figure 3.13: Received power vs. time delay for receiver at position (45m, 5m, 1m)

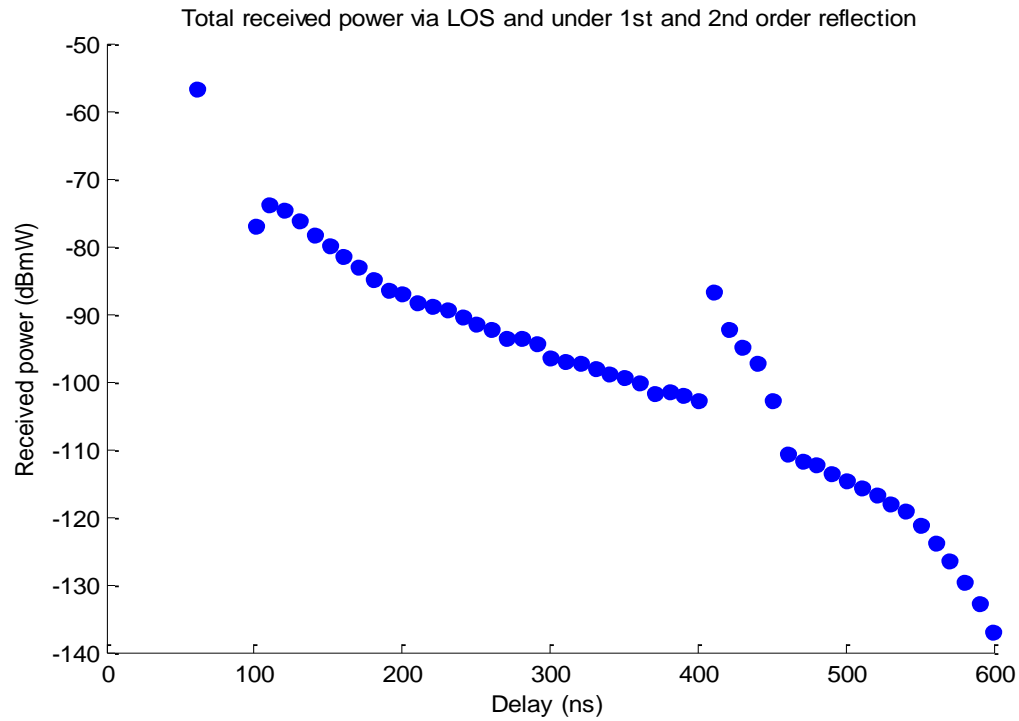


Figure 3.14: Received power vs. time delay for receiver at position (10m,5m,1m)

3.5 Simulation result of single reflection model with four radiators

In most cases, more than one source is used in a conferencing hall so that the whole room can be covered. Therefore, let's consider configurations with multiple sources. First we assume that the four radiators are positioned on the same wall as shown in Figure 3.15 (a) and in a second configuration Figure 3.15(b) they are positioned in the four corners of the room. We only consider one selected position for the receiver as shown with the red point at (63m, 5m, 1m). The power distribution vs. time delay is represented in the following graphs for these two configurations

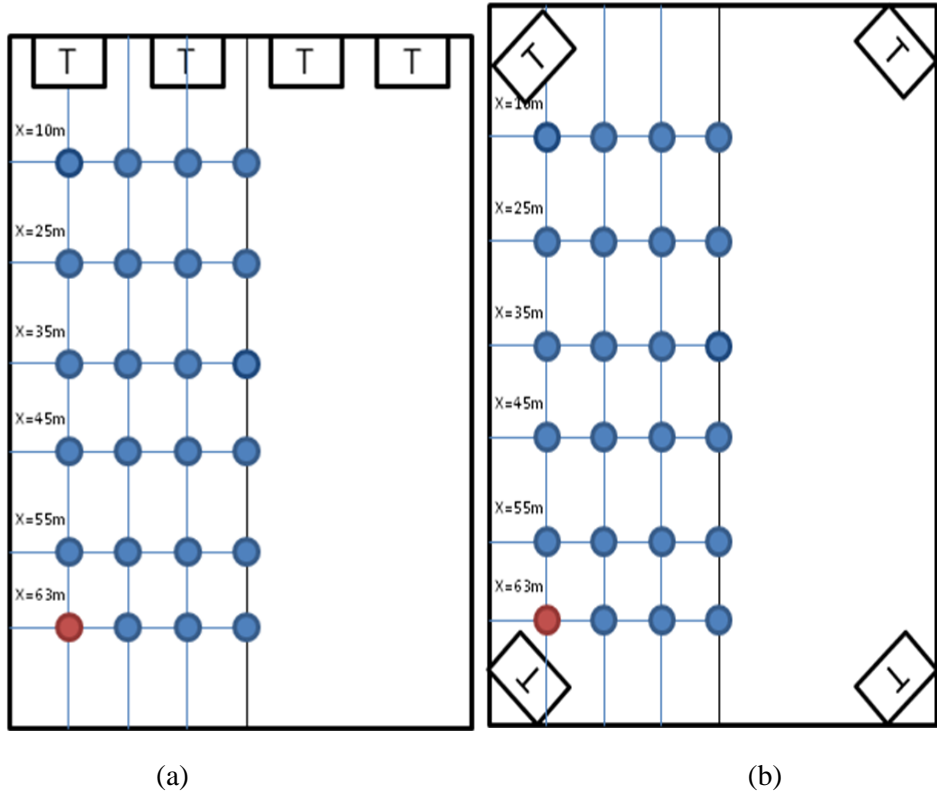


Figure 3.15: Two configurations of four radiators in the room

Figure 3.16 shows the received power vs. the excess delay for the first configuration (a). The first four points on the graph belong to the LOS received power of the four radiators which arrive with about the same delay. Following that there is an exponential decay of power due to diffuse components which arrive at the receiver. A large excess delay is also generated from the signal dispersion.

Figure 3.17 represents the power distribution for the second configuration and the same receiver position. The first point is the LOS received power of the transmitter in the vicinity of the receiver and three other LOS received powers arrive after that. Because of the orientation angle of the transmitter there is little received power at a delay about 150ns due to the reflection from very close reflectors to the transmitter. The amount of the power that is arrived at a large delay is between -70dBm and -100dBm which are coming from far away reflectors. Since there are four radiators on each corner of the room, it is obvious that the level of received power does not decrease significantly for larger delay.

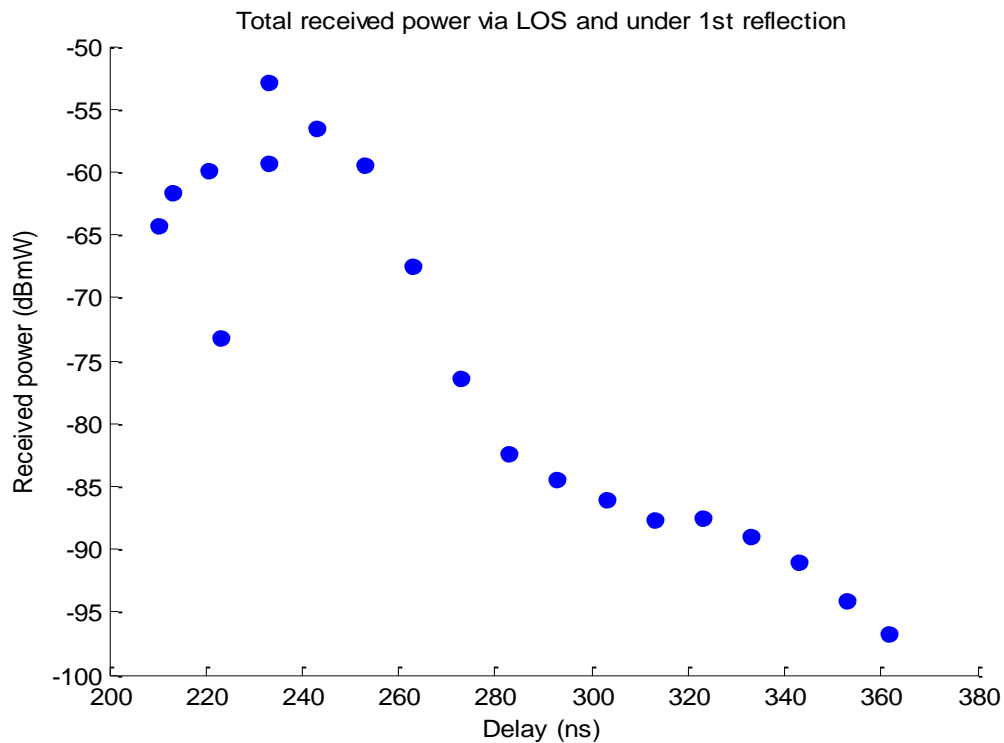


Figure 3.16: Received power vs. delay for the receiver shown in first conjunction

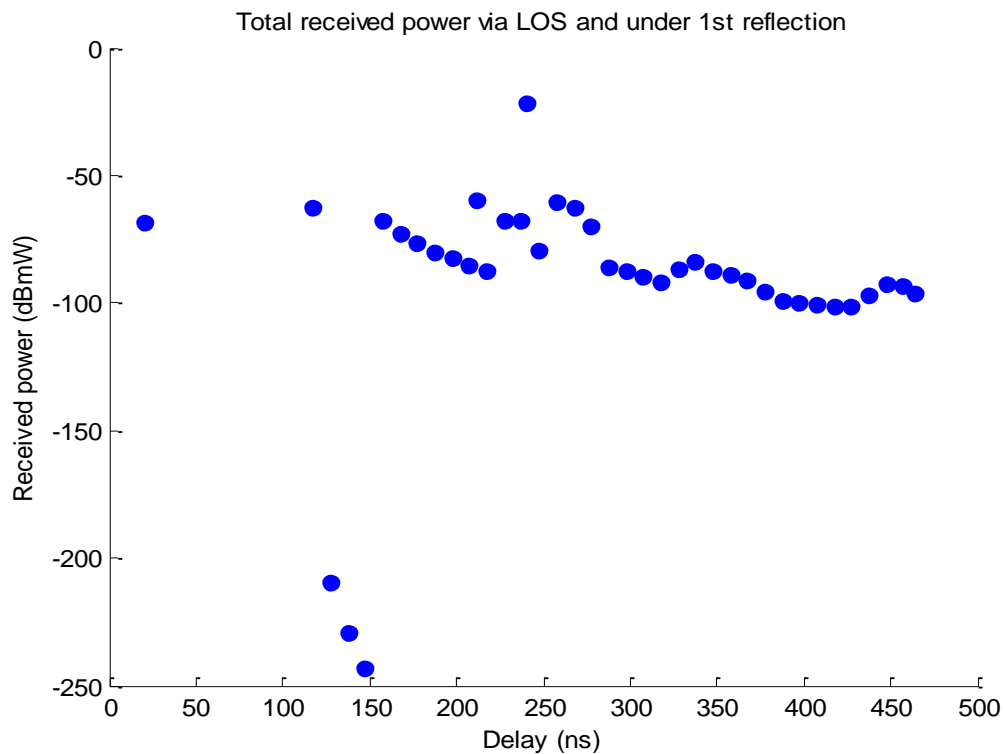


Figure 3.17: Received power vs. delay for the receiver shown in second configuration

3.6 Calculation of delay spread and RMS delay

The importance of calculating delay spread and RMS delay has been discussed in detail in chapter 2. The channel delay spread qualifies the multipath channel in the time domain and RMS delay limits the maximum symbol rate of the system. Therefore, in this section, we are going to find these two important parameters which affect the choice of applying multicarrier or single carrier modulation for the system.

The maximum excess delay is measured with respect to the power level of -30dB and -40dB below the first received signal. When the received signal is less than this threshold, it is not considered. Furthermore, if there is a LOS path between transmitter and receiver it is considered as the first arrival component but in a worse case, it is assumed that the LOS is blocked.

Therefore, in the following graphs, the channel delay spread with -30dB and -40dB thresholds and RMS delay are presented based on the single and multiple reflections model. Also the assumption of blocked LOS is considered.

Figures 3.18 and 3.19 show the distribution of the delay spread with -30dB and -40dB threshold respectively, when the receiver is placed in 24 different positions used in the single reflection model. The horizontal axis represents receiver positions such that the position 24 is when the detector is too close to the transmitter. These Figures also show that the delay spread of a NLOS channel is larger than a LOS channel. It is because the difference between first arrival component and the -30dB and -40dB ones increase in NLOS channel.

In both Figures, as the receiver is close to the transmitter, there is a rise in the delay spread. In the worst case when the receiver is located at position (10m, 5m, 1m) the maximum delay spread is 350ns. However, there is an exception in graph 3.17 but it can be neglected.

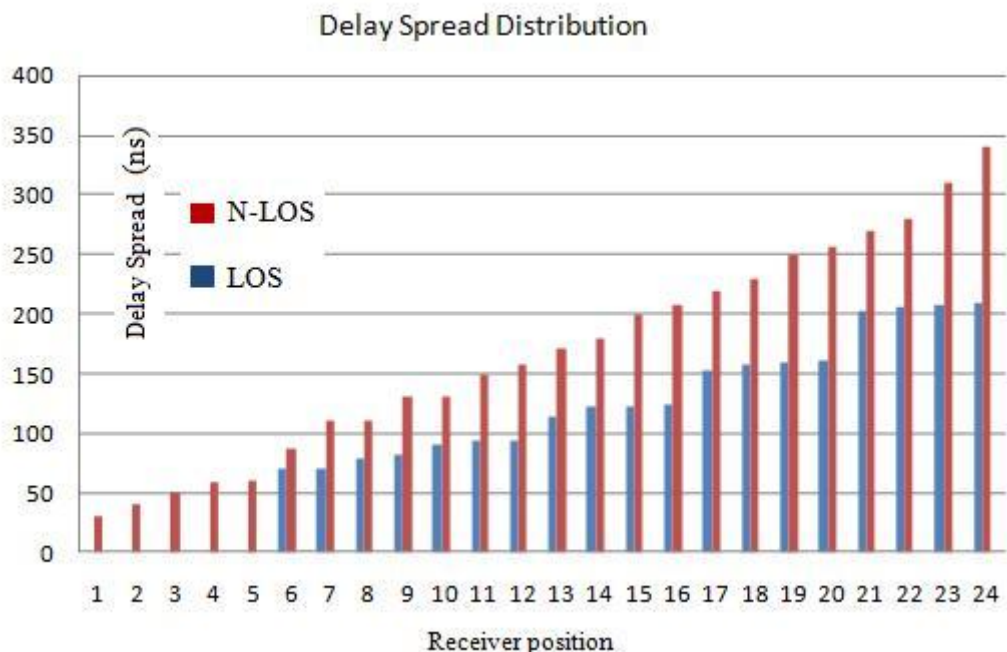


Figure 3.18: 30dB delay spread with LOS and N-LOS in single reflection channel model

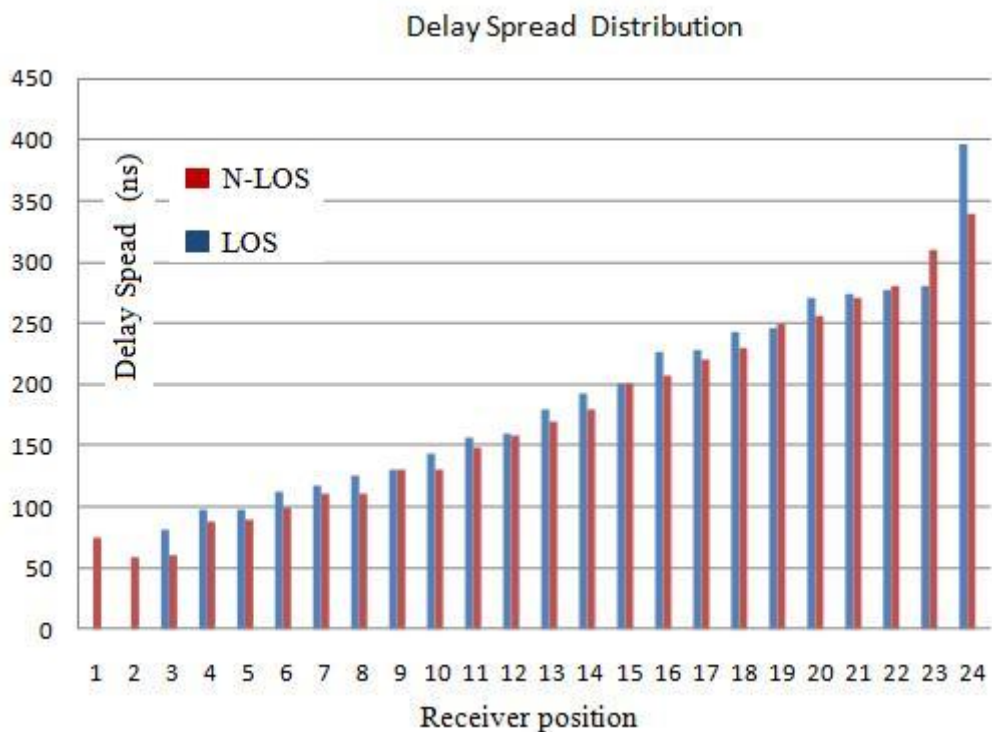


Figure 3.19: 40dB delay spread with LOS and N-LOS in single reflection channel model

Figure 3.20 illustrates the RMS delay of LOS and NLOS single reflection channel model. Clearly, the RMS delay of NLOS channel (red bars) is significantly greater than that of LOS (blue bars). The maximum RMS delay is about 90ns when the receiver is placed at the position closer to the transmitter because of more reflection paths.

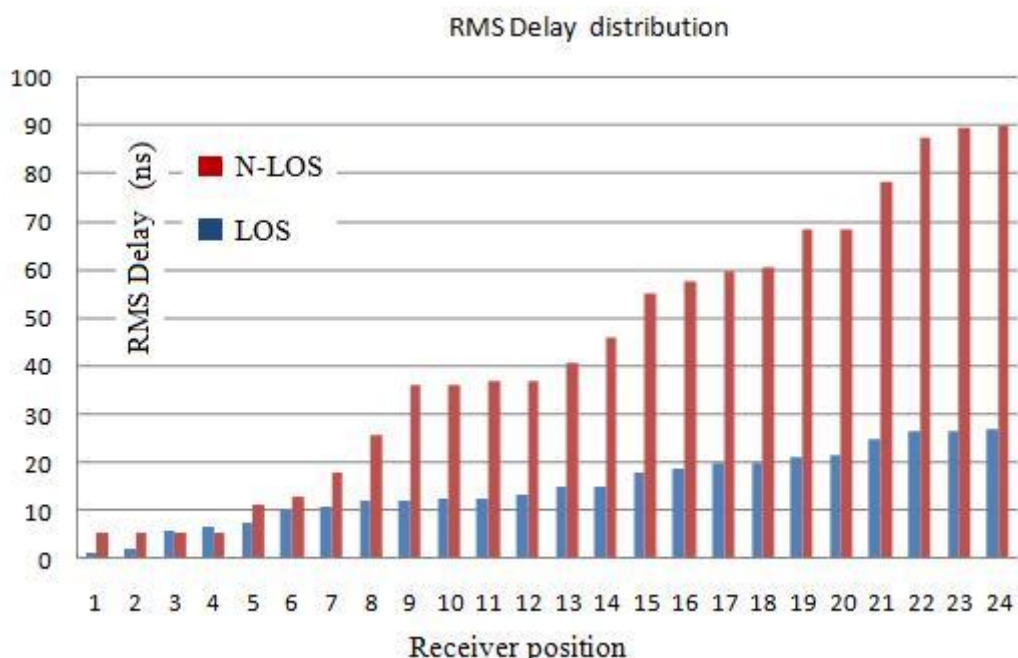


Figure 3.20: RMS delay spread with LOS and N-LOS in single reflection channel model

In Figure 3.21 and 3.22, the delay spread of the multiple reflection channel model are shown for -30dB and -40B respectively. The same behavior as seen in single reflection model is formed in the following Figures. It is very interesting to be noted that considering second reflections don't influence the maximum delay spread. Maximum delay spread is about 350ns in both Figures.

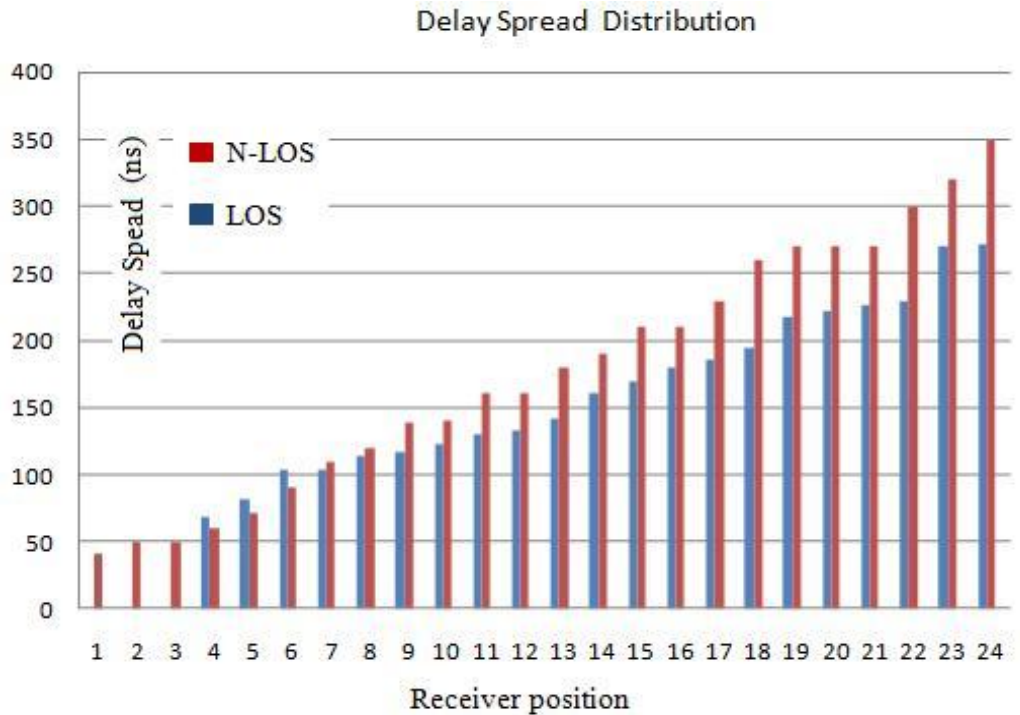


Figure 3.21: 30dB delay spread with LOS and N-LOS in multi reflections channel model

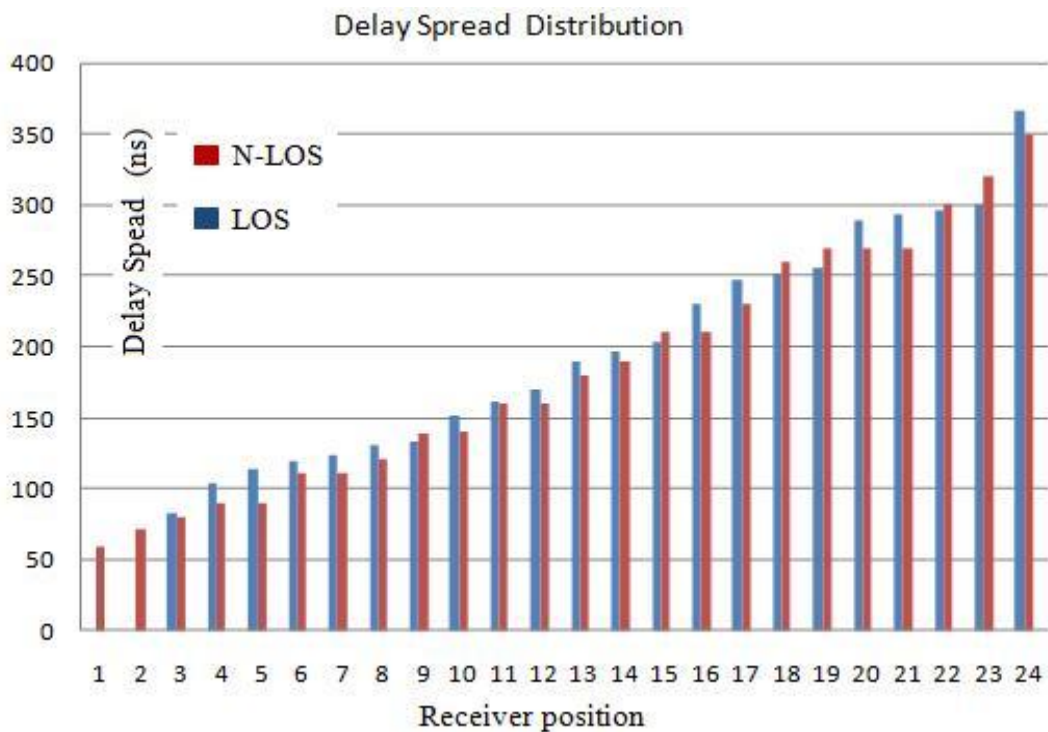


Figure 3.22: 40dB delay spread with LOS and N-LOS in multi reflections channel model

Finally, Figure 3.23 displays the RMS delay spread in the multiple reflections channel with considering LOS and NLOS paths. Again it is seen that the RMS delay is not influenced with considering second order reflections. It was seen from the power distribution graphs that higher order reflections only affect the amount of the power received.

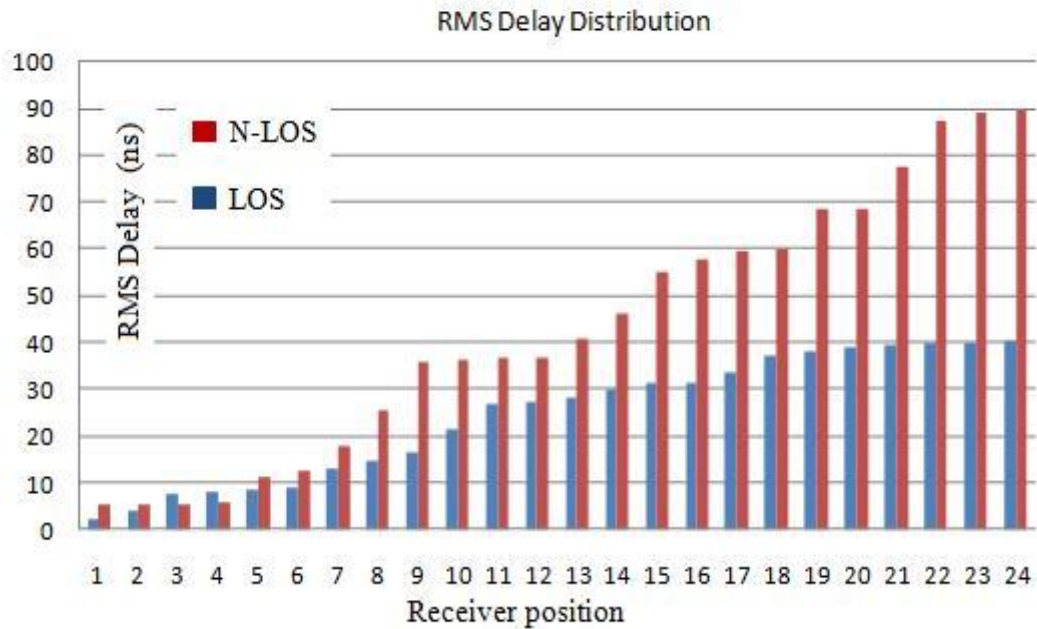


Figure 3.23: RMS delay spread with LOS and N-LOS in multi reflections channel

To sum up the results of this chapter, we present a method for evaluating the impulse response of an arbitrary room with Lambertian reflectors. This method can account for first and second order reflected paths. The results of the simulations indicate that reflections of multiple order increase the excess delay spread but they don't influence RMS delay and maximum delay spread of the channel with considering -30dB and -40dB level of the threshold. The maximum delay spread and RMS delay are determined to be 350ns and 90ns respectively; however, for further analysis, we will use 400ns and 100ns for maximum delay spread and RMS delay, respectively.

These results are applicable only for the particular room configuration which is the common configuration of conferencing rooms and the system deployment, but we cannot make a general statement about all room configurations. Future work in channel characterization can concentrate on filling this gap by examining the effect of irregularly shape for room, furniture, non-Lambertian and specular reflector. In addition, the number of second reflection in the room is limited to decrease the computation time, therefore, further work on the modeling can improve the accuracy of the model.

4. Opto-Electronic Front-Ends

As a prerequisite for investigation of the transmission technique, Chapter 4 focuses on opto-electrical front-ends of the system which play an important role in designing a good transmitter and receiver. In that sense, there will be a comparison between characteristics of available components. We are going to obtain the bandwidth limiting factor of all the components and also discuss important parameters of each component.

As shown in Figure 4.1, a basic optical wireless system consists of a transmitter, a free space as propagation channel and a receiver. The transmitter consists of one or more optical sources which convert an electrical signal into an optical signal. The receiver or detector performs the inverse operation of the optical source by detecting the photon flux on the detector surface and converts it into an electrical signal. In choosing transmitter and receiver for a high speed non-directed link, a quick comparison between some of the characteristics of the available options is investigated in the following.

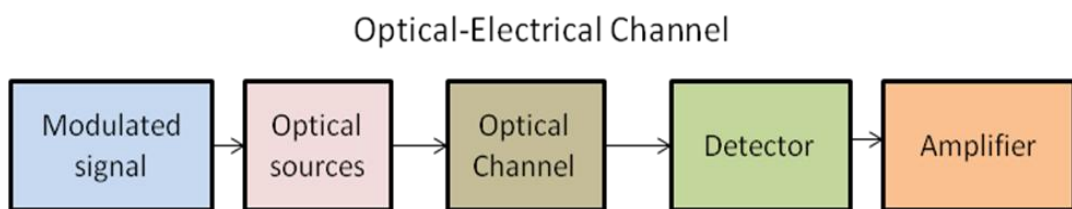


Figure 4.1: A schematic of electrical-optical channel

4.1 Optical source

Two most commonly used light emitting devices in wireless infrared communication system are Light Emitting Diode (LED) and Laser Diodes (LD) operating in forward bias.

The output optical intensity of a LED is proportional to the drive current. As a result of the drive current generated at the device input, electron and hole pairs are recombined after injection into the active region of the diode. Due to their recombination, energy is released as emitted photons. If the thickness of active region increases, then the device can have a wide range of input currents over which it has a linear behavior. However, a wide active region limits the bandwidth of the device. To increase the probability of recombination, causing more photon emission, a LED is constructed of materials known as direct band gap semiconductors [17].

On the other hand, the output intensity of LDs is similar to that of semiconductor LEDs and depends on the transition of charge carriers into the active region, but the device structure is different. Unlike LED, LDs are threshold devices; at low drive currents, the device operates like a low intensity LED, however, after the current exceeds the threshold level, it operates as a very high efficient optical device.

Table 4.1 presents a comparison between LED and LD characteristics. LEDs are commonly used due to their very low cost which is a key factor for the wide spread use of LEDs. Because of wide angular radiation pattern of the LEDs, they are generally considered eye-safe and a good option for non-directed transmission. The bandwidth of typical LEDs is limited in tens of MHz and increasing the bandwidth comes at the cost of reduction in electro-optical conversion efficiency [6].

LEDs also suffer from a broad angular radiation pattern which requires the use of a detector with a wide field of view leading to poor rejection of ambient light. The main advantages of LDs are the speed of operation and much higher electro-optical conversion efficiency. On the other hand, LDs are more complex and more expensive than LEDs. LDs are considered as a point source and they need to be rendered eye safe. To achieve eye safety, the output light must be diffused with the help of a diffuser such that high intensity of emitted radiation is spread over an extended emission aperture and angle [3].

Characteristic	LED	LD
Optical Spectral Width	25-100 nm	0.1 to 5nm
Modulation bandwidth	10s of kHz to 100s of MHz	10s of kHz to 10s of GHz
E/O Conversion efficiency	10 to 20%	30 to 70%
Eye Safety	Considered Eye safe	Must be rendered eye safe
Reliability	High	Moderate
Cost	Low	Moderate to High

Table 4.1: Comparison between LED and LD

There are a number of international standards which provide guidelines on LED and LD emissions. The eye safety of infrared transmission is determined by the Electro-technical Commission (IEC). Table 4.2 includes a list of the classes under which optical radiators can transmit; the IEC Class 1 allowable exposure limit (AEL) is the most desirable class for an infrared system since its emissions under any circumstance are safe without warning labels to be applied. Further information can be found in [18].

Safety Class	Interpretation
Class1	Safe under reasonably foreseeable conditions of operation
Class2	Eye protection afforded by aversion responses including blink reflex
Class3A	Safe for viewing with unaided eye. Direct intra-beam viewing with optical aids may be hazardous
Class3B	Direct intra-beam viewing is always hazardous. viewing diffuse reflections is normally safe

Table 4.2: Interpretation of LED safety classification for optical sources [18]

Because of the mentioned advantages of LEDs and the system required bandwidth in tens of MHz, the optical sources for the system in this work are chosen to be LEDs.

In general, there are a few characteristics of LEDs that designers have to consider: rise and fall time, peak wavelength, radiant power P , radiation pattern and ($P-I$) current to power characteristic. The mentioned parameters are discussed briefly in the following and used in the next step to select an appropriate LED.

LED Bandwidth

The main disadvantage of the LED is its low modulation bandwidth as compared with the laser diode. Modulation bandwidth is determined by the minority carrier lifetime, τ_{life} , in the light emitting active region as

$$f_{3dB} = \frac{1}{2\pi\tau_{life}} \text{ Hz} \quad (4.1)$$

In addition, carrier life time determines the rise and fall times of the LED which is approximately $\tau_{rise} = 2.2\tau$. Therefore, In order to achieve high speed data transmission, the LED should have small rise and fall times to make it fast.

Peak Wavelength

Peak wavelength (λ_p) refers to the wavelength at which the light source produce its maximum emission intensity. Manufacturers usually specify the maximum and minimum value for λp and it is temperature dependent such that the optical spectrum becomes wider with increasing temperature.

Radiant Power

The total radiated power of the LED is called radiant power or radiant intensity and measured in watt or watt per steradian (W/sr), respectively. The light detected by a receiver depends on the radian intensity emitted toward the receiver. Suppose a transmitter emits a radiation pattern described by the radiant intensity (W/sr) $P_i R(\phi)$ where $R(\phi)$ is the radiation pattern (Eq.2.5). At the receiver located at distance r and angle ϕ with respect to the transmitter, the irradiance (W/cm²) is $I_{ir}(d, \phi) = P_i R(\phi) / r^2$. Then the received power (W) is $P_r = I_{ir}(d, \phi) A_{Rx}$ where, A_{Rx} is area of the detector.

Radiant power - Current (P - I) curve

The radiant output power vs. forward current characteristic shows the linearity of the LED. The linearity curve of the LED can be found in the data sheet of LED. It represents the degree to which the optical output is directly proportional to the electrical current input. The radiant power-current characteristic is temperature dependent, it means for a given input current, the optical output power falls as temperature increases.

4.2 Infrared receiver

A typical optical wireless receiver consists of an optical lens and optical filter, photo-detector and preamplifier as shown in Figure 4.2. The optical lens is used to increase the effective area of the photo-detector and collects radiation. The optical filter is used to reject the out of band ambient illumination. The photo detector converts optical radiation into a photo-current and the preamplifier amplify the signal and converts it into voltage. In this section we only focus on the photo detector and the preamplifier.

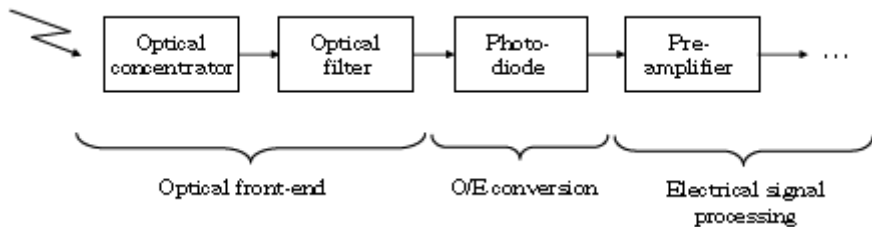


Figure 4.2: A typical OW receiver [7]

4.2.1 Photo-detector

The main component of an optical wireless receiver is the photo detector which converts light into electrical current. When light reaches a photo detector, the incident photons generate free electron-hole pairs if they have sufficient energy. The diffusion of these charge carriers in the detector constitutes the detected photo-current. To collect sufficient energy, a large area photo-detector must be used. A large photo diode is of the interest but it limits electrical due to high capacitance.

There are two practical options for a detector: Positive-Intrinsic-Negative Diode (PIN) and avalanche photodiodes (APD) in Si-technology.

PIN diodes are constructed by placing high-resistivity intrinsic I region between a P-type and N-type region. When photons arrive at the detector, they are observed in the intrinsic region and every absorbed photon generates one electron-hole pair in the intrinsic region. Because of the electric field generated in this region, these carriers are swept up and collected across the junction which is the origin of the photo-current [17]. The APD is constructed similar to PIN diode and the

only difference is that every photon absorbed by the intrinsic layer may generate more than one electron-hole pair.

APDs have photocurrent gain, while PIN photodiodes generate only one electron-hole per photon leading to unit gain. However, the APD gain may not improve the signal-to-noise ratio (SNR) in every case. APDs can lead to impressive infrared link performance when there is little ambient-induced shot noise; because their internal gain overcomes preamplifier thermal noise, increasing the receiver SNR. However, when ambient-induced shot noise is the dominant source of noise, then use of an avalanche diode results in reduction of SNR because the random nature of an APD internal gain increases the variance of the shot noise [3]. In addition, APDs require an additional circuitry to generate the required high bias voltages and to control their temperature [18]. Therefore, APDs are not appropriate for portable devices with limited supplies.

PIN diode receivers are commonly used due to their lower cost, excellent linearity, long life time, tolerance to wide temperature fluctuations and operation with an inexpensive low-bias voltage power supply [3]. A comparison between PIN and APD is illustrated in Table 4.3. The main issue of the PIN diode is the thickness of depletion region; the capacitance of the diode is dependent on the depletion width. Increasing the bias voltage of the PIN diode increases the depth of this region and lowers the capacitance until the fully depleted condition is achieved.

In this thesis, PIN diodes are more preferable to the APD because of the mentioned characteristics.

Characteristic	PIN Photo Diodes	Avalanche Photo Diode
Modulation Bandwidth	10s of MHz to 10s of GHz	10s of MHz to 10s of GHz
Photocurrent gain	1	10e2 to 10e4
Special Circuitry required	None	Temperature Compensation Circuitry
Linearity	High	Low-suited to digital application
Cost	Low	Moderate to High

Table 4.3: Comparison of PIN and APD for wireless optical link

The important parameters of PIN diode are rise and fall time, capacitance, spectral efficiency, relative spectral efficiency and noise equivalent power (NEP).

Photo-detector Bandwidth

The bandwidth of a photo-detector is determined by the speed with which it responds to variations of the incident optical power. The speed is generally expressed as the rise time or cut off frequency. There are three frequency limiting mechanisms for a PIN diode [19]: drift transit time in the depletion region, diffusion time of carriers, and the RC time constant of the diode circuit combination. Thus, the above three factors determine the rise time of a photo diode as seen in Eq (4.2). In properly designed PIN diodes, the diffusion time effects are reduced to a negligible level, leaving only the drift transit time and the junction capacitance.

$$t_{rise} = \sqrt{t_{drift}^2 + t_{diff}^2 + t_{RC}^2} \quad (4.2)$$

where, $t_{RC} = 2.2 \times C_t \times R_L$ and $t_{drift} = d / v_d = d^2 / \mu V_R$, d is depletion layer width, μ is the traveling rate, V_R the reverse voltage, C_t is the sum of the photodiode junction and input capacitances on the inverting terminal of the amplifier and R_L the load resistance. Consequently, the rise time roughly relates to the cutoff frequency, f_c in the formula:

$$f_c = \frac{0.35}{t_{rise}} \quad (4.3)$$

Spectral efficiency [AW]

Spectral efficiency is the ratio of the radiant power to the resulting photo current. The higher is the value of spectral efficiency, the larger is the current generated by the PIN diode. So it is necessary to have as spectral efficiency as large possible.

Relative spectral efficiency

The PIN diode needs to have maximum relative radiant power at the same wavelength as LED.

Noise equivalent power (NEP)

There are two sources of noise in a high speed PIN diode: shot noise, and electronic Johnson noise. Shot noise is related to the statistical fluctuation in both photocurrent and dark current. The magnitude of the shot noise is expressed as

$$I_{sn} = \sqrt{2q(I_p + I_D)f} \quad (4.4)$$

where $q = 1.6 \times 10^{-19} \text{C}$, is the electron charge, I_p is the photo-generated current, I_D is the photo-detector dark current and f is measurement bandwidth. The load resistance of a photo detector generates the Johnson noise due to the thermal generation of carriers. The magnitude of this generated current noise is:

$$I_{jn} = \sqrt{\frac{4k_B T_m f}{R_L}} \quad (4.5)$$

Where $k_B = 1.38 \times 10^{-23}$ is the Boltzmann Constant, T_m is the absolute temperature in degrees Kelvin, f is the bandwidth and R_L is the load resistance of the photodiode. The total noise current generated in a photo-detector is determined by:

$$I_{tn} = \sqrt{I_{sn}^2 + I_{jn}^2} \quad (4.6)$$

In order to quantify the noise performance of a photo-detector, following definition of noise equivalent power (NEP) is used: “Noise Equivalent Power is the amount of incident light power on a photo-detector in order to generate a photocurrent equal to the noise current of the detector” [20]. It is desirable to have NEP as low as possible which leads to a high SNR [19].

$$NEP = \frac{I_{in}}{R_p}, \quad R_p = \text{responsivity in A/W} \quad (4.7)$$

These parameters are the important parameters to be looked when a PIN diode is selected for the system design.

4.2.2 PIN diode with preamplifier

The purpose of using a preamplifier is first to convert the current into a voltage signal and then to amplify the signal. Preamplifiers can be designed as low-impedance (typically 50Ω), high impedance and trans-impedance (TIA) amplifier. A typical circuit model of a detector with low and high impedance amplifier and its small signal circuit are shown in Figure 4.3.

The input of the preamplifier is terminated by an external load resistor. The PIN diode can be equivalently represented by a current source parallel to the depletion capacitance, (C_{det}).

C_{stray} shows the parasitic effect of the interconnection between the PIN diode and preamplifier.

The gate capacitance of the transistor circuit used in the amplifier is shown by C_{FET} .

The value of the load resistor is chosen small for low-impedance amplifiers allowing a wide receiver bandwidth. On the other hand, a small resistor generates a large thermal noise reducing receiver sensitivity. Inversely, a large resistor is chosen for a high-impedance amplifier which diminishes the effect of thermal noise but the resulting bandwidth is small. In addition, it requires an equalization step right after the preamplifier which is not attractive. Therefore, the low and high impedance amplifiers are not further discussed in this work.

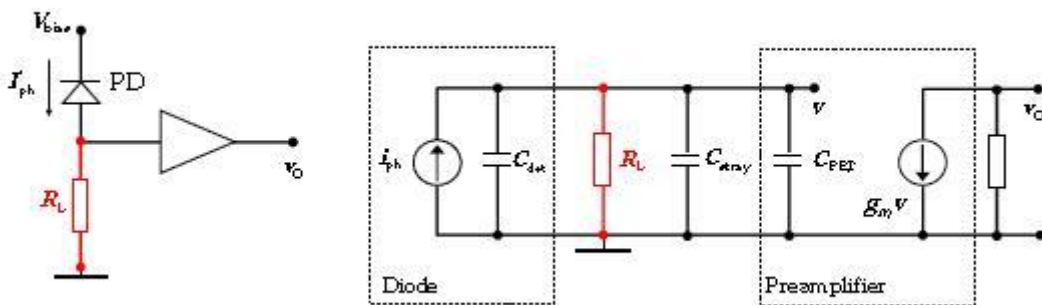


Figure 4.3: Circuit model and equivalent small circuit of a detector with low/ high impedance amplifier[7]

A trans-impedance amplifier design with its equivalent small signal circuit is represented in Figure 4.4. In this receiver the feedback resistor (R_f) is used and it is connected around an inverting amplifier. In this way, the output voltage is proportional to the input current amplified by feedback resistor. Therefore, a large resistor generates high gain amplifier. However, the feedback resistor must be chosen very carefully because it affects the bandwidth of the circuit as

$$f_{-3dB} = \sqrt{\frac{GBP}{2\pi R_f C_{det}}} \quad (4.8)$$

where, C_{det} is the photo diode capacitance and its value depends on the biasing voltage, GBP is the gain bandwidth product of amplifier. The maximum achievable bandwidth can be calculated by knowing the PIN diode capacitance and trans-impedance gain. In case of a high bandwidth requirement and a large capacitance, a good approach is to have a high GBP and a moderate or low gain amplifier and follow this stage by a broadband voltage gain stage.

The input capacitance of amplifier is influenced by capacitance of the photo-diode such that C_{stray} has a pF order of magnitude and C_{FET} is almost negligible because of small width of the transistor gate.

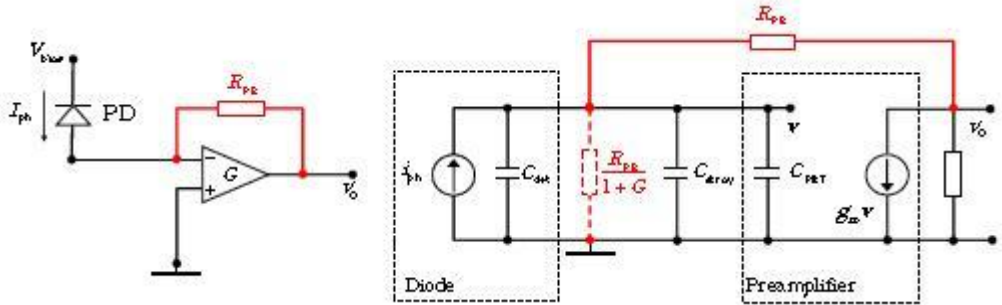


Figure 4.4: Basic scheme of a detector with trans-impedance and its equivalent small circuit[7]

In addition, the noise gain of the preamplifier determines the stability of the circuit. The reason is that any noise signal can trigger an unstable circuit into oscillation. The stability can be reached by adding a feedback capacitor (C_f). Feedback resistor also affects the bandwidth of the amplifier but because it is in the range of pF it can be neglected. C_f is set by several parameters including the trans-impedance gain (R_f), the gain bandwidth product and input capacitance of the PIN diode. The minimum value if the feedback capacitor is calculated by

$$C_f = \frac{1}{4\pi R_f GBW} [1 + \sqrt{(1 + 8\pi R_f C_{det} GBW)}] \quad (4.9)$$

In the following, a few characteristics of the trans-impedance amplifier are introduced; input current noise, input current voltage, input equivalent noise.

Input current and voltage noise

The noise of an amplifier can be completely specified in terms of two noise sources, input current noise \bar{i}_n and input voltage noise \bar{e}_n as shown in Figure 4.5. \bar{i}_n is the noise that occurs at the input of the noiseless amplifier due to fluctuations in the current and it is expressed in (pA/\sqrt{Hz}). \bar{e}_n is the voltage noise seen at the input of the noiseless amplifier if the input terminal is shorted and it is expressed in (nV/\sqrt{Hz}). These values are provided in the amplifier data sheets.

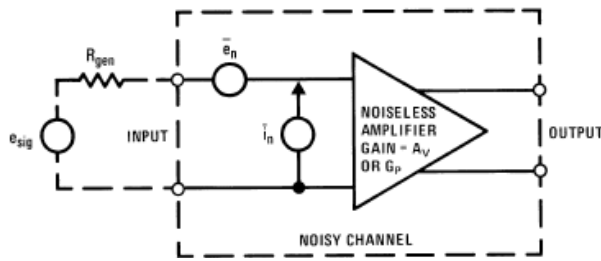


Figure 4.5: Noise characteristic of a amplifier [21]

Input equivalent noise

Input equivalent noise is the relationship in which all noise sources are added at the input of the amplifier in RMS fashion; that is, as the square root of the sum of the squares and generates the equivalent current noise if the total output noise is band limited to a frequency less than the feedback pole frequency. The feedback pole frequency is defined by $f = 1/2\pi R_F C_F$ to provide stability of the amplifier. A very simple expression for the equivalent input noise current can be derived as [22]

$$I_{EQ} = \sqrt{i_n^2 + \left(\frac{4kT}{R_F}\right)^2 + \frac{e_n}{R_F} + \left(\frac{e_N 2\pi C_{det} F}{3}\right)^2} \quad (4.10)$$

where:

I_{EQ} = Equivalent input noise current if the output noise is band limited to $f < 1/2\pi R_F C_F$

i_n = Input current noise for the op amp inverting input

e_n = Input voltage noise for the op amp

C_{det} = Diode capacitance

F = Band limiting frequency in Hz (usually a post filter prior to further signal processing)

If phase modulation techniques are used to transmit information, another important parameter is the phase characteristic of the signal.

This chapter has looked at various important parameters of LED, PIN diode and preamplifier. We presented a detailed noise and bandwidth analysis for a PIN diode and a preamplifier. The results indicate that to achieve large bandwidth, a detector with small capacitance and large area is required. Hence, the area of the detector can be calculated if for example the bandwidth of 20MHz is required. As mentioned in chapter 2, for an infrared system, the noise is generated from internal component as well, which the noise of two main components in the receiver front-end was discussed here.

With respect to the current system design, input equivalent noise is the dominate source of the noise which is used to determine SNR. As future work, the noise power of the receiver front-end can be easily determined for a specific design.

5.

Experimental investigation to increase the bandwidth

In this chapter, first we will show the new available opto-electrical components in the market and discuss their characteristics. The suitable LED, PIN diode and trans-impedance amplifier will be chosen. Finally, a measurement set up is defined with the selected components to verify the possibility of increasing the bandwidth of the system.

In chapter 4, we discussed the main characteristics of the opto-electrical components. The optical source and detector for the system were considered to be a LED and a PIN diode. In this chapter, we are going to explore whether there are new components available which support a large bandwidth compared to the components used in the current system.

5.1 Light Emitting Diode

After intensive research through the different manufactures such as Vishay and Osram, several new light emitting diodes are chosen. Table 5.1 summarizes the primary specifications of these LEDs. Common IR LEDs are low power emitters, designed for operation at 100mA forward current and 1.5V forward voltage. Most IR LEDs are intended for tight half beam angle between 10° and 40° and have a cut off frequency between 18 and 35MHz.

Part Number	Peak wavelength (nm)	Radiant intensity(mW/sr)	Angle of half intensity	Rise time	Cut off frequency
TSFF5400	870	60	22°	10ns	35MHz
TSFF5200		160	10°		
VSMF4710		10	60°		24MHz
TSFF5410		70	22°		
TSFF6210		180	10°		
TSFF5510		32	38°		
TSHG6210	850	230	10°	15ns	18MHz
TSHG6410		90	18°		
TSHG6400		70	22°		
TSHG6200		160	10°		
TSHG5510	830	32	38°	20ns	24MHz
TSHG8400		70	22°		
TSHG8200		180	10°		
SFH 4595	880	60	14°	10ns	35MHz
SFH 4500	950	80	10°	10ns	35MHz

Table 5.1: Light emitting diodes

The LED of the current system is TSHF5410 with modulation bandwidth of 12MHz, 22° half angle, 30ns rise and fall time, 890nm peak wavelength and radiant intensity of 70mW/sr. As mentioned in 4.1, the rise time is inversely proportional to frequency bandwidth of LED. This LED is quite slow compared to the new components. Hence, even LED is a bandwidth limiting factor in the current system design. However, new LEDs support a larger bandwidth compared to the bandwidth of new PIN diodes, therefore, they are not considered as a bandwidth limiting components.

As seen in the Table 5.1, LEDs are categorized in terms of peak wavelengths and in the following the characteristics of some categories are discussed.

Figure 5.1 shows the radiant intensity of the LEDs vs. the angle of half intensity for LEDs with peak wavelength of 870nm. The red bars represent radiant density of LEDs with rise time of 10ns relatively 35 MHz bandwidth and green bars are LEDs with 15ns rise time relatively 24MHz bandwidth.

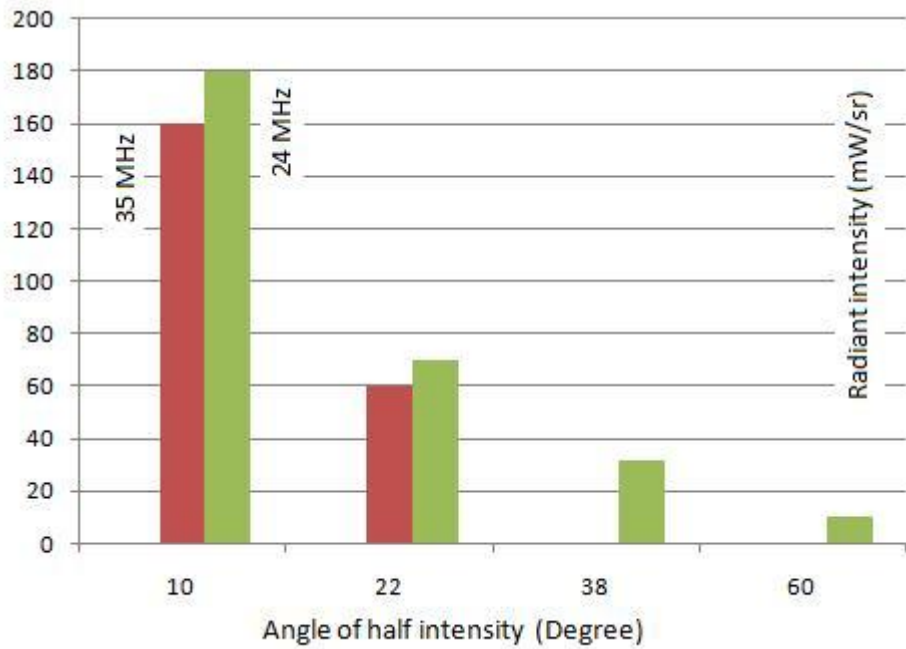


Figure 5.1: Radiant intensity of the LEDs vs. angle of half intensity, $\lambda=870\text{nm}$

The chart indicates that radiant intensity significantly decays as the angle of half intensity becomes larger due to wide beam pattern. Although a LED with an angle of 10° has high a radiant intensity, it has a very narrow beam pattern. Therefore, the radiation pattern is not wide enough to cover a large area unless these LEDs are mounted in different direction. The effects of the larger bandwidth results in slightly decrease in radiant intensity of the LEDs.

Figure 5.2 also shows the relationship between radiant intensity and angle of half intensity for LED with peak wavelength of 850nm for which the same trend is visible. LEDs listed in Table 5.1 are all faster than the LED used in the current system and applying any of these components result in an increase in the bandwidth of the transmitter.

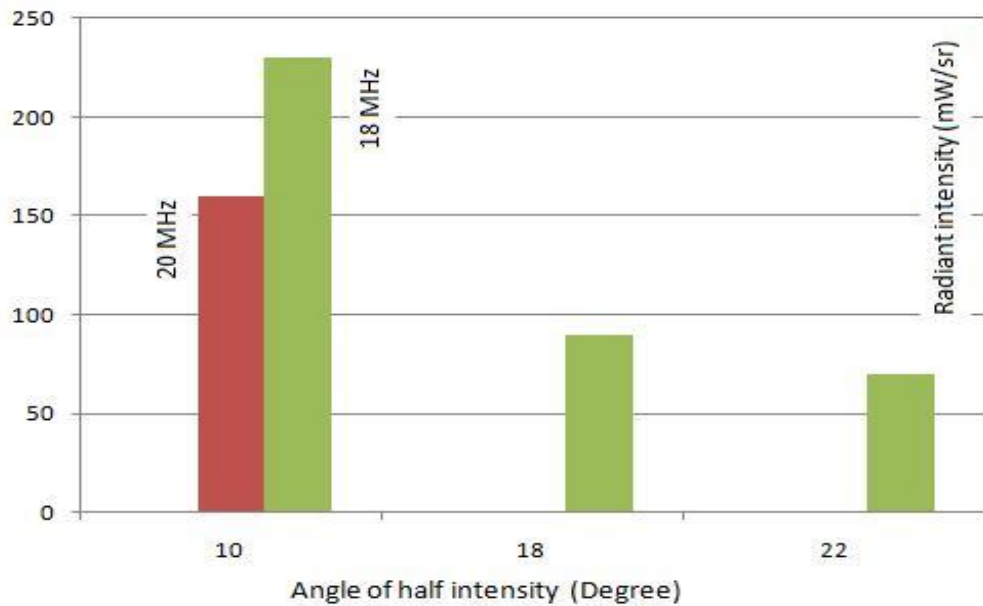


Figure 5.2: Radiant intensity of the LED vs. angle of half intensity, $\lambda=850\text{nm}$

As mentioned, light emitting diodes are not considered as a bandwidth limiting factor for the required bandwidth below 35MHz. TSFF5400 which has the highest bandwidth is not produced anymore by Vishay. Therefore, the next good option in order to support large bandwidth is TSFF5410 which has reasonable output intensity and half angle compared to the others. It can support the frequency bandwidth of 24MHz.

TSHG6400 is also a good option with bandwidth of 18MHz. Final selection of the appropriate LED has to be made after choosing the PIN diodes because if there does not exist a PIN-diode supporting 24MHz bandwidth then using a LED with 24 MHz bandwidth only results in intensity reduction.

5.2 PIN-diode

To select an appropriate PIN photodiode, the important factors of several PIN diodes are listed in Table 5.2. These parameters were discussed in detail in chapter 4. As seen from Table 5.2, the junction capacitance is proportional to the area of the PIN diode. Increasing the bias voltage of the photodiode reduces the junction capacitance and increases the bandwidth.

PIN photodiode used for the current system is SHF235 FA with a rise time of 20ns resulting in bandwidth of 17.5MHz, which is a common rise time of many PIN diodes. One high speed PIN diode alternative is TESP5700 which has a 10ns rise time supporting a 35MHz bandwidth and includes day light filter. However, the fast rise time is achieved at the expense of small area and low output current. In addition, it was also mentioned in chapter 4 that the small area of the PIN diode can be compensated by using several PIN diodes or a hemispherical lens with the gain n_d^2 , n_d^2 is lens index. The peak wavelength for this diode is equal to the infrared emitter TSFF5410 chosen for high speed communication. Whether there is a lens to provide enough gain needs to be checked.

Part Number	Spectral efficiency	Rise time	Peak Wavelength (nm)	Capacitance (pF)	NEP	Area (mm ²)	angle	output
BP 104 F,FS	0.70	20ns	950	48	3.6e-14	4.48	60	35μA
BF 104 FAS	0.65		880					34μA
BF 104 S,BS104 SR	0.62		850					55μA
BPW 34 F	0.59		950		72	4.3e-14	7	80μA
SFH2400,FA	-	5	850	11	2.9e-14	1		10μA
SFH 2701	0.5	1.2	820	5	6.3e-15	0.36		1.2μA
BPW 34,FS,FSR	0.59	25	950	72	4.3e-14	7		50μA
SFH 225 FA	0.63	20	900	48	3.6e-14	4.48	60	34μA
SFH 235 FA	0.63	20	900	72	4e-14	7	65	50μA
TESP5700	0.57	10	870	17	-	2.2	60	25 μA
BPV10	0.55	2.5	920	11	3e-14	0.78	20	70 μA
BPV10NF	0.55	2.5	940	11				60μA
BPW 34 FA, FAS,R18R	0.65	20	880	72	3.9e-14	7	60	50μA
S6968-01	0.55	-	850	50	6.3e-15	150	35	1.2μA

Table 5.2: PIN diodes

5.3 Trans-impedance amplifier (TIA)

A typical trans-impedance amplifier circuit with all necessary components was shown previously in Figure 4.4. Figure 5.3 shows an example of achievable bandwidth versus trans-impedance gain for a 10pF source capacitance for various amplifiers.

The OPA847 has a 3.9GHz GBP with 0.85nV/√Hz input voltage noise. The OPA846 has a 1.75GHz GBP with a 1.2nV/√Hz input voltage noise. The OPA843 is an 800MHz GBP device with a 2nV/√Hz input voltage noise. Finally, the OPA657 is a 1.65GHz GBP device with a 4.8nV/√Hz input voltage noise. Unlike the other three devices, the OPA657 is a FET input amplifier.

Looking at achievable bandwidth, OP847 provides the highest supporting bandwidth for different trans-impedance gains. Looking at the noise, OP847 yields a 2.5pA/√Hz input noise current and 0.85nV/√Hz input noise voltage. This amplifier has a much lower voltage noise and higher noise current. Low input voltage noise is required for best sensitivity in wideband trans-impedance application [23].

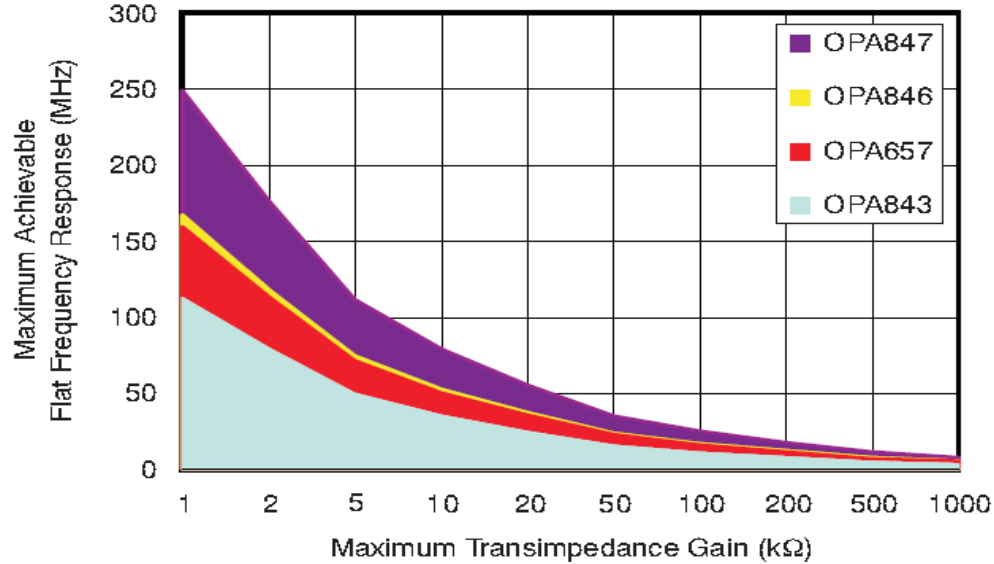


Figure 5.3: Maximum achievable bandwidth for selected Op-amps [23]

5.4 Summary of chosen components

The discussion in this chapter was not intended to optimize the transmitter and receiver design but has the goal to provide a verified set of components useful for further investigations. Table 5.3 summarizes the OW transmitter and receiver elements

Components	Parameters	Values
LED	Type Manufactury Peak wavelength Cut-off frequency Angle of half intensity Radiant intensity	TSFF5410 Vishay 870nm 24MHz 22° 70(mW/sr)
PIN diode	Type Manufactury Peak wavelength Cut-off frequency Angle of half intensity Input capacitance Responsivity	TESP5700 Vishay 870nm 35MHz 60° 17pF 0.57 (A/W)
Preamplifier	Type GBP	TIA- OPA 847 3900MHz

Table 5.3: Summary of the OW components for target system

5.5 Measurement set up

In order to verify the possibility of increasing the current bandwidth, a simple measurement set up with chosen components is constructed. According to the datasheet of the components, the bandwidth of 24 MHz is expected to be seen at the detector output. The measurement set up consists of a signal generator, a LED as transmitter, a PIN diode as receiver and the final stage is the signal analyzer to see the spectrum of the received current as shown in Figure 5.4.

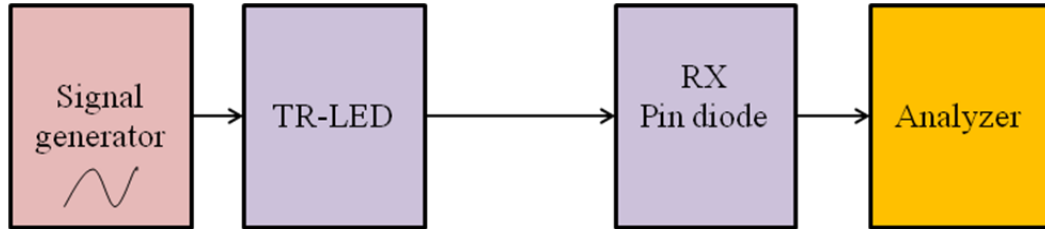


Figure 5.4: General measurement set up

The LED and the PIN diode are located close to each other to cancel the effects of the not ideal optical channel. A sine wave in frequency range between 1 kHz to 24MHz is generated and passed through the LED driver circuit. It is received via the PIN diode and the spectrum of the signal is viewed on the spectrum analyzer screen. It is important to be mentioned that the PIN diode has been included a day light blocking filtering.

5.5.1 LED driver circuit

LEDs are current-driven devices whose brightness is proportional to their forward current. Fluctuation in forward current is controlled by changing the input voltage. The important task in designing a LED driver is to generate the required biasing current to ensure the signal is always positive. The circuit diagram of LED driver circuit is shown in Figure 5.5.

The signal generator can generate a 0.36V peak to peak voltage signal. The gain of the transistor is unit, and then the 36mA peak to peak current signal can be seen at emitter of the transistor. The current needs to be positive for which a biasing is required. Because there is always a distortion in signal around zero, it is better to have large a DC biasing which is taken here to be 66mA. Therefore, the peak of the current signal is at 84mA and minimum at 48mA. It also needs to be checked that the transistor works in its active region for maximum current passed through the LED.

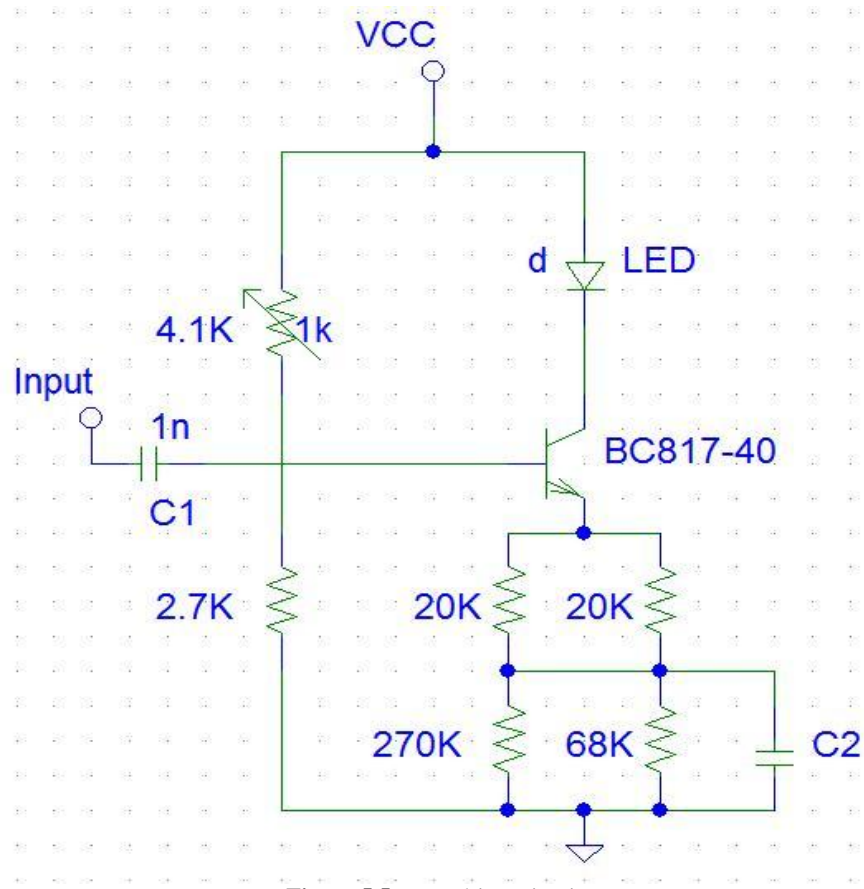


Figure 5.5: LED driver circuit

5.5.2 PIN diode driver circuit

The PIN diode driver circuit should be designed such that the amplitude and frequency response of the detector can be observed by the analyzer. Because the received current is very small, the signal needs to be amplified. Therefore, an amplifier is used in this circuit with configuration different than trans-impedance amplifier and it is capable of supporting a large bandwidth. The driver circuit of PIN diode is illustrated in Figure 5.6. In the circuit, two bipolar transistors are used, one an NPN-type, the other PNP-type which they can significantly amplify the signal.

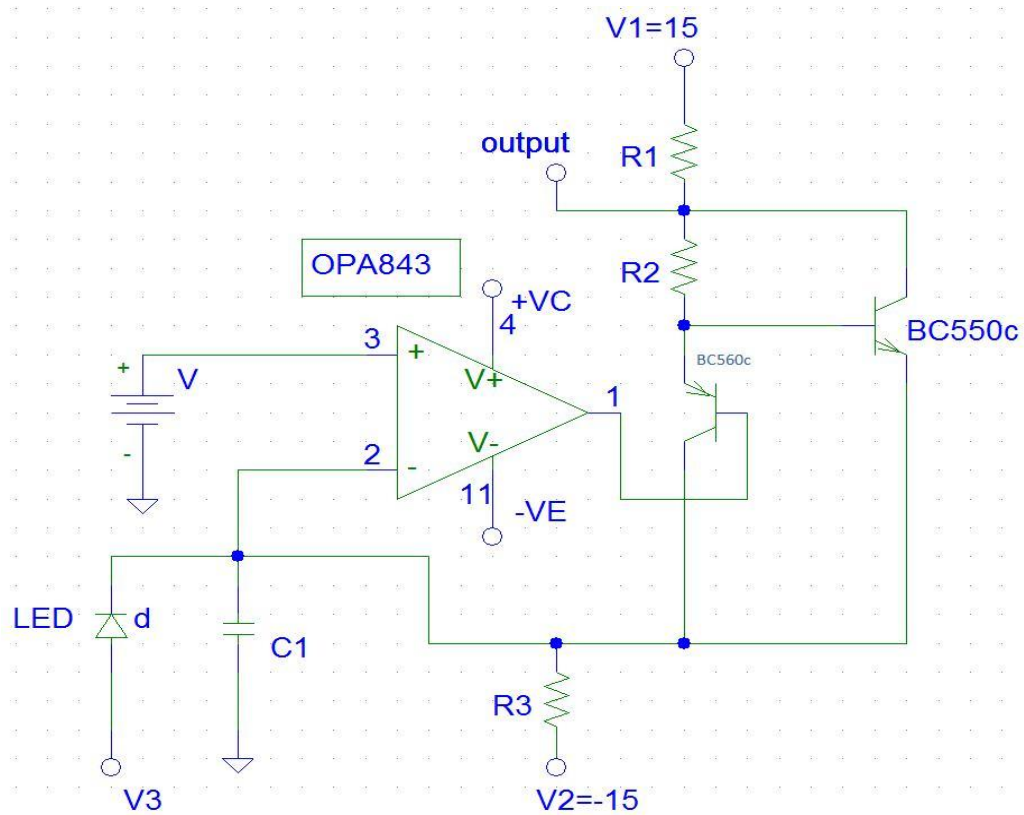


Figure 5.6: PIN diode driver circuit

5.6 Results of the measurement

The picture of the set up is shown in Figure 5.7. The measurements are based on a LOS path between transmitter and detector. A sinusoid is generated by the analyzer injected into the transmitter. The DC level generated by the constant current determines the required bias current. The light is detected by PIN diode and the received electrical power is read from the electrical spectrum analyzer. The procedure is repeated for different distance between transmitter and receiver (2cm, 5cm, 10cm). For further investigation, the results with transmitting a greater input current or adding more LEDs should be checked to see the spectrum at longer distances.

It can be seen from the measurement results shown in Figure 5.8 that, the maximum bandwidth of 22MHz is achievable. With this result, the system transmission bandwidth can increase from 8MHz to 22MHz. However, the 2MHz lower bound limit is considered due to IEC-regulation. It can be considered to be 1MHz as well but below that would not be recommended because of the interference from fluorescent lighting. In addition, the upper bound of the bandwidth is limited to 20MHz to accommodate the variation in the electrical components. As a consequence, the achievable bandwidth with the regarded components is 18MHz.

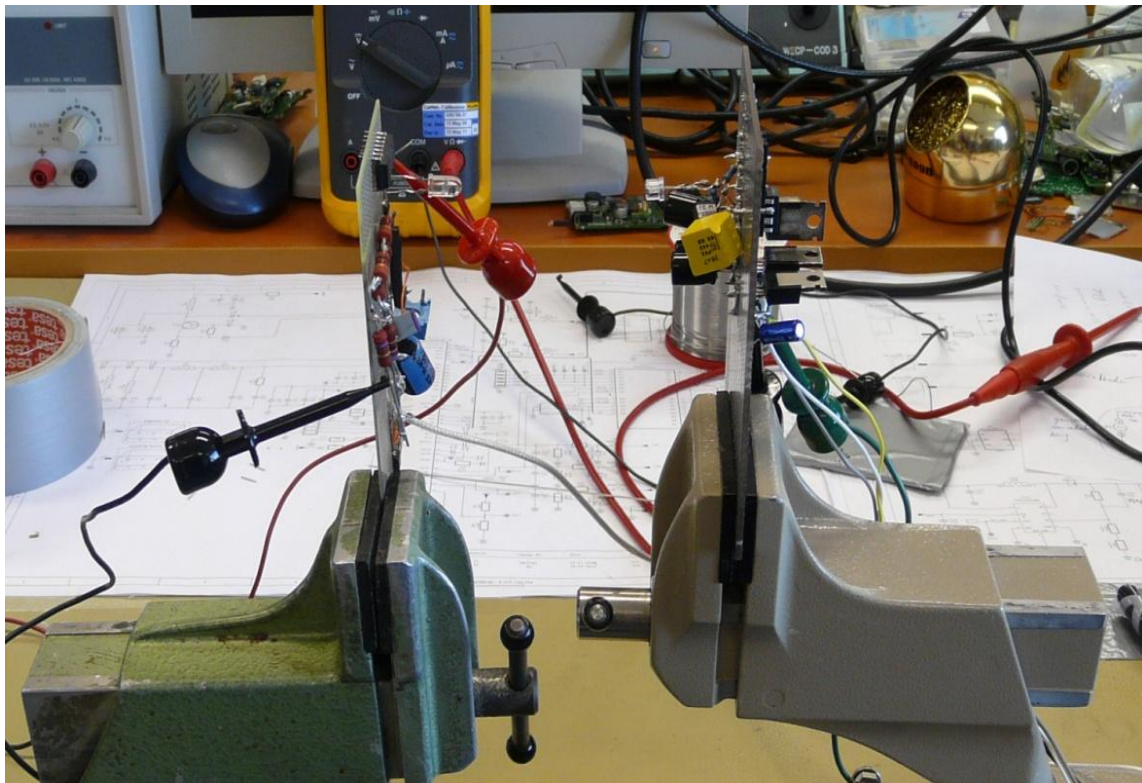


Figure 5.7: Measurement set up



Figure 5.8: Spectrum of the received signal

6. Digital Modulation Techniques

In this chapter, various modulation schemes will be introduced. Then it will focus on the comparison of these modulations in terms of bandwidth and power efficiency. It is followed by discussing the bit error rate and peak to average power ratio for different modulations.

6.1 Modulation scheme classification

There exist a multitude of modulation techniques which are generated by combining and varying of basic modulations, amplitude shift keying (ASK), frequency shift keying (FSK) and phase shift keying (PSK). In general, the modulation schemes can be classified into two groups based on their sensitivity to non-linear distortion: 1. constant envelope modulation and, 2. variable envelope modulation schemes as shown in Figure 6.1.

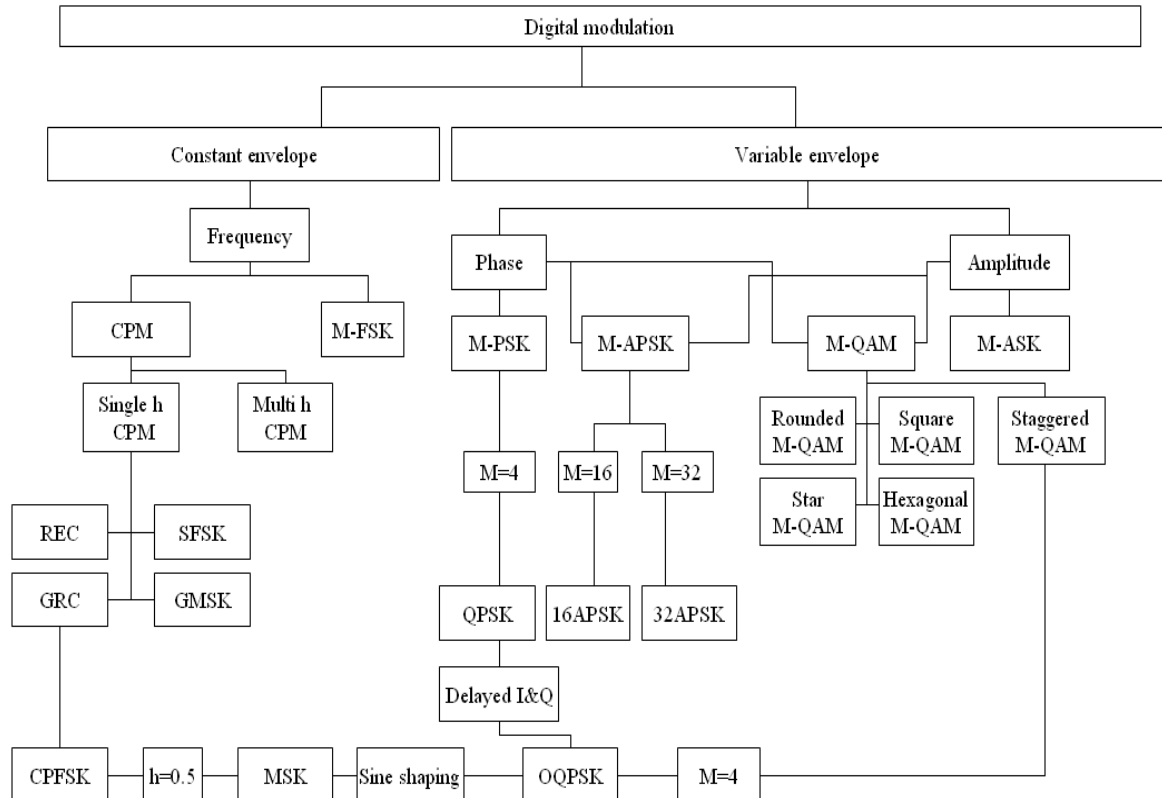


Figure 6.1: Modulation scheme classification

6.1.1 Constant envelop modulation (CE)

Constant envelope modulation is categorized into two groups: continuous phase modulation (CPM) and frequency shift key (FSK). CPM includes minimum shift key (MSK), sinusoidal frequency shift key (SFSK) and Gaussian minimum shift key (GMSK). Thus, the information bits are encoded either in the frequency or continuous phase. In this sense, signals suffer less distortion in high power amplifiers. It means that the amplifier device can operate in a nonlinear mode or near saturation. However, they don't permit high bandwidth efficiency as compared with variable envelope modulation. Because the modulation schemes are non-linear it requires higher bandwidth occupancy than amplitude and phase modulation techniques [9]. Consequently, because the bandwidth limitation is the primary concern of this project, FSK and CPM schemes are not considered in this work.

6.1.2 Variable Envelop Modulation

Variable envelope modulation has better spectral properties than constant envelope. However, because the information bits are encoded in both amplitude and phase of the transmitted signal, they are more susceptible to variation from fading and interference. In addition, they also require linear amplifiers which are expensive and less power efficient than non-linear amplifier. Therefore, the trade off between variable and constant envelope is for better spectral efficiency, better power efficiency and resistance to channel impairment.

For variable envelope modulation, the size of the constellation must be chosen. The larger the constellation, the higher data rate is achievable for a given signal bandwidth, but, the signal is more susceptible to noise fading and the system is hard to implement.

Generally, variable envelop modulation is categorized into the two groups: phase shift keying (PSK) and amplitude shift keying (ASK). PSK is not classified as a constant envelope because of its discontinuous phase shift. Amplitude and phase shift keying (MAPSK) is another type of PSK. Quadrature amplitude modulation is combination of ASK and PSK and it has different constellation shape, square QAM, star QAM, hexagonal QAM, rounded QAM, staggered QAM (SQAM).

6.1.2.1 Phase shift keying (MPSK)

In multi level phase shift key (MPSK), the phase of the carrier is shifted to one of the M possible values $\phi = 2\pi(i-1)/M$ where $i=1\dots M$. The constellation points are positioned on a circle which it provides the highest immunity to corruption and maximum separation in phase between adjacent points. Another advantage of this is that the symbols are transmitted with the same energy. In practice, 8PSK is usually the highest order of PSK and more than 8 phases result in power penalty [9].

6.1.2.2 Amplitude Phase shift keying (MAPSK)

MAPSK methods generate transmitted signal by varying both amplitude and phase of the carrier signal. The constellation of MAPSK is made up of concentric PSK rings as shown in Figure 6.2. It is widely used in satellite communication including European digital video broadcasting where high transfer efficiency is essential. MAPSK has various signal constellations which 16 APSK shows a good performance in case of nonlinear characteristics of an amplifier [23]. One advantage of 16APSK is to have two concentric-rings with only two amplitude levels. This gives a reduction in amplitude levels and decrease peak to average power ratio (PAPR) when the 16APSK is used in Orthogonal Frequency Division Multiplexing (OFDM) systems [24]. Practically, for 16APSK the symbol energy has to be kept large enough to compensate for the close distance between the adjacent points in the constellation. Otherwise symbols are highly sensitive to noise.

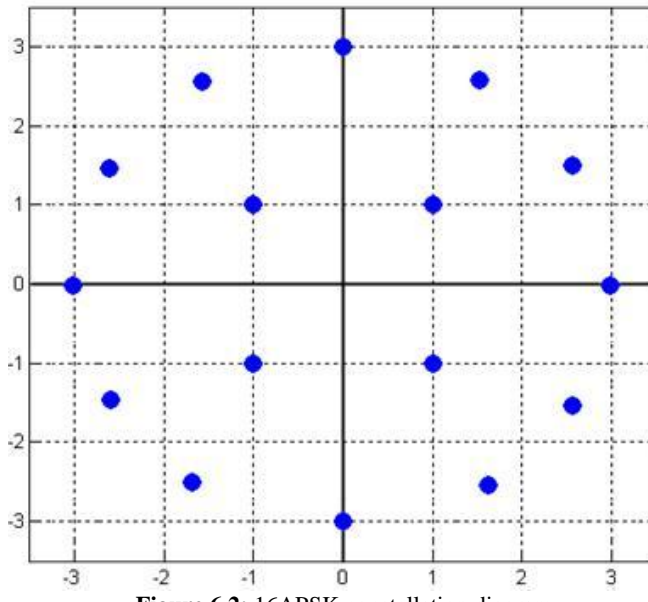


Figure 6.2: 16APSK constellation diagram

6.1.2.3 Quadrature Amplitude Modulation (M-QAM)

In quadrature amplitude modulation (M-QAM), the information bits are encoded in both amplitude and phase of the transmitted signal. Common square constellations are 4-QAM and 16-QAM. In case of 16-QAM, 4 bits are transmitted per symbol and they are mapped onto the In-phase and quadrature symbols. Therefore, each constellation point would represent four bits with two bits on the (I) axis and two bits on the (Q) axis. QAM is more bandwidth efficient than QPSK but it is vulnerable to non-linear distortion and channel fading effects because distance between the symbols points on the constellation diagram decreases and to achieve same performance as QPSK more transmitted power is required.

6.2 Comparison of digital modulation schemes

The choice of modulation technique is influenced by several factors such as high spectral efficiency, high power efficiency, robustness to channel impairment and low implementation cost. Hence, a desirable modulation provides low bit error rates at low received signal-to-noise ratios (SNR), performs well in multipath and fading conditions, occupies a minimum bandwidth, and is cost effective to implement [9]. These requirements are often conflicting and a modulation scheme does not simultaneously satisfy all of them. The choice of modulation is a trade off between these requirements and the demand of a particular application. These factors are discussed in the following for several modulation schemes.

6.2.1 Bandwidth and power efficiency

The Shannon theory states there is upper bound on achievable bandwidth efficiency over a noisy communication channel and is given by

$$R_b = B \log_2 \left(1 + \frac{P_r}{N_0 B} \right) \text{ (bits/sec)} \quad (6.1)$$

where R_b is data rate, P_r is received signal power, N_0 is noise power spectral density (PSD) and B is bandwidth (Hz). From (6.1), the designers attempt to optimize a system to have a maximum capacity, however, it can easily be concluded that maximum capacity of the system depends on the received signal to noise ratio. Therefore, capacity can reach its maximum if input power is chosen optimally.

As mentioned, designing a digital communication system is a tradeoff between bandwidth and power efficiency. In many systems, one of them is more valuable than the other. Therefore, researchers classify systems as either bandwidth or power limited. In case of bandwidth limited system, spectrally efficient modulation techniques can be used to save bandwidth at the expense of power. In power limited system, power efficient modulation is used to save power at the expense of bandwidth. In addition, error correction coding is applied to save the power [25].

Bandwidth efficiency reflects how efficiently a limited bandwidth is utilized and is defined as the ratio of the data rate per Hertz in a given bandwidth

$$\eta = \frac{R_b}{B} = \frac{1/T_b}{2/lT_b} = \frac{R_b}{2R_s} = \frac{l}{2} \left[\frac{\text{bit / s}}{\text{Hz}} \right] \quad (6.2)$$

where l is number of bits per symbol.

Higher level modulation schemes except FSK have high bandwidth efficiency. On the other hand, they suffer from poor power efficiency. Power efficiency describes the ability of a modulation technique to protect the reliability of the digital message at low power levels. It is expressed as the ratio of the signal energy per bit to noise power spectral density (E_b/N_0) required at the receiver to

achieve a certain probability of error. According to Shannon's theorem the relation between bandwidth and power efficiency is given by

$$\frac{R_b}{B} < \log_2\left(1 + \frac{E_b}{N_0} \cdot \frac{R_b}{B}\right) \quad (6.3)$$

$$\frac{E_b}{N_0} > \frac{2^{R_b/B} - 1}{R_b / B}. \quad (6.4)$$

Figure 6.3 represents bandwidth efficiency vs. power efficiency for different modulation schemes for a given bit error rate of 10^{-5} . The best modulation scheme is the one closest to the left-hand corner. As it is observed, QPSK requires $E_b / N_0 = 10dB$ achieving bandwidth efficiency $\eta = 2$ (bit/s/Hz). 16QAM allows $\eta = 4$ (bit/s/Hz) of transmission bandwidth at $E_b / N_0 = 14dB$. This is because the spacing between the points in the signal constellation decreases. In order to achieve the same bit error rate more energy per bit is required.

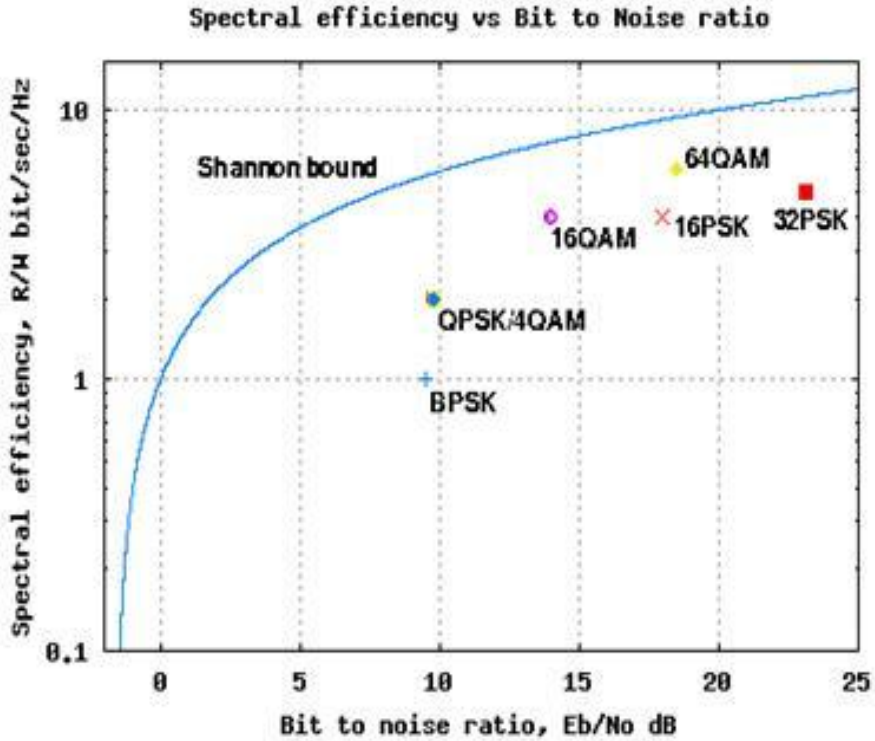


Figure 6.3: Bandwidth efficiency vs. power efficiency [26]

6.2.2 Bit error probability

The performance of the system affected by the noise is measured by the probability of error of the received signal. It is a function of the ratio of the energy per bit to noise spectral density and measured at the detector input. Furthermore, the relationship between BER and E_b / N_0 depends on the modulation technique. Figure 6.4 illustrates the Bit error rate vs. energy per bit for different modulation schemes assuming an AWGN channel. To obtain very small BER , the system design becomes very complex. However, there are many coding techniques to achieve a good performance. As Figure 6.4 reveals, QPSK requires the least amount of energy and it is followed by 16-QAM, 16PSK, 64-QAM and 32PSK. The required energy for 16-QAM is approximately 4dB more than QPSK for $BER = 10^{-6}$. Therefore, if the system is power limited then higher level modulation schemes can't be considered as good option unless using coding to reduce required power.

Another issue when choosing the modulation technique is immunity of the scheme to channel impairment such as amplitude nonlinearities and channel fading. If the signal is highly attenuated over the channel then FSK and PSK are more appropriate. The QAM detection depends strongly on the received signal level and they are more sensitive to channel characteristics.

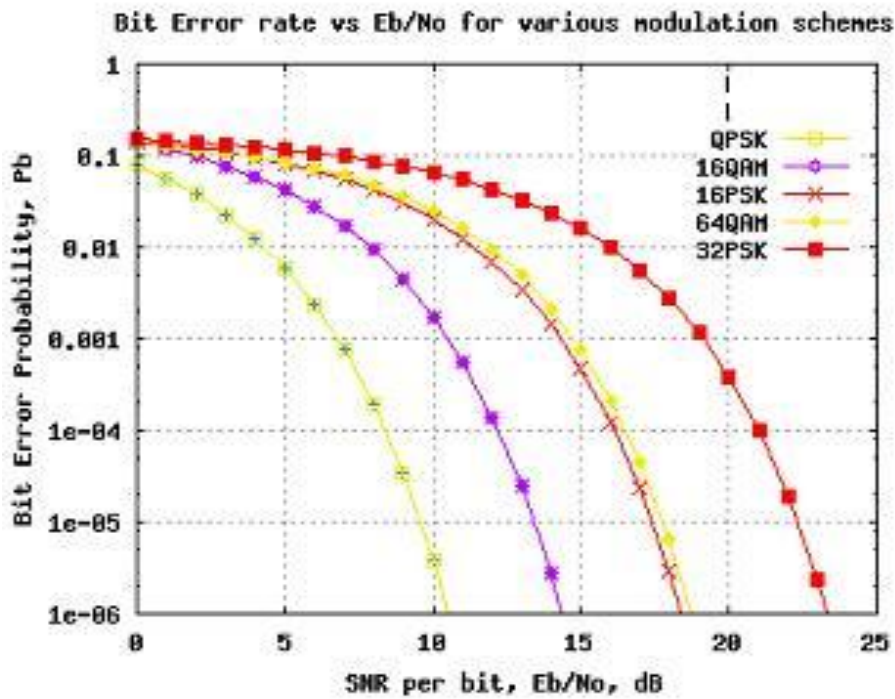


Figure 6.4: Bit error rate vs. bit to noise ratio[26]

6.2.3 Peak to average power ratio

The sensitivity of the modulation scheme to non-linear distortion depends on peak to average power ratio (PAPR), which is defined as a ratio of the peak power of the modulated signal to the average power of the modulated signal. When PAPR is 0 dB there is no variation in amplitude of the modulated signal. Therefore, the signal is constant envelope and insensitive to nonlinear distortions. In contrast, amplitude signals (QAM) are subject to non-linear power amplification with PAPR higher than 0dB.

PAPR values for different modulation schemes with Nyquist filter and with roll cosine factor $r_N = 1$ are shown in Table 6.1. The PAPR depends on factor of raised cosine filter for a single carrier. Furthermore, higher level QAM schemes have higher PAPR.

Characteristic	Un-filter	Nyquist filter($r_N = 1$)
QPSK	0.00 dB	1.80 dB
8-PSK	0.00 dB	1.80 dB
16-QAM	2.55dB	4.35 dB
64-QAM	3.68 dB	5.50 dB

Table 6.1: Peak to average power ratio (PAPR) of several modulation schemes

7.

Multicarrier modulation-OFDM

This chapter discusses single and multicarrier transmission. It is followed by describing the concept of an OFDM system as a promising approach to handle channel dynamics and signal degradation. Finally, challenges in the design an OFDM system are discussed.

7.1 Multicarrier

The delay of the channel causes a stretching of the input signal which creates signal distortion referred to as ISI. One way to reduce ISI is to use adaptive filters for equalization. However, to some extent, it can be complicated due to the filter taps which often increase with number of reflected channel paths.

ISI can also be significantly reduced by the employment of multicarrier modulation (MCM) technique. The basic idea of multicarrier modulation is to divide the total bandwidth into many narrow sub-channels and transmit several bit streams in parallel. Importantly, the number of sub streams is selected to insure each sub-channel has a bandwidth smaller than the coherent bandwidth of the channel. Then for a sufficiently large number of sub-channels (N_{sc}), it can be assumed that each narrow band sub-channel experiences flat fading.

Figure 7.1 shows how the frequency selective channel affects the signal with a bandwidth B . In single carrier system, each data symbol occupies the total available bandwidth. Therefore, at the output of the channel $|H(f)|$, different parts of the transmitted signal spectrum are attenuated differently and reconstruction of the signal requires a complex equalization. Consequently, a narrow band interference or strong frequency band attenuation can cause single carrier transmission to completely fail.

Multicarrier modulation makes the equalization at the receiver very simple and efficient. In such system, a data symbol only occupies a fraction of the available bandwidth and different symbols are transmitted by different sub-bands in parallel. Thus, each sub-channel experiences less ISI and then the equalization of the signal in each sub-band requires a filter with only one tap. That is the reason equalization becomes simple [27], [7].

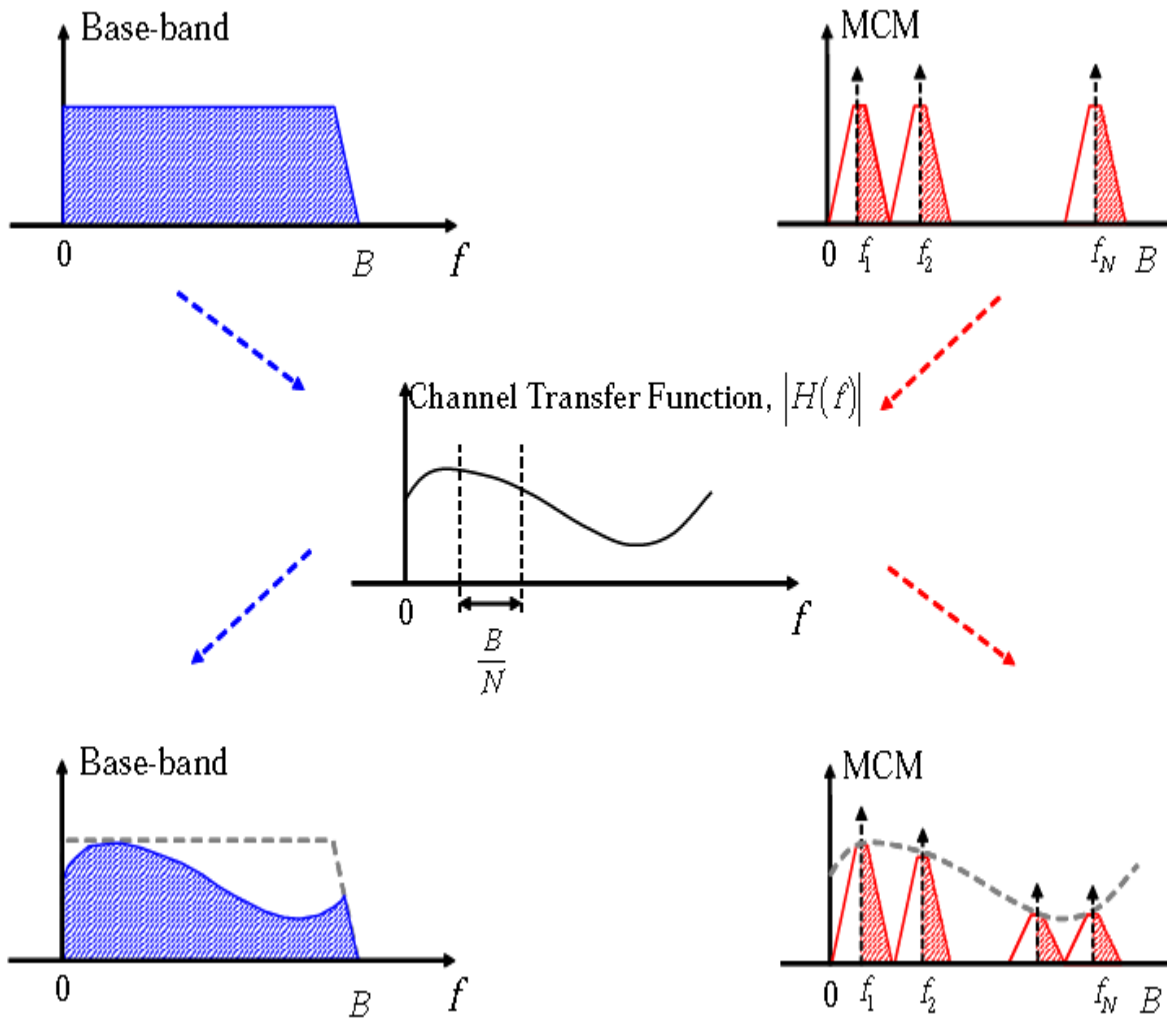


Figure 7.1: Passing of baseband and MCM signal through a frequency selective channel [7]

MCM can be implemented using several techniques. The first multicarrier system was introduced as Frequency Division Multiplexing (FDM). In FDM, the composite multicarrier signal is obtained by shifting baseband parallel data streams upwards in frequency by modulating them on different sinusoidal carriers.

The subcarriers of a FDM system must not have overlapping spectra to prevent the channels from crosstalk that would occur between different sub-channels. To generate non overlapping subcarriers, frequency guard bands are commonly inserted between subcarriers as shown in Figure 7.2. The benefit of a guard interval comes at the cost of reducing spectral efficiency.

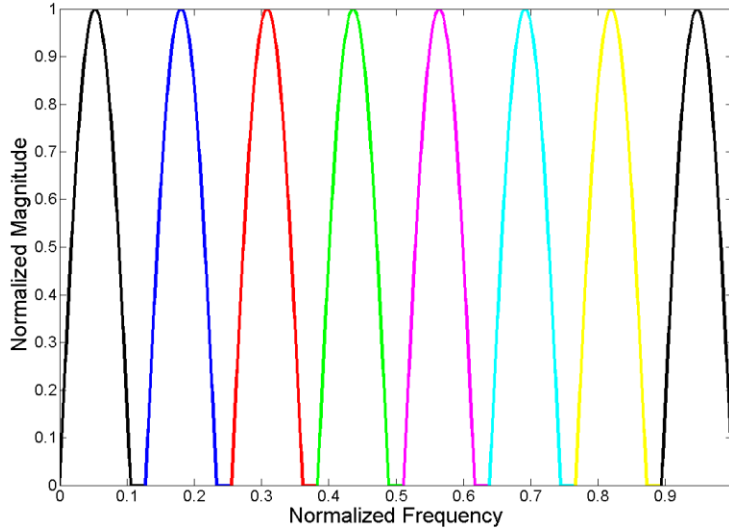


Figure 7.2: FDM spectrum with 8 subcarriers and guard bands

Orthogonal Frequency Division Multiplexing (OFDM) is one of the spectrally efficient multicarrier methods. It has been used for European Digital Audio Broadcasting (DAB) back in 1995 and other standards such as Digital Video Broadcasting (DVB), WiFi (IEEE 802.11a/g/j/n), WiMAX (IEEE 802.16) and UWB WPAN (IEEE 802.15.3a).

OFDM is special case of FDM that offers a high spectral efficiency due to its orthogonal subcarriers which allow their spectra to overlap. Two complex functions are said to be orthogonal if the integration of one to the conjugate of other over the domain of interest is equal to zero:

$$\int_{t \in D} e^{j2\pi f_n t} e^{-j2\pi f_m t} dt = \begin{cases} 1, & \text{for } n = m \\ 0, & \text{for } n \neq m \end{cases} \quad (7.1)$$

where f_n and f_m are frequencies of two orthogonal subcarrier on the time domain D .

As long as subcarriers are orthogonal to each other, they don't interfere with each other. Figure 7.3 illustrates the spectrum of OFDM with 8 subcarriers. In addition, the guard bands that are necessary in an FDM system would no longer be necessary.

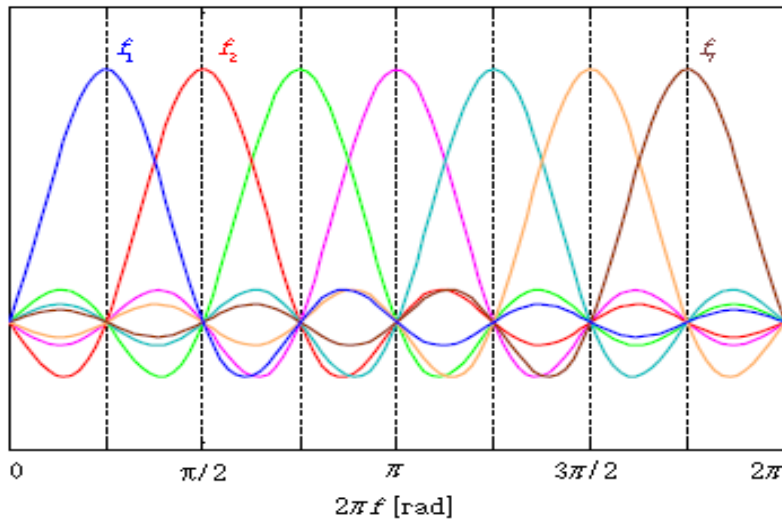


Figure 7.3: Spectrum of 8 equally modulated subcarriers in OFDM [7]

A comparison between bandwidth efficiency of FDM and OFDM are show in Figure 7.4. Assume a system has a baseband occupied bandwidth (B). The required transmission bandwidth of FDM for any number of subcarriers is always $2B$ because in FDM the entire bandwidth is divided to the number of non overlapping sub-channel. In OFDM system, transmission bandwidth depends on number of subcarrier (N_{sc}) as $(N_{sc} + 1)B / N_{sc}$ such that for large number of subcarriers, the subcarrier spacing decreases.

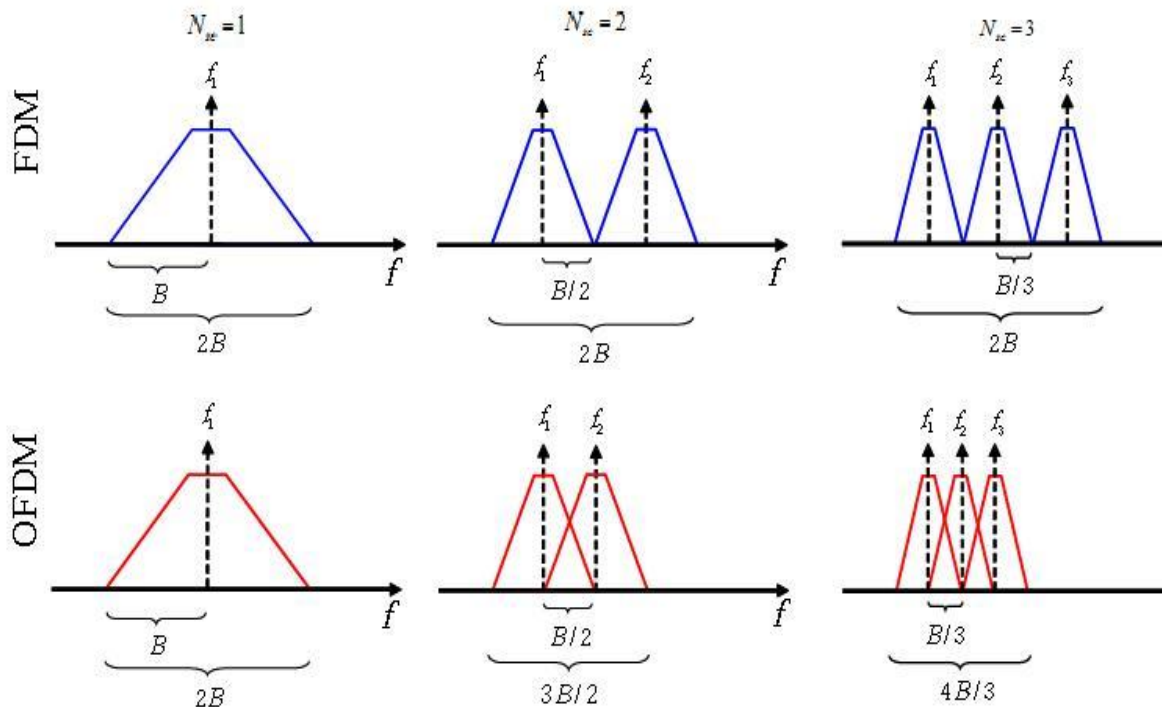


Figure 7.4: Comparison of spectral efficiency of FDM and OFDM

7.2 OFDM signal structure

In the 1960s, an OFDM modulator was implemented with analog oscillators. The main reason that the OFDM technique has taken a long time to become a prominence was the practical implementation of this method. It was extremely difficult to generate such a signal and even harder to receive and demodulate the signal [30]. Later on, Weinstein and Ebert generated a fully digital OFDM scheme by means of the discrete Fourier transform, DFT [28]. Its implementation even became simpler by using the fast Fourier transform (FFT) algorithm.

The DFT approach is shown in Figure 7.5. By performing DFT on the complex input symbols $(a_n + jb_n), n = 0, \dots, N_{sc} - 1$ the data symbols are imprinted on N_{sc} mutually orthogonal subcarriers $f_n = n/T$.

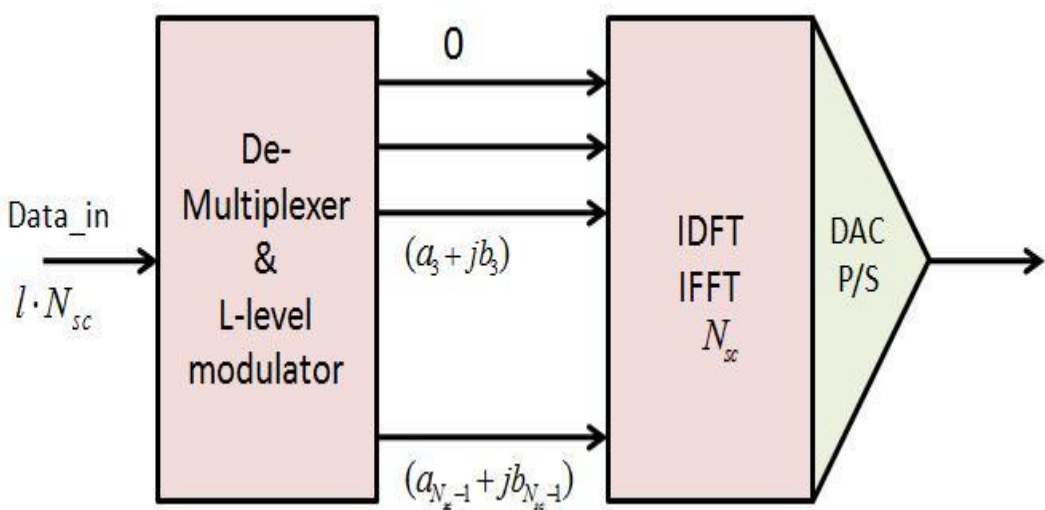


Figure 7.5: Digital implementation of multi-carrier modulator. P/S denotes parallel-to-serial and DAC digital-to-analogue conversion.

The IDFT converts the data symbol $[X]$ from frequency domain into the time domain $[x]$ with

$$x[k] = \frac{1}{N_{sc}} \sum_{n=0}^{N_{sc}-1} X[n] e^{j(\frac{2\pi}{N_{sc}} kn)}, k = 0, \dots, N_{sc} - 1 \quad (7.2)$$

Since the first input of IFFT is zero, this subcarrier is considered as DC and left un-modulated. At the receiver, the received OFDM signal in the time domain is converted to the frequency domain by performing a DFT

$$Y[n] = \sum_{k=0}^{N_{sc}-1} y[k] e^{-j(\frac{2\pi}{N_{sc}} kn)}, n = 0, \dots, N_{sc} - 1 \quad (7.3)$$

The above scenario describes a situation when the OFDM signal is transmitted over a channel without ISI. However, in practice, in order to overcome the effect of channel delay spread, a

special guard interval is inserted in each OFDM symbol referred to as cyclic prefix (CP). The cyclic prefix is formed by appending N_{CP} symbol of OFDM symbol sequences from the back to the beginning of the sequence as illustrated in Figure 7.6. The receiver is instructed to ignore the first N_{CP} received samples and only the rest of the samples are demodulated by the FFT which are unaffected by the channel response. Usually, the cyclic prefix is set longer than the maximum delay spread of channel. Since it does not contain useful data it reduces the spectral efficiency.

In addition, there exists another method to remove the effects of the multipath channel, named zero-padding (ZP). The only difference between ZP and CP is that CP is replaced with appending zeros at the end of the symbol. ZP is also able to remove ISI when the length of appended zeros is longer than the maximum delay of the channel. It is claimed in [27], ZP-OFDM outperforms CP-OFDM in terms of better bit error rate (*BER*) performance and lower peak to average power ratio. Because when the ZP prefix replaces the CP in OFDM symbols, the ripples in the power spectral density can be reduced significantly.

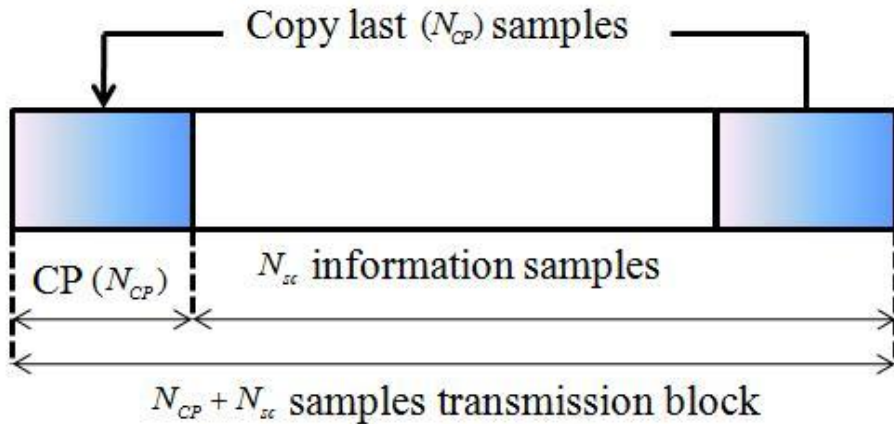


Figure 7.6: Generation of cyclic prefix guard interval

A simplified block scheme of OFDM is shown in Figure 7.7. The signal in frequency domain is denoted by capital letter and in time domain by small letter. ICP and RCP stand for insertion and removal of cyclic prefix respectively.

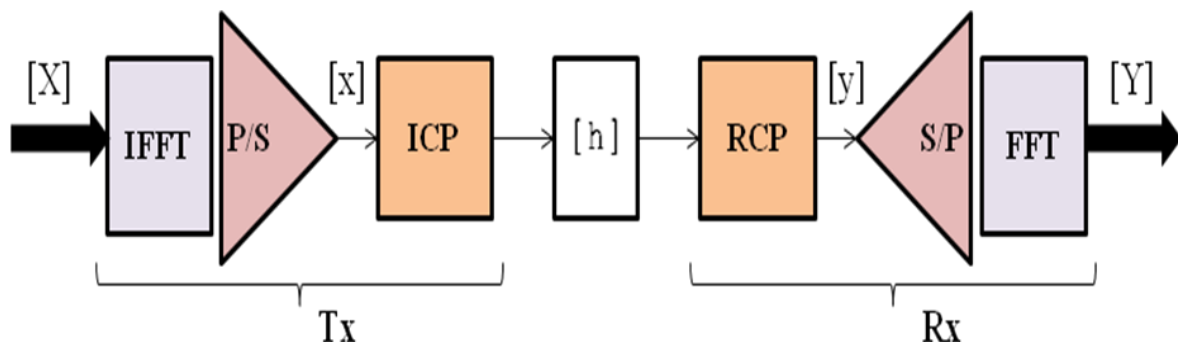


Figure 7.7: Simplified OFDM transmitter and receiver blocks

7.3 Advantages of OFDM

The main advantages of OFDM which differentiates it from a single carrier modulation are:

- Its robustness against frequency selective fading of the channel because of dividing the channel bandwidth into many narrow sub-bands.
- Mitigation of ISI by inserting cyclic prefix.
- High bandwidth efficiency due to overlapping of subcarriers which result in higher data rate transmission.

7.4 OFDM challenges

Below we will explore challenging issues in OFDM system and introduce potential method to improve these disadvantages.

7.4.1 Peak to average power ratio (PAPR)

One of the major disadvantages of OFDM is its experience of large peak to average power ratio when all subcarriers are added up coherently. If the transmitter contains a nonlinear power amplifier then high PAPR forces it to operate in nonlinear region causing signal distortion. If the linearity cannot be fulfilled, it causes both in-band and out-of-band interference to signals. The in-band interference degrades system performance and the out-of-band interference causes adjacent channel interference (ACI) that disturbs systems working in the neighbor bands [29]. However, ACI does not occur in optical communication, because there are no applications in the neighboring frequency bands and IR radiation is blocked by the walls. Systems with high PAPR require power amplifier with a large dynamic range equal to the PAPR for distortion less transmission which decreases amplifier efficiency. Therefore, reducing PAPR is necessary [29]. The PAPR is defined as the ratio of the maximum power occurring in OFDM symbol to the average power of the same OFDM symbol.

$$PAPR = \frac{\max |x(t)|^2}{E[|x(t)|^2]} \quad (7.4)$$

where E [...] denotes expectation.

PAPR is mainly dependent on the number of subcarriers and selected digital modulation scheme. As mentioned earlier, its maximum value occurs when all subcarriers are added coherently. In that case, the maximum PAPR is N_{sc} for N_{sc} subcarriers [9]. However, in practice, full coherent addition of all subcarriers is highly improbable. Therefore, although it is good to have a large number of subcarriers to keep the overhead associated with cyclic prefix down, a large PAPR is a significant penalty for large N_{sc} .

A large amount of research has been done to reduce PAPR of OFDM signal which are briefly discuss in the following section.

7.4.1.1 PAPR reduction method

Generally, PAPR reduction techniques are categorized into two groups, the distortion based techniques and the redundancy techniques. Clipping is a simple example of the distortion based technique which limits the time-domain signal for which the signal power goes beyond a certain threshold [30]. Clipping results in out of band radiation and poor error performance due to the distortion of the original signal. The redundancy based techniques are categorized into the following groups: coding, selective mapping and tone reservation, etc.

In selective mapping (SLM), a set of sequences from the original signal are generated and then the sequence with the lowest PAPR is selected to transmit. Usually, transmission of side information is required to inform the receiver which pattern is selection by transmitter, and then the receiver can recover the information. The reliability of the side information has to be considered [30].

Another popular method is tone reservations (TR) in which some of subcarriers are reserved to reduce the peak power. These reserved subcarriers don't carry any information. TR does not need transmission of side information as in SLM. However, the receiver has to know the position of the reserved subcarriers and ignores them. There are many strategies discussed in the literature to find the proper subset of subcarriers, or reduce the computational cost for searching the best results. The complexity is one serious drawback of TR. In addition, this set has to be calculated for every OFDM frame individually [31].

Active constellation extension (ACE) reduces PAPR by changing the signal constellation without affecting the BER performance. The challenge in this method is to find a unique way to map the input data to the constellation point. The inverse process is needed to be implemented in the receiver as well which is quite complex [32].

Coded OFDM is another promising technique which has received high attention due to its capability to contest with multipath fading. The concept of the method is to apply those code words that generate low PAPR. Besides, it can easily correct the errors due to frequency selective fading. The use of coding for PAPR was a brilliant idea and realized by Jones, Wilkinson and Barton [33].

The performance of TR and SLM are compared in [31] in which SLM presents better PAPR reduction and power efficiency. TR suffers from lower power efficiency due to optimization problems for tone reservation. In [29] turbo coding and selective mapping are used together to reduce PAPR. The turbo encoder is applied to generate SLM sequences and it offers two advantages of significant reduction in PAPR and bit error rate. It showed this combination can reduce the probability of the PAPR exceeding 7dB from 70% to 0.25 % for a bit error rate $=10^{-5}$, SNR= 4dB and 128 subcarriers. Combination of selective mapping and clipping techniques are applied to OFDM in [34]. If there is no error in the side information of SLM selected sequence, then SLM does not cause any distortion affecting the error performance. Clipping causes an effective reduction in PAPR but results in a large *BER* performance degradation. Therefore, combining these two methods result in effective PAPR reduction and reasonable BER performance.

In an optical Multicarrier (MCM) system, the main drawback is poor optical average power efficiency. “Because the MCM electrical signal is a summation of modulated sinusoids and takes on both negative and positive values, optical intensity (instantaneous power) must be nonnegative. Hence, a DC bias must be added to the MCM electrical signal in order to modulate it onto the intensity of an optical carrier. As the number of subcarriers increases, the minimum value of the MCM electrical signal decreases (becomes more negative) and the required DC bias increases. Since the average optical power is proportional to this DC bias, the optical average-power efficiency worsens as the number of subcarriers increases “[35], [36].

Therefore, many techniques used to reduce PAPR in a RF system are insufficient to reduce the DC bias in an optical MCM system [35]. The impact of large DC biasing influences the choice of the LED operating point. There are a few techniques introduced to reduce PAPR and DC biasing of an optical MCM system.

Reference [35] discusses two classes of techniques for reducing the optical average power requirement in MCM with IM/DD system. The first class of techniques involves block coding between the information bits to be transmitted and the symbol amplitudes modulated onto subcarriers. The second class of techniques involves replacing the fixed DC bias by a bias signal that varies on a symbol-by-symbol. Reference [36] also proposes two techniques to reduce the average optical power in wireless optical MCM systems, namely in-band trellis coding and out-of-band carrier design.

7.4.2 Frequency and timing offset

As shown in Figure 7.3, the input data is modulated onto orthogonal subcarriers separated by subcarrier spacing Δf and these subcarriers overlap in the frequency domain. However, in practice, the frequency orthogonality is not perfect due to time synchronization error, Doppler frequency shift and oscillator mismatch [9]. Synchronization of an OFDM signal is important step at the receiver because if it is not performed very accurately the orthogonality between subcarriers is lost resulting in inter-carrier interference (ICI).

Sensitivity to frequency and timing offset is higher in multicarrier system. When the number of subcarriers grows, it forces OFDM symbol time to be larger which causes the subcarriers to be closer together. Narrower sub-bands are more susceptible to ICI.

A wide variety of techniques have been proposed for estimating and correcting both time and frequency offsets at OFDM receiver. Some of these techniques are introduced in the following section.

7.4.2.1 Timing and frequency synchronization techniques

OFDM synchronization methods are categorized into data-aided and non-data-aided groups. In the data-aided category, a training sequence or pilot symbols are used for estimation. It is highly accurate and simple; however, it wastes bandwidth and reduces data transmission speed. On the other hand, the non-data aided category uses the cyclic prefix for estimation. Reduction in bandwidth efficiency is less compared to data-aid category but it does not have high accuracy in estimation [37].

Schmidl and Cox [38] proposed a method for time and frequency synchronization by using two training symbols placed at the start of the frame. The first symbol has two identical halves in the time domain. The correlation between these two halves can be performed to find the beginning of the symbol and then, the carrier frequency offset is corrected.

Nogami and Nagashima [39] presented an algorithm to find time and frequency offset by using a null symbol. In this symbol period, nothing is transmitted so that the received power is dropped and it can be detected to find the beginning of the frame.

Beek and Sandell [40] described a method which jointly finds both time and frequency offset called joint maximum likelihood estimator (ML). In this method, redundant information is contained within cyclic prefix which enable the estimation without additional pilot.

7.5 Summary

In this chapter we have studied the effect of the channel on a single and multicarrier system. In multicarrier system, dividing the serial data stream to the number of parallel data streams brings two advantages: first, due to the decreasing symbol rate on each sub-channel, the probability that the symbol being completely corrupted in a fading channel is reduced. Second, the narrow sub-channel diminishes the need for a channel equalizer. In addition, using multilevel digital modulation on each subcarrier increases transmission data rate. In OFDM, the major advantage is that the interference is reduced by applying a cyclic prefix. OFDM has two main drawbacks which affect the performance of the system: frequency offset and high PAPR. However, many methods have been introduced to improve the impairments of OFDM. For example coded and clipping OFDM are the promising alternatives in multipath and fading environment. For an optical MCM with large number of subcarriers, besides a high PAPR, requirement of a large DC biasing to drive the optical source is a major concern. Due to the limitation in generating a large DC bias, the number of subcarriers cannot be increased infinitely to compensate cyclic prefix overhead or to increase the data rate in an optical MCM system.

8.

Modulation choice for the system

This chapter starts with calculation of data rate for supporting 100 audio channels for infrared language distribution system. We will compare and analyse the application of single and multi-carrier modulation for the system according to methods introduced in previous chapters and show how the results differ for each approach. To that end, there is a brief discussion on the challenges of the selected approach for the system design.

In chapter 2 and 3, we discussed the different aspects of wireless optical communication and a method for evaluating the impulse response of the infrared channel. Therefore, the maximum delay spread and RMS delay of the channel was determined based on ray-tracing simulation model, where are found 400ns and 100ns, respectively, for a room with size of 2600m². In chapters 4 and 5, we demonstrated the feasibility of increasing the bandwidth of the system from 8MHz to 18MHz with applying new opto-electrical components. In this chapter, depending on the characteristics of the channel and system requirement we are going to compare different modulation schemes and select the option which proves a better fit than others.

As mentioned in chapter 1, the current system supports 32 audio channels in bandwidth between 2 and 8MHz with 8 non-overlapping subcarriers. For each subcarrier DQPSK modulation and raised cosine pulse with factor $r_N = 0.4$ are applied. Each subcarrier has a bandwidth of 586.53 kHz; therefore, the data rate per transmission channel is given by

$$R_b = \frac{B \times l}{(1 + r_N)} = \frac{2 \times 586.53 \text{kHz}}{1.4} = 837.9 \text{ kbps} \quad (8.1)$$

The total data rate 32 channels is $8 \times 837.9 \text{ kbps} = 6.7 \text{ Mbps}$.

8.1 General system requirement

The next generation of the Bosch infrared language distribution system needs to support 100 audio channels. To realize a larger number of audio channels, it is needed to increase the data rate of the overall system. As mentioned before, there exist two options to increase the data rate of the system. First, increase the currently used bandwidth and second, make a more efficient use of the available bandwidth. In case of the first option, the current bandwidth of the system can be increased to 18MHz. In case of the second option; several techniques were discussed such as higher order digital modulation and multicarrier modulation.

In the following, a simple calculation is set up to define the total data rate required for a system supporting 100 audio channels. The sampling frequency (f_s) and Reed-Solomon (RS) code are chosen equal to those applied in the current system. Therefore, the raw bit rate corresponding to each audio channel is given by

$$R_r = f_s \times n_{wd} \times \frac{1}{R_c Cf} \quad (8.2)$$

where $f_s = 44.1$ kHz is sample frequency, $n_{wd} = 16$ sampling word, $R_c = 24/28$ is the coding rate and $Cf = 4$ is compression factor. Thus, the total data rate for 100 audio channels is given

$$R_T = R_r \times 100 \approx 20.58 \text{ Mb/s} \quad (8.3)$$

To make it more clear, Figure 8.1 shows the raw data rate generated in each stage at transmitter side before modulation is applied.

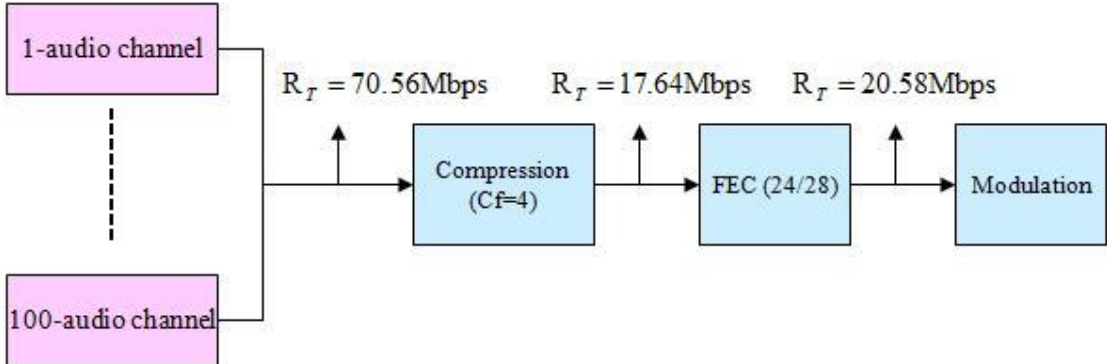


Figure 8.1: Raw data rate in different stages of transmitter

8.2 Single carrier approach with multilevel modulation

When a signal is wideband and symbol duration is less than the RMS delay spread. In that case, if the signal is transmitted over a multipath channel, each of the different multipath components will interfere with subsequently transmitted symbols and generate ISI.

From chapter 2, the maximum delay spread and RMS delay were considered to be 400ns and 100ns respectively. Therefore, the modulated signal experiences negligible ISI if the symbol rate is limited to $R_s = 1/10\tau_{RMS} = 1 \text{ Msymbol/s}$.

Consequently, the large RMS delay spread creates a significant constraint on the data rate of the system. To increase the data rate in such approach, a high level modulation method must be used.

Thus, if the carrier of such a system is modulated by DQPSK, 16QAM and 64QAM, the maximum symbol rate and required transmission bandwidth of each modulation are determined as listed in Table 8.1.

Modulation	Data rate (R_b)	Transmission bandwidth (B)
QPSK	2Mb/s	2MHz
16QAM	4Mb/s	2MHz
64QAM	6Mb/s	2MHz

Table 8.1: The maximum symbol rate and required transmission bandwidth of each modulation

As seen here, even though, QPSK is a very robust technique, its main drawback is its low data rate efficiency. 16QAM has twice the bandwidth efficiency of QPSK but it is more sensitive to amplitude distortion. Finally the highest data rate of 6 Mb/s can be provided by applying 64QAM at the expense of an increase in complexity of the system and transmission power. Hence, to achieve the same bit error rate and coverage area as QPSK, 4dB more E_b / N_0 is required at the receiver.

The maximum achievable data rate is limited to 6Mb/s applying 64QAM and still it does not provide the data rate required for the new system. In addition, this leads to a required transmission bandwidth of 2MHz. It means that only 2 MHz of 18MHz bandwidth is used for this system. In other word, the overall transmission bandwidth is wasted.

Therefore, no further investigation for this approach is considered in this chapter.

8.3 Non-overlapping multicarrier approach with multilevel digital modulation

In a multicarrier system, the performance of the system is strongly affected by the number of narrowband subcarriers. To avoid the reduction of the performance, the number of sub-channels must be chosen to insure that each channel has a bandwidth less than the coherence bandwidth ($B_N \ll B_{coh}$) of the channel for which the channel experiences flat fading. In other words, the symbol time is chosen to be much larger than the delay spread of the channel.

The bandwidth of each subcarrier using Pre-modulation raised cosine roll off filter with factor r_N is calculated by

$$B_N = \frac{(1+r_N)}{T_N} \quad (8.4)$$

where T_N is subcarrier symbol time.

To insure flat fading on each sub-channel, the bandwidth of each subcarrier is approximated to be $B_N = \frac{1}{3} B_{coh}$. The factor (1/3) is chosen such that the bandwidth of each sub-channel is almost

the same as the sub-channel bandwidth of the current system. The coherence bandwidth is $B_{coh} = 1/2\pi\tau_{RMS} = 1.6$ MHz with respect to 100ns RMS delay spread. So the resultant bandwidth of each sub-channel is

$$B_N = \frac{1}{3} B_{coh} = \frac{1}{3} \times 1.6 \text{MHz} \times 1.4 = 533 \text{kHz} \quad (8.5)$$

Consider multicarrier system with transmission bandwidth of $B_T = 18$ MHz and bandwidth of $B_N = 533$ kHz per each sub-channel, then number of sub-channel (N_{sc}) is determined by

$$N_{sc} = B_T / B_N = 18 \text{MHz} / 533 \text{kHz} = 33 \quad (8.6)$$

Total data rate of the system with QPSK modulation ($l=2$) on each carrier is given by

$$R_b \simeq N_{sc} \frac{B_N l}{1 + r_N} = 33 \frac{533 \text{kHz} \cdot 2}{1.4} \simeq 25 \text{Mb/s} \quad (8.7)$$

If subcarriers are modulated by 16QAM then data rate increases to $R_b = 50$ Mb/s.

8.3.1 Effective bandwidth per carrier

In a realistic implementation, a sub-channel will occupy a larger bandwidth than under ideal raised cosine pulse shaping. It is because from the total bandwidth, a factor of x is reserved as guard band (B_G) between subcarriers and it discards the imperfect matching of the filters in transmitter and receiver. The factor x denotes the sum of all the guard bands relative to the total bandwidth, so:

$$\sum B_G = x B_T \quad \text{with } 0 \leq x \leq 1, \quad (8.8)$$

Then, the actual available bandwidth considered for data transmission is

$$B_{avail} = B_T - \sum B_G = (1-x)B_T \quad (8.9)$$

The efficient bandwidth and available data rate per subcarrier are obtained by

$$B_{eff} = \frac{(1-x)B_T}{N_{sc}}, \quad R_b = B_{eff} \times \frac{l}{1+r_N} \quad (8.10)$$

where N_{sc} is number of subcarrier.

Using $x = 0.2$ as considered in the design of the current system results in available bandwidth of $B_{avail} = 14.4\text{MHz}$. Considering $B_{eff} = 533\text{ kHz}$ as efficient bandwidth per carrier results in 27 subcarriers. In this case, with QPSK per carrier, the total data rate is

$$R_b \simeq N_{sc} \frac{B_{eff} l}{1 + r_N} = 27 \frac{533\text{kHz} \cdot 2}{1.4} \simeq 20\text{Mb/s} \quad (8.11)$$

As seen from (8.7) and (8.11), this approach can provide the required data rate of the new system. However, due to the guard band insertion, there is a large reduction in bandwidth efficiency. In addition, implementation of this method requires separate modulators and demodulators for each subcarrier which make the system design rather complex for a large number of subcarriers.

8.4 OFDM approach

The OFDM scheme has been discussed in details in previous chapter. Briefly, in OFDM, the input data stream is divided into data blocks of size N_{sc} where each block is referred to as an OFDM symbol. A cyclic prefix is added to each OFDM symbol to eliminate ISI between the data blocks. The spectral efficiency increases due to overlapping of sub-channels and it is easily implemented with performing of IFFT and FFT.

8.4.1 OFDM system parameters

The key parameter to start the design of an OFDM system is maximum channel delay spread which was determined to be 400ns (τ_{max}). Therefore, the guard interval must be at least as long as τ_{max} . We choose the guard time to be about $T_g = 2\tau_{max}$ so that the design is sufficiently immune against delay spread variation. The useful symbol duration (T_u) of an OFDM block is equal to inverse of the subcarrier spacing (Δf).

When the subcarrier spacing increases, then automatically the symbol period decreases. It is desirable to have symbol duration much larger than the guard time to compensate the overhead of the guard interval. However, it can't be arbitrarily large because large symbol duration means more subcarriers, small subcarrier spacing and more sensitivity to frequency offset. Also there is an increase of the peak to average power ratio. In addition, for an optical OFDM system, more subcarriers result in large DC biasing which means poor average optical power efficiency.

By referring to the literature, typically, useful symbol period is $T_u = \Delta T_g$ for which $\Delta = \{4, 8, 16, 32\}$. After adding the guard interval, the actual duration of an OFDM symbol is $T_{OFDM} = T_g + T_u$. The total data rate of an OFDM system is now calculated by

$$R_{b-OFDM} = N_{data} \times l \times R_c \times \frac{1}{T_g + T_u} \quad (8.12)$$

where l is number of bits per modulated symbol, N_{data} number of subcarriers for data transmission and R_c is the coding rate (24/28).

To calculate the achievable data rate, the guard interval, number of bit per symbol and coding rate are known. Therefore, this equation shows a tradeoff between number of subcarrier and useful symbol time.

In OFDM, usually, not all subcarriers of an OFDM are used for data transmission. There are four types of subcarrier

- Data subcarriers (N_{data}): useful data transmission.
- Pilot subcarriers (N_{pilot}): as discussed in (5.5.1) they are mainly used for channel estimation and synchronization.
- Null subcarriers (N_{null}): these subcarriers usually are near two edges of the assigned band. No information is transmitted by these subcarriers and they are only used to prevent significant leakage to adjacent band. They are also known as guard subcarriers or virtual subcarriers. When the OFDM signal power spectrum has high side lobes, generation of this guard band helps to reduce the out of band emission and thus eases the requirement on transmitter front-end filters. Insertion of guard bands wastes some assigned bandwidth and decreases spectral efficiency of the OFDM system [41].
- DC subcarrier: it is a subcarrier whose frequency is equal zero.

Therefore, the total number of subcarrier used for transmitting a modulated data symbol is $N_{data} = N_{ifft} - N_{pilot} - N_{null} - 1$.

Returning to the OFDM system analysis, in order to exploit the channel bandwidth in an efficient way, no pilot and null subcarriers are considered for synchronization and frequency band, respectively. Pilot subcarriers are not necessary because the optical wireless channel changes very slowly and Doppler frequency is considered zero. Thus, a reference symbol can be used for channel estimation and synchronization. As the channel is assumed to be only very slowly time-varying, this reference symbol can be transmitted every n symbols and causes an overhead. In addition, null subcarriers are not required because in optical wireless communication, there is no application in the adjacent frequency band. The parameters of an OFDM system for different values of Δ are calculated and listed in Table 3.

Δ	4	8	16	32
Overall bandwidth (MHz)	18	18	18	18
Guard interval (ns)	800	800	800	800
Useful symbol duration(μ s)	3.2	6.4	12.8	25.6
OFDM symbol duration (μ s)	4	7.2	13.6	26.4
Subcarrier spacing (kHz)	312	156	78.12	39.6
Number of data subcarrier	57	115	230	460
Number of bits per symbol	2	2	2	2
OFDM data rate (Mbps)	24.42	27.3	28.99	32.16
FFT size	64	128	256	512
Cyclic prefix overhead	20%	11%	5.9%	3%

Table 8.1: QPSK-OFDM parameters

We have proposed an OFDM system with different number of subcarriers. We have considered optical channel properties to determine guard interval and the useful symbol duration of OFDM. It was also considered to transmit low information redundancy such as pilot insertion. Therefore, since the chosen design of opto-electrical front-ends allows the bandwidth of 18 MHz, if QPSK modulation is applied on each subcarrier, it can fulfill the required data rate for the new system. In addition, QPSK is a good option for optical channel because it is less sensitive to high channel path loss.

As mentioned before, the larger the number of subcarriers, the greater the symbol period on each carrier leading to higher bandwidth efficiency and a smaller cyclic prefix overhead. On the other hand, the large number of subcarriers results in high PAPR, large DC biasing required for optical source and the complexity in the implementation increases. As seen in Table 8.2, an OFDM with 57 data subcarriers, carrier spacing of 312 kHz and 64IFFT can provide the data rate of 24Mbps with small number of subcarriers. Therefore, all mentioned reasons result in the choice for the size of 64FFT.

Later in this chapter, the challenges with the selected option are investigated.

8.4.2 Challenges with chosen OFDM parameters

Based on the system constraints and channel information, chosen method faces some issues in the design which are discussed briefly in the following

Linearity of the optical source

For wireless optical systems, since the OFDM modulating signal at the LED input is a sum of N_{data} signals on equidistant subcarrier frequency, then the amplitude of modulating signal may exceed the maximum value defined for linearity of the LED. However, As long as the linearity is achieved, having large number of subcarrier is minor issue. Therefore, whether LED output power experience distortion if an OFDM signal (summation of 57 subcarriers) is transmitted must be checked.

Peak to average power ratio

Multicarrier systems suffer from a high peak to average power ratio due to the addition of many independent frequency carriers. This results in nonlinear distortion due to clipping in transmitted signal. If the modulated signal at the LED input is a sum of $N_{data} = 57$ signals on equidistant subcarrier frequencies with equal amplitude, the maximum PAPR is approximately given by [9]

$$PAPR = 10 \log_{10}(N_{data} = 57) = 17.55 \text{ dB} \quad (8.13)$$

This value is still high and PAPR reduction methods are still of great interest because if the PAPR is reduced then more average power can be transmitted and it means increase in the coverage area. Figure 8.2 shows PAPR for proposed OFDM parameters listed in Table 8.2 when they transmit same data rate.

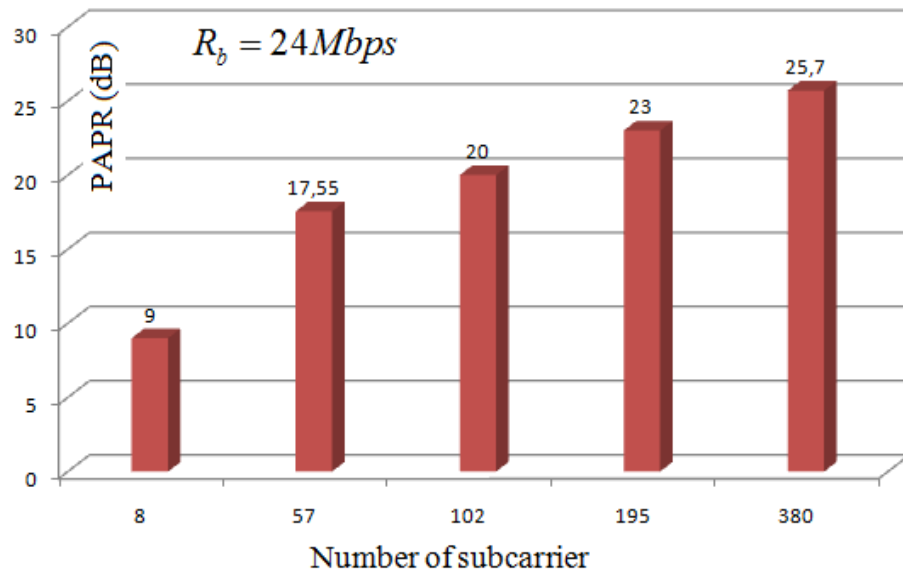


Figure 8.2: PAPR vs. Number of subcarriers

Average optical power requirement

As said earlier, transmission of the optical multicarrier signal is translated in a requirement for a large DC signal which in turn implies a large average optical power requirement. Many approaches proposed in literature to improve the power efficiency (in terms of DC) are based on block-coding and other techniques proposed for RF OFDM. Nevertheless, these techniques reduce the transmission rate and may have large implementation complexity like TR or SLM.

The power penalty for a multicarrier MQAM modulation is determined by [1]

$$\text{power penalty} = \underbrace{1.5}_{\text{offset penalty}} + \underbrace{5\log_{10} N_{data}}_{\text{multi-subcarrier penalty}} + \underbrace{5\log_{10} \left(\frac{(\sqrt{M} - 1)^2}{\log_2 \sqrt{M}} \right)}_{\text{multi-level penalty}} \quad [dB] \quad (8.14)$$

where, 1.5 is the offset penalty due to power wasted in the DC. The multicarrier penalty which is zero for $N_{data} = 1$, represents the penalty when more than one subcarrier is used. The multilevel penalty, which is zero for 4QAM and QPSK, represents the penalty due to larger constellation diagram. Figure 8.2 shows the power penalty for 16QAM and QPSK vs. the number of subcarriers. In Table 8.3 the power penalty for number of subcarrier used data transmission in the purposed OFDM are shown using QPSK and 16QAM.

According to (8.14), doubling the number of subcarriers results in 1.5dB increase in required optical power. Power penalty for different number of subcarriers are listed in table 8.2. The optical power penalty for a QPSK system with 57 subcarriers is 10.27dB which is 4.5dB more when eight subcarriers used. It is seen that using 16QAM increases the power penalty 3dB more than when QPSK is applied with 57 subcarriers.

As previously mentioned, since phase modulation is applied and data is transmitted on the phase of each subcarrier, to reduce the optical average power, the bias can be reduced to the point that some clipping occurs. If clipping is permitted, then the modulating power of the transmission signal can be increased. In other words, the power can be increased by increasing the sum of the subcarrier amplitude until the error performance reaches its threshold. The effect of the clipping on the system performance was investigated in details in [7].

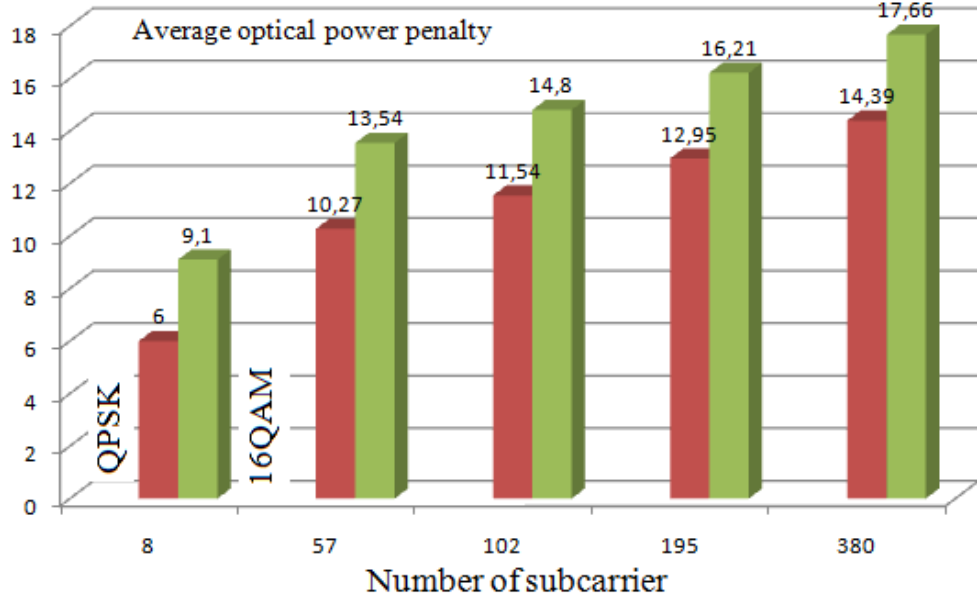


Figure 8.3: Power Penalty vs. number of subcarrier

Transmission power and coverage area

The ratio of the received signal to the noise (SNR) at the receiver output is the most important factor in designing a system. Hence, it is necessary for a receiver to achieve a certain level of signal to noise ratio which is given by

$$\frac{E_b}{N_0} = \frac{P_r}{N_0 R_b} \quad (8.15)$$

where, P_r is received electrical power and N_0 is noise spectral density. The received LOS optical power was determined by Eq. (2.6). The received electrical signal after (amplifying assuming trans-impedance amplifier) is given by

$$P_{elec} = \left[\left(P_t \frac{(n+1)A \cos^n(\phi) \cos^m(\theta)}{2\pi r^2} \right) * R_p R_f \right]^2 [W] \quad (8.16)$$

where, P_t is transmitter optical power, R_p is the responsivity of the receiver (A/W), r is distance between transmitter and receiver and R_f is feedback resistor of trans-impedance amplifier. Therefore, by substituting (8.14) into (8.13)

$$E_b R_b = \left[\left(P_t \frac{(n+1)A \cos^n(\phi) \cos^m(\theta)}{2\pi r^2} \right) * R_p R_f \right]^2 \quad (8.17)$$

Eq. (8.17) shows that increasing the data rate of the system and keeping both coverage area and transmitted power similar to the current system, the received energy per bit decreases significantly resulting in high bit error rate. Therefore, to obtain the same energy per bit at receiver, either transmitted power must be increased or the coverage area decreased. In the proposed OFDM model, the transmission data rate is approximately $R_{b-OFDM} = 24\text{Mb/s}$ which is almost three times more than that in current system. This results in power penalty of 5dB for new system to achieve the same performance as current system. In addition, as shown in Figure 8.3 increase in the number of subcarriers results in 4dB power penalty. Therefore, total power penalty due to large number of subcarriers and high data rate transmission is 9dB. Number of subcarriers and high data rate transmission also affect converge area. Increase in data rate from 6.7Mbps to 24Mbps leads to reduction of 0.5 in coverage area and increase in the number of subcarrier leads to reduction of 0.33 in coverage area.

On the other hands, it can be observed that the received power depends on area and responsivity of the detector as well as gain of the amplifier. Using a detector with large area and good responsivity provides more power at receiver without the need of large increase in transmitted power.

9.

Conclusion and further research

9.1 Conclusion

This thesis provides system design in order to increase the data rate of wireless infrared multi language distribution system. **In short the results of this thesis confirm that it is possible to increase the data rate of the system and OFDM is a suitable method for the system whose parameters can be tailored according to the system requirement.** To make OFDM less sensitive to optical channel loss and have low PAPR, we offered OFDM with small number of subcarriers and phase modulation on each subcarrier. As seen in chapter 8, OFDM with 57 subcarriers for data transmission, 64IFFT size and QPSK modulation can provide the required data rate of the new system. The contributions of this thesis work are summarized as follows:

- Firstly, single and multi reflection optical channel for any room size and any transmitter and receiver configurations are modelled by using ray- tracing model. The results show reasonable agreement with the simulation model of Philips. In single reflection model, received power, maximum delay spread and RMS delay spread with respect to power level of -30dB and -40dB as a threshold of the received signal are determined. In multiple reflection models, the same parameters are found with considering limited number of second reflections; it shows that considering second reflections slightly increase amount of received power and also there is an increase in excess delay due to second reflections from far away reflectors. **Therefore, based on the simulation results, the single reflection paths have the most effect on the characteristics of the optical channel. The important parameters of the multipath optical channel have been determined, the maximum delay spread of 400ns and RMS delay of 100ns which affect the choice of applying multicarrier or single carrier modulation.**
- Opto-electrical front-ends are analyzed and their relevant components and parameters are discussed in order to achieve a design as simple as possible, which allows a wide transmission bandwidth. A simple measurement set up is used to determine whether the frequency bandwidth represented on the datasheet of components can be achieved in different distances. At the transmitter side, LED (TSFF5410) is chosen as a transmitter. At the receiver side, a PIN diode (TESP5700) and a preamplifier (OPA847) are considered as main components. The discussion of the opto-electrical front-ends is not intended to optimize the receiver design, but aimed to provide a set of realistic receiver parameters useful for further investigations. **The desired bandwidth of 18 MHz resulted from the choice of the source, detector and preamplifier types. It is clear that the**

transmission bandwidth of the current system is limited by the bandwidth of the photo-detector.

- Theoretical approaches for increasing the data rate of the system are investigated by comparing several modulation techniques in terms of bandwidth and power efficiency. The result shown that single carrier modulation with even 64QAM modulation in the bandwidth of 18MHz cannot provide the required data rate of the system. Therefore, no more investigation is considered for this approach. From analysis of a non-overlapping multicarrier approach for the system, it is represented that a multicarrier system is defined with 33 sub-channels and bandwidth of 533 kHz for each sub-channel. In this case, the transmission data rate of the system using QPSK is 25Mbps. In addition, it was discussed that in a realistic implementation, a guard interval is inserted between each sub-channel in order to discard the imperfect matching in transmitter and receiver filters. In this case, if 3.6MHz of the bandwidth is considered as overall guard band, the available bandwidth and number of subcarriers are decreased to 14MHz and 27, respectively. Then the data rate of the system decreases to 20Mbp. Consequently, although this approach can provide the required data rate to support 100 audio channels, the implementation of this method requires separate modulators and demodulator for each subcarriers which the system design becomes rather complex for large number of subcarriers. **Therefore, the single carrier and non-overlapping multicarrier modulation are not good approaches to increase the data rate of the system because of low bandwidth efficiency and high complexity.**
- Finally, the OFDM approach is introduced as a good option for the system. Deployment of OFDM in an optical wireless system brings various benefits, among which are providing large bandwidth efficiency with simple front-end design and its robustness to frequency selective fading response. The influence of OFDM on peak to average power ratio, optical power penalty, large DC basing for optical MCM system are discussed. **Since the chosen opto-electrical front-ends allow a signal bandwidth of 18MHz, the choice for 64 IFFT with 57 subcarriers for data transmission, guard interval twice the maximum delay spread of the optical channel and QPSK modulation on each subcarrier can achieve the transmission data rate of 24Mbps with small number of subcarriers. Therefore, among analyzed methods, OFDM is a better option due to make efficient use of the bandwidth and simple implementation.**
- **In addition, the increase in transmission data rate results in a reduction in the received energy per bit to achieve the same coverage area and transmitted power as the current system. Therefore, to obtain the same performance as current system, either transmitted power must be increased or the coverage area decreased.**

9.2 Further work

There are fundamental recommendations for further research:

- The optical channel model is defined for a limiting number of second reflections; therefore, further work on the modeling of the channel can improve the accuracy of the model even considering third and fourth order reflections. Despite the advantages of the simulation, many issue can only be resolved through an experimentation for example, the model is applied for an empty room; however, objects in the room must be taken into account with which impulse response varies. Therefore, it is necessary to obtain impulse channel characteristics by measurement.
- The measurement set up to determine transmission bandwidth of the new opt-electrical components is performed when distances between transmitter and receiver are 2cm, 5cm and 10cm. It can be shown that the same bandwidth can be achieved for larger distances if more than one LED or PIN diodes are used. Especially, since the PIN diode is the bandwidth limiting factor, by using 2 PIN diodes, the amount of the reduction in the bandwidth for the introduced receiver front-end can be viewed.
- The investigations conducted in OFDM analysis is based on the theoretical calculation, therefore, another important step in future work that can be accomplished is to determine the permitted power of the LED that it does not experience distortion when an OFDM signal (summation of 57 subcarriers) is transmitted which it can be used to determine the level of the permitted clipping
- In this work many methods are introduced to reduce PAPR and it was not foreseen that which method is a suitable option for optical OFDM system and how much they can reduce PAPR. However, according to many references the suitable PAPR reduction method for an optical OFDM system is clipping. Therefore, the effect of the clipping on *BER* can be evaluated.
- The last interesting topic would be to implement the OFDM transmitter and receiver.

10.

References

- [1] Barry, J. (1986). *Wireless Communication Using Non-Directed Infrared Radiation*. University of California.
- [2] Ramirez, R., & Green, R. J. (1999). *Indoor Optical Wireless Communications*. London: IEE, Savoy Place.
- [3] Kahn, J., & Barry, J. (1997). Wireless INfrared Communication. Proceeding of the *IEEE*, 265-298.
- [4] Singh, C., & John, J. *A Review on INdorr Optical Wireless System*.
- [5] Gfeller, F., & Bapst, U. (1997). Wireless In-house Data Communication via Diffuse INfrared Radiation. *IEEE* , 1472-1492.
- [6] Kahn, J., & You, R. (1998). Imaging Diversity Recievers for High-Speed Infrared Wireless Communication. *IEEE Communication magazine* .
- [7] Grubor, J. (2009). *Adaptive Modulation Technique for Broadband Communication in Indoor Optical Wireless Systems*. Berlin. Berlin: Technical University of Berlin.
- [8] Hashemi, H. (1994). Indoor Propagation Measurement at infrared frequency for wireless local area network applications. Vehicular Technology, *IEEE Transactions*, 562 - 576
- [9] Goldsmith, A. (2005). *Wireless Communications*. Cambridge University Press.
- [10] Hernandez, L. (1997). Algorithm for calculation of impulse response on IR wireless indoor channels. Electronic letters, *IEEE*, 1804 - 1806
- [11] Lopez-Hernandez, F., & Perez, R. (1998). Monte Carlo calculation of impulse response on diffuse IR wireless indoor channels. *ELECTRONIC LETTERS* , 1260-1262.
- [12] Carruthers, J., & Kannan, P. (2002). Iterative Site-Based Modeling for Wireless Infrared Channels. *IEEE ANTENA AND PROPAGATION* .
- [13] lomba, C., & Valadas, R. *Efficient Simulation of the Impulse Response of the Wireless Optical Channel*. Potugal.
- [14] Moreira, A., & Valadas, R. (1997). Optical interference produced by artificial light. *Wireless Network* , 131-140.
- [15] Moreira, A., & Valadas, R. (1995). Characterisation and Modelling of Artificial Light Interference in Optical Wireless Communication Systems. Toronto: PIMRC.
- [16] Mathias, J. (2007). *eetimes*. Retrieved from Wi-Fi Channel Emulation Goes Mainstream: <http://www.eetimes.com/design/rf-microwave-design/4012902/Wi-Fi-channel-emulation-goes-mainstream>

- [17] Hranilovic, S. (2005). *Wireless Optical Communication Systems*. United State of America: Springer.
- [18] IEC. (1993). International Electro-technical Commission. *Safety of laser products. Equipment classification requirements and user's guide*. Group safety publication.
- [19] Retrieved from PHOTODIODE CHARACTERISTICS: <http://www.udt.com>
- [20] T1A1, A. C. (2008). Retrieved from Noise-equivalent power: <http://en.wikipedia.org/wiki/Noise-equivalentpower>
- [21] *Noise Specs Confusing*. (n.d.). Retrieved from National Semiconductor.
- [22] *Wideband, Ultra-Low Noise, Voltage-Feedback Operational Amplifier with Shutdown*. (n.d.). Retrieved from Texas Instruments: www.ti.com
- [23] Kim, S., & Lee, U. (2007). Improved Performance of APSK Modulation Scheme for Satellite System. Information, Communication and Signal Processing, *IEEE*, 1- 4.
- [24] Ali, P., Hussain, F., & Jeong, G. (2008). . A low complexity De-mapping Technique for 16-APSK Modulation for Digital Video Broadcasting in AWGN Channel. *International Conference on Convergence and Hybrid Information Technology*. Seoul: Hanyang University.
- [25] Sklar, B. (1993). Defining, Designing, and Evaluating Digital Communication Systems. *IEEE Communication Magazine* .
- [26] Sankar, K. (2008). *Signal Processing for Communication*. Retrieved from Comparing BPSK, QPSK,16QAM, 16PSK, 64QAM and 32PSK: <http://www.dspslog.com>
- [27] Lu, G., & Nikookar, H. (2009). On The Potential of ZP-OFDM for Cognitive Radio. *Wireless Personal Multimedia Communication* .
- [28] Matiæ, D. OFDM as a possible modulation technique for multimedia applications in the range of mm waves. In *Introduction to OFDM*.
- [29] Abouda, A. (2004). PAPR REDUCTION OF OFDM SIGNAL USING TURBO CODING AND SELECTIVE MAPPING. *Nordic Signal Processing Symposium* .
- [30] Lin, M., Tsai, Y., & Yang, C. (2005). Selective-Mapping Type Peak Power Reduction Techniques for Turbo Coded OFDM. *IEEE* .
- [31] Siegl, C., & Fischer, R. (n.d.). Tone Reservation for Peak-to-Average Power Ratio Reduction in OFDM under Different Optimization Constraints.
- [32] Kumara, A., & Sim, M. (2008). PAR Reduction in Space-Time Coded OFDM via Modified Active Constellation Extension. *Innovative Technologies in Intelligent Systems and Industrial Applications*, (pp. 12-13). Malaysia.
- [33] Zafar, Q., Taha, Q., & Xian, L. *A PAPR REDUCTION TECHNIQUE USING EXPURGATED CYCLIC CODES FOR COFDM*,. Arkansas: University of Arkansas.
- [34] Wang, L., Cho, K., & Yoon, D. *PAPR Reduction of OFDM Signals Using Deliberate Clipping and Pre-scrambling Technique*. seoul: Hanyang University.
- [35] You, Y., & Kahn, J. (2001). Power Reduction Techniques for Multiple-Subcarrier Intensity-Modulated Optical Signals. Communications,*IEEE*, 1620 – 1627.
- [36] Kang, W., & Hranilovic, S. (2008). . Power Reduction Techniques for Multiple-Subcarrier Modulated Diffuse Wireless Optical Channels. Communcation, *IEEE Transactions*, 279 – 288.

- [37] Wu, F., & Abu-Rgheff, M. *Time and Frequency Synchronization Techniques for OFDM Systems operating in Gaussian and Fading Channels*. University of Plymouth.
- [38] Schmidl, T., & Cox, D. (1997). Robust Frequency and Timing Synchronization for OFDM. Communication, *IEEE Transactions*, 1613 – 1621.
- [39] Nogami, H., & Nagashima, T. A frequency and timing period acquisition technique for OFDM systems, Personal, Indoor and Mobile Radio Communication. *PIRMC*, (p. 1995).
- [40] Beek, J., & Sandell, M. (1997). ML Estimation of Time and Frequency Offset in OFDM Systems. *IEEE Transactions on Signal Processing* .
- [41] Chiueh, T., & Tsai, P. (2007). *OFDM baseband receiver design for wireless communication*. Singapore: Wiley.